



POLITECNICO DI TORINO

MECHANICAL AND AEROSPACE ENGINEERING DEPARTMENT

Master degree course in Aerospace Engineering

Master Degree Thesis

**Methodology and tools to improve
the aerodynamic characterization
of high-speed vehicles during the
conceptual design phase**

Supervisors

Prof. Nicole Viola

Dr. Davide Ferretto

Dr. Roberta Fusaro

Candidate

Luca Nepote Fus
s265759

ACADEMIC YEAR 2020-2021

Abstract

Over the last years, innovative concepts of civil high-speed transportation vehicles were proposed. These aircraft have a strong potential to increase the cruise range efficiency at high Mach numbers, due to efficient propulsion units combined with high-lifting vehicle concepts. In this context, the necessity to have a simple and reliable tool for the estimation of the aerodynamic performance of such vehicles is of primary importance in the first phases of the design, when a quick response is needed for each design modification/improvement that is made.

The objective of this thesis is to improve the prediction of the aerodynamic performance of a new high-speed vehicle since the conceptual design phase. The goal is to define a new aerodynamic performances characterization routine as complete as possible, capable of supporting a wide range of users and vehicle configurations.

The first part of this project focuses on the analysis and description of four preliminary aerodynamic estimation models taken from the literature: their main theoretical aspects, limitations and capabilities have been listed. The next step is to implement them in Matlab, test them with existing aircraft whose main geometric characteristics are known, and compare the obtained results with the available aerodynamic coefficients. Finally, in order to better estimate the aerodynamic behaviour of the aircraft under investigation for the whole mission profile, the basic models have been adapted by adding corrective coefficients.

The analysis focuses on the combined cycle engine launchers, which include hypersonic cruise aircraft, powered by air-breathing propulsion over all or part of their flight mission. In particular, the aerodynamic coefficients of eight different high-speed vehicles are studied, grouped into four different configurational families: Waverider configuration, Blended body configuration, Wing body configuration and Cylinder wing configuration.

The main effort of this work was spent on the application to the STRATOFly MR3 vehicle case study. STRATOFly MR3 is a Mach 8 waverider configuration that stems from more than a decade of European research activities, under the framework of Horizon 2020 research and innovation programme. In particular, for this vehicle it is possible to estimate the aerodynamic coefficients for a Mach number between 0.4 to 8, for an angle of attack between 1° to 5° and for all operative conditions, including the case in which the engines are switched on or off.

Finally, in order to allow any user to take advantage of these results, it was necessary to implement a simple and intuitive Graphical User Interface (GUI). The work is also contributing to the improvement of ASTRID-H, a conceptual design tool currently under development by Politecnico di Torino.

Ringraziamenti

Prima di procedere con la trattazione, vorrei dedicare qualche riga a tutte le persone che mi sono state vicine in questo percorso ed hanno contribuito alla realizzazione della mia tesi di laurea.

In primo luogo, grazie alle professoresse Nicole Viola, Roberta Fusaro ed al professore Davide Ferretto, per il loro supporto tecnico e per essersi sempre dimostrati pazienti e disponibili nei miei confronti. Mi hanno dato la possibilità, inoltre, di prender parte a questo progetto interessante.

Grazie ai miei genitori Fabrizio e Luisa, che mi hanno permesso di intraprendere questo percorso di studi ed hanno creduto in me fin dal primo momento. Grazie alle mie sorelle Valentina e Sara, a mia nonna Daniela e a tutta la mia famiglia, per essermi stati sempre accanto.

Grazie ai miei amici d'infanzia Simone Coletti, Alessandro Peirone, Francesco Rotella, Francesco Contis e Matteo Vottero. Con voi sono cresciuto e tuttora condivido buona parte della mia vita. Siete fondamentali e mi avete regalato momenti indimenticabili.

Grazie ai miei amici di Università Simone Moino, Davide Neglia, Luca Narcisi, Greta Montaldo, Gabriele Vittori, Alessandro Princi e Lorenzo Montagna, che hanno reso questi anni speciali. E' stato bello aiutarsi nei momenti di difficoltà e festeggiare insieme ogni piccolo traguardo. Senza di voi non sarei qui oggi.

Grazie ai miei compagni di pallavolo Arturo Bertero, Luca Bagetto, Umberto Cena e Riccardo Arnaud. In campo eravamo più che semplici amici e nonostante le circostanze ci abbiano fatto allontanare, saremo sempre una squadra.

Infine, grazie alla persona più importante, Marta. Grazie per tutto il sostegno e la forza che mi regali ogni giorno, per credere in me più di quanto non lo faccia io stesso e per esserci sempre. Hai un ruolo determinante nella mia vita e non ti ringrazierò mai abbastanza.

Contents

List of Tables	6
List of Figures	7
1 Introduction	12
2 Aerodynamic Models	15
2.1 Model I (Curran Model)	15
2.2 Model II (All-Body Hypersonic Aircraft)	19
2.3 Model III (Raymer Model)	26
2.4 Model IV (Torenbeek Model)	34
3 Final Aerodynamic Models	43
3.1 Dorsal Waverider Configuration	45
3.1.1 STRATOFly MR3 project	46
3.1.2 Curran Model Results	52
3.1.3 All-Body Hypersonic Aircraft Model Results	55
3.1.4 Raymer Model Results	58
3.1.5 Torenbeek Model Results	61
3.1.6 Engine - ON Final Results	63
3.1.7 Engine - OFF Final Results	65
3.2 Ventral Waverider Configuration	69
3.2.1 NASA X-43A	69
3.2.2 Results	71
3.3 High - AR Wing Body Configuration	76
3.3.1 X-34	76
3.3.2 PRORA USV-FTB-1	78
3.3.3 Results	80
3.4 Low - AR Wing Body Configuration	87
3.4.1 HYPLANE	87
3.4.2 Results	89
3.5 Cylinder Wing Configuration	94

3.5.1	VTO-HOPPER	94
3.5.2	Results	96
3.6	Blended Body Configuration	101
3.6.1	ELAC	101
3.6.2	SAENGER	103
3.6.3	Results	105
4	Aerodynamic Graphical User Interface Tools	112
4.1	GUI Architecture and Capabilities	113
4.2	User Guide	118
4.2.1	Simplified analysis	119
4.2.2	Accurate analysis	121
4.2.3	Both analysis and comparison	124
4.2.4	Other Results	125
5	Conclusions	129
	Bibliography	132

List of Tables

2.1	Model I - Input and Output	17
2.2	Model II - Input and Output	25
2.3	Model III - Input and Output	33
2.4	Model IV - Input and Output	41
3.1	STRATOFLY MR3 geometrical data	48
3.2	Curran Model Corrective Coefficients for the all angles of attack analysed, Engine - ON condition	54
3.3	All-Body Hypersonic Aircraft Model Corrective Coefficients for the all angles of attack analysed, Engine - ON condition	57
3.4	Raymer Model Corrective Coefficients for the all angles of attack analysed, Engine - ON condition	60
3.5	Torenbeek Model Corrective Coefficients for the all angles of attack analysed, Engine - ON condition	62
3.6	Corrective Coefficients for the all angles of attack analysed, Engine - OFF condition	66
3.7	X-43A geometrical data	70
3.8	Corrective coefficients for ventral waverider configuration	75
3.9	X-34 geometrical data	77
3.10	USV-FTB-1 geometrical data	79
3.11	Corrective coefficients for High AR wing-body configuration	81
3.12	HYPLANE geometrical data	88
3.13	Corrective coefficients for Low AR wing-body configuration	93
3.14	VTO - HOPPER geometrical data	95
3.15	Corrective coefficients for Cylinder Wing configuration	100
3.16	ELAC geometrical data	102
3.17	SAENGER geometrical data	104
3.18	Corrective coefficients for Blended Body configuration	106

List of Figures

2.1	τ effects on the vehicle configuration [1]	16
2.2	Model II - nominal configuration [3]	19
2.3	Model II - configurational parameters [3]	20
2.4	Model III - nominal configuration[4]	26
2.5	Basic wing geometry and definitions of flow parameters [5]	34
2.6	Arrow wing geometry [5]	38
2.7	Blended-body geometry [5]	40
3.1	Surface and Volume Characteristics of Hypersonic Configuration Concepts [1]	44
3.2	Nonweiler (Caret) Waverider showing the attached shock [6]	45
3.3	STRATOFLY MR3 Vehicle [29]	47
3.4	STRATOFLY MR3 aerodynamic coefficients in the engine operative condition	50
3.5	STRATOFLY MR3 aerodynamic coefficients in the engine off condition	51
3.6	Aerodynamic coefficients of the basic Curran Model compared with the aerodynamic coefficients of the modified Curran Model	52
3.7	Confidence bound for the Curran Model supersonic Drag Coefficients, $\alpha = 1^\circ$	55
3.8	Aerodynamic coefficients of the basic All-Body Hypersonic Aircraft Model compared with the aerodynamic coefficients of the modified All-Body Hypersonic Aircraft Model	56
3.9	Aerodynamic coefficients of the basic Raymer Model compared with the aerodynamic coefficients of the modified Raymer Model	58
3.10	Aerodynamic coefficients of the basic Torenbeek Model compared with the aerodynamic coefficients of the modified Torenbeek Model	61
3.11	Lift Coefficient - Engine ON condition - Mach and Alpha variation	63
3.12	Drag Coefficient and Efficiency - Engine ON condition - Mach and Alpha variation	64
3.13	Lift Coefficient and Drag Coefficient - Engine OFF condition - Mach and Alpha variation	67
3.14	Efficiency - Engine OFF condition - Mach and Alpha variation	68
3.15	X-43A vehicle configuration [11]	69

3.16	Aerodynamic coefficients of the basic Curran Model compared with the aerodynamic coefficients of the modified Curran Model for ventral waverider configuration	71
3.17	Aerodynamic coefficients of the basic All-Body Hypersonic Aircraft Model compared with the aerodynamic coefficients of the modified All-Body Hypersonic Aircraft Model for ventral waverider configuration	72
3.18	Aerodynamic coefficients of the basic Raymer Model compared with the aerodynamic coefficients of the modified Raymer Model for ventral waverider configuration	73
3.19	Aerodynamic coefficients of the basic Torenbeek Model compared with the aerodynamic coefficients of the modified Torenbeek Model for ventral waverider configuration	74
3.20	X-34 vehicle configuration	76
3.21	PRORA USV-FTB-1 vehicle configuration [16]	78
3.22	Aerodynamic coefficients of the basic Curran Model compared with the aerodynamic coefficients of the modified Curran Model for High AR Wing Body configuration	82
3.23	Aerodynamic coefficients of the basic All-Body Hypersonic Aircraft Model compared with the aerodynamic coefficients of the modified All-Body Hypersonic Aircraft Model for High AR Wing Body configuration	83
3.24	Aerodynamic coefficients of the Raymer Model compared with the aerodynamic coefficients of the modified Raymer Model for High AR Wing Body configuration	84
3.25	Aerodynamic coefficients of the Torenbeek Model compared with the aerodynamic coefficients of the modified Torenbeek Model for High AR Wing Body configuration	85
3.26	HYPLANE vehicle configuration [20]	87
3.27	Aerodynamic coefficients of the basic Curran Model compared with the aerodynamic coefficients of the modified Curran Model for Low AR Wing Body configuration	89
3.28	Aerodynamic coefficients of the basic All-Body Hypersonic Aircraft Model compared with the aerodynamic coefficients of the modified All-Body Hypersonic Aircraft Model for Low AR Wing Body configuration	90
3.29	Aerodynamic coefficients of the basic Raymer Model compared with the aerodynamic coefficients of the modified Raymer Model for Low AR Wing Body configuration	91
3.30	Aerodynamic coefficients of the basic Torenbeek Model compared with the aerodynamic coefficients of the modified Torenbeek Model for Low AR Wing Body configuration	92

3.31	VTO-HOPPER reusable booster stage configuration [23]	94
3.32	Aerodynamic coefficients of the basic Curran Model compared with the aerodynamic coefficients of the modified Curran Model for Cylinder Wing configuration	96
3.33	Aerodynamic coefficients of the basic All-Body Hypersonic Aircraft Model for Cylinder Wing configuration	97
3.34	Aerodynamic coefficients of the basic Raymer Model compared with the aerodynamic coefficients of the modified Raymer Model for Cylinder Wing configuration	98
3.35	Aerodynamic coefficients of the basic Torenbeek Model compared with the aerodynamic coefficients of the modified Torenbeek Model for Cylinder Wing configuration	99
3.36	ELAC vehicle configuration [25]	101
3.37	Saenger vehicle configuration [14]	103
3.38	Aerodynamic coefficients of the basic Curran Model compared with the aerodynamic coefficients of the modified Curran Model for Blended Body configuration	107
3.39	Aerodynamic coefficients of the basic All-Body Hypersonic Aircraft Model compared with the aerodynamic coefficients of the modified All-Body Hypersonic Aircraft Model for Blended Body configuration	108
3.40	Aerodynamic coefficients of the basic Raymer Model compared with the aerodynamic coefficients of the modified Raymer Model for Blended Body configuration	109
3.41	Aerodynamic coefficients of the basic Torenbeek Model compared with the aerodynamic coefficients of the modified Torenbeek Model for Blended Body configuration	110
4.1	Structure of the Aerodynamic GUI, simplified analysis.	115
4.2	Structure of the Aerodynamic GUI, more accurate analysis.	116
4.3	Structure of the Aerodynamic GUI, more accurate analysis.	117
4.4	First choice of the Aerodynamic tool	118
4.5	Second choice of the Aerodynamic tool	119
4.6	Cylinder wing - simplified analysis - INPUT	119
4.7	Cylinder wing - simplified analysis - OUTPUT	120
4.8	Dorsal waverider - accurate analysis - first INPUT screen	121
4.9	Dorsal waverider - accurate analysis - second INPUT screen	122
4.10	Dorsal waverider - accurate analysis - third INPUT screen	122
4.11	Dorsal waverider - accurate analysis - fourth INPUT screen	123
4.12	Dorsal waverider - accurate analysis - OUTPUT screen	123
4.13	Dorsal waverider - both analysis and comparison - Engine ON	124
4.14	Dorsal waverider - both analysis and comparison - Engine OFF	125
4.15	Dorsal waverider - Mach and α variation - Engine ON - Raymer Model results	126

4.16 Dorsal waverider - Mach and α variation - Engine OFF - Raymer	
Model results	126

Chapter 1

Introduction

Current and future aviation trends are focused on the fields of high-speed flight, in order to sustain the air traffic expansion, while ensuring compliance with the required safety levels. The future vision for civil aviation foresees an increase of 6 times in passengers number over the next 30 years [30]. In order to support this significant growth, the worldwide aerospace community is increasingly opening to find alternative approaches: one of the main goals is to reduce the flight time by one order of magnitude, with respect to the state of the art of civil aviation and all the societal, economical and technological aspects. As a result, nowadays, conventional subsonic aircraft may be insufficient to meet the ever-increasing demand: high-speed civil transportation vehicles have a strong potential to enhance the efficiency of the cruise range at high Mach numbers, thanks to efficient propulsion units combined with high-lifting vehicle concepts.

As well as the willingness to improve the performance of current civil aircraft, a worldwide growing attention to drastically reduce the climate impact of aviation in the next years is clear. In particular, the aim is to pursue the abatement of greenhouse gases and pollutant emissions, thanks to high-efficient vehicles and low-emissions combustors propelled by liquid hydrogen (LH_2). The main advantages of this fuel are firstly a higher energy content and secondly it has no carbon atoms so CO_2 emissions are eliminated [31].

Within this global research landscape, several projects have been founded with the aim of investigating and developing new high-speed technologies. A concrete example is the STRATOFly project (STRATOspheric FLYing opportunities for high-speed propulsion concepts) which has been funded by the European Commission, under the framework of Horizon 2020 research and innovation programme. The aim was to conceive a hypersonic civil passenger vehicle (STRATOFly MR3), able to flight along unexploited routes at 30 km altitude and Mach number equal to 8, consequently reducing flight time and ensuring a minimum level of both noise and greenhouse gasses emissions [9].

The design of an aircraft such as the one mentioned above is a very complex process that can only be achieved thanks to a high level of integration between the airframe and the on-board subsystems that most affect the layout. It is possible to subdivide this procedure in two different layers: the conceptual design phase and the subsystems preliminary design phase, which are strictly interrelated. The first one aims at providing an assessment of the vehicle feasibility and mission concepts from both the operational and technical aspects. In order to achieve this goal, it is extremely important to estimate the basic aerodynamic performance and geometrical parameters for the reference design point selection [29]. It is clear that the necessity to have a simple and reliable tool for the estimation of the aerodynamic coefficients is crucial in these first steps, when a quick response is needed for each design modification/improvement that is made.

This thesis work aims to satisfy this need, by improving the prediction of aerodynamic performance of a new high-speed vehicle, since the conceptual design phase. The goal is to develop a tool capable of supporting a large number of users and vehicle configurations. In addition, it is possible to consider this effort as a starting point for the improvement of the aerodynamic calculation routine implemented in ASTRID-H, which is already installed at the moment, but it is quite simplified. ASTRID-H (Aircraft on-board Systems sizing and TRade-off analysis in Initial Design - High speed) is a software that has been developed at Politecnico di Torino and, as its name suggests, it provides a reliable support for the the conceptual and preliminary design phases of a new high-speed vehicle.

Therefore, the first part of this work consists of the analysis and description of four aerodynamic estimation models taken from the literature, whose limitations and theoretical aspects have been listed. After that, these models were implemented in Matlab and tested with geometrical data of existing aircraft: the obtained results were then compared with the available aerodynamic coefficients. In order to improve the prediction of the aerodynamic characteristics for the whole mission profile, the basic models have been adapted for each configurational family studied, by adding corrective coefficients. Finally, a simple and intuitive Aerodynamic Graphical User Interface (GUI) has been implemented, with the aim to allow any user to enter the required inputs and simply obtain the desired outcomes, in terms of Lift coefficient, Drag coefficient and Efficiency as a function of both Mach number and angle of attack.

Chapter 2

Aerodynamic Models

This thesis' objective is to improve the prediction of the aerodynamic performance of a new high-speed vehicle since the conceptual design phase. The results of the mathematical models in depth investigated and described in this chapter are also contributing to the improvement of ASTRID-H, the conceptual design tool described in the Chapter 4. The goal is to define a new aerodynamic performance characterization routine as complete as possible and capable of supporting a wide range of users and vehicle configurations. In the following section of this chapter, four models are presented, in order of increasing complexity. For each model, the main assumptions, limits and capabilities are discussed.

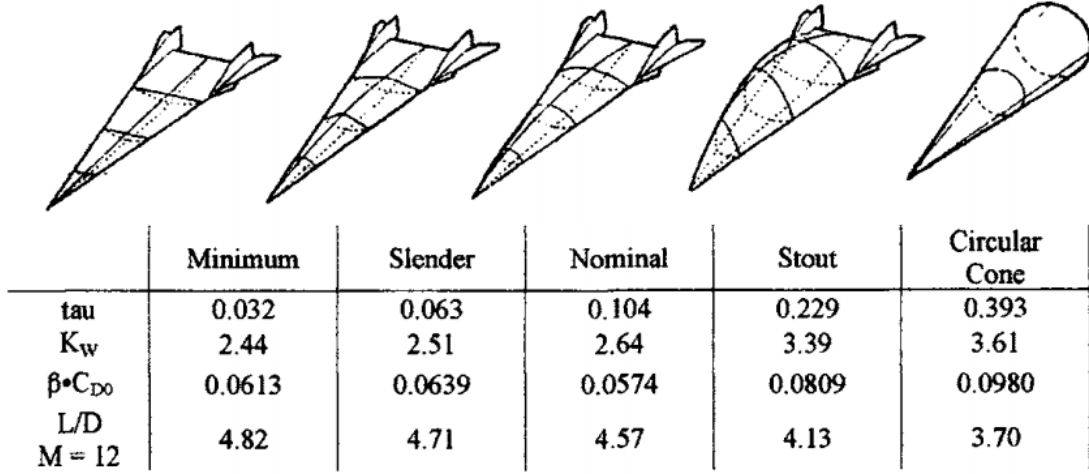
2.1 Model I (Curran Model)

This first model has been taken from the reference “*S. N. B. M. E. T. Curran, Scramjet propulsion, Cambridge, Massachusetts, 2000*” [1]. This is the simplest of those analysed in this thesis and it consists of a set of parametric equations that allows a simple estimate of the external aerodynamics of a generic high speed vehicle. Due to its restricted number of input required, this model is widely used and extremely useful in conceptual design.

The model is based on two configurational parameters which are the Küchemann's τ and the ratio of wetted to planform surface \mathbf{K}_w . The first one is defined as $\tau = \sqrt{\frac{V_{tot}}{S_{plan}^{1.5}}}$, where V_{tot} is the total vehicle volume and S_{plan} is the planform area, also known as reference surface; the second one is defined as $K_w = \frac{S_{wet}}{S_{plan}}$, where S_{wet} is the wetted surface.

Although Küchemann introduced τ as a volume parameter, it can be considered a slenderness one and in the figure 2.1 it's possible to see its effect on the vehicle configuration: the higher is the τ , the lower is the slenderness.

In the following lines, all the model is reported. first of all, there is the correlation


 Figure 2.1. τ effects on the vehicle configuration [1]

between the two most important parameters, first proposed by Dwight Taylor[1]:

$$F = \sqrt{\left(\frac{V_{tot}^{0.667}}{S_{plan}}\right) \cdot \left(\frac{S_{wet}}{S_{plan}}\right)^{1.5}} = \tau^{0.3333} \cdot K_w^{0.75} \quad (2.1)$$

thanks to which it's possible to estimate the maximum efficiency, eq. 2.2

$$\left(\frac{L}{D}\right)_{\max} = E_{\max} = \frac{a}{M} \cdot (M + b) \cdot (c - d \cdot F) \quad (2.2)$$

where M is the Mach number; the semi-empirical coefficients given in this equation have been statistically evaluated for a CAV (cruise and acceleration vehicle) and their value is $a = 3.063$, $b = 3$, $c = 1.11238$ and $d = 0.1866$.

Then, it's possible to estimate the Drag coefficient and the Lift one.

- Drag Coefficient

$$C_{D0} = \frac{f \cdot e^{g \cdot F}}{\sqrt{|(M^2 - 1)|}} \quad (2.3)$$

The zero lift drag coefficient (eq. 2.3) is a function of the total volume, wetted surface and Mach number. It is not necessary to do a complete drag build-up to determine total drag. The latter can then be estimated using the approach of Vinh[2]:

$$C_D = C_{D0} \cdot (1 + B) \quad (2.4)$$

where it's possible to use three different value of $(1+B)$ for three different main mission phases wich are the acceleration one (representative of all climb phases

and the first part of the cruise) $(1+B) = 1.075$, the minimum fuel flow cruise one (representative of the cruise phase at constant speed) $(1+B) = 1.75$ and the maximum efficiency one (representative of descending phases) $(1+B) = 2$.

• **Lift Coefficient**

Thanks to the Drag coefficient for the maximum efficiency phase and the maximum efficiency value, it's possible to evaluate the Lift coefficient for the maximum efficiency phase (eq.2.5).

$$C_{L_{E_{\max}}} = C_{D_{E_{\max}}} \cdot E_{\max}; \quad (2.5)$$

then, the Lift coefficient for the acceleration phase and the minimum fuel flow cruise one is evaluated (eq.2.6) where the i value is respectively 0.1 and 0.82 .

$$C_L = i \cdot C_{L_{E_{\max}}} \quad (2.6)$$

How it's possible to see, this aerodynamic model is very simple and allows to obtain a very quick estimation of the aerodynamic coefficients for three different mission phases. moreover, it requires very few input, as shown in the table 2.1.

INPUT		<i>Unit of measure</i>
Mach number	M	none
Total volume	V_{tot}	$[m^3]$
Planform surface	S_{plan}	$[m^2]$
Wetted surface	S_{wet}	$[m^2]$
OUTPUT		
$C_L = f(M)$		
$C_D = f(M)$		
$E = f(M)$		

Table 2.1. Model I - Input and Output

The downside, however, is that the estimation may be quite inaccurate given the very small amount of data useful for the characterisation of the aircraft being analysed. In addition, the output aerodynamic coefficients are a function of the Mach number only, without considering the angle of attack at which the estimate is being made. In conclusion, this method could be useful for the first design steps, when very few inputs data are available.

In terms of limitations and applicability, this model can be used for a wide range of configurational concepts, on which the relationship between τ and K_w is dependent. The most interesting family for this study is the Combined cycle engine launchers one (which include hypersonic cruise aircraft), powered by airbreathing propulsion

over all or part of their flight path. In particular, it is important to mention the Blended Body, Wing-Body, Cylinder wing and Nonweiler Waverider configurations [1]. The speed range in which the model can be applied included subsonic regime up to hypersonic regime.

2.2 Model II (All-Body Hypersonic Aircraft)

This second aerodynamic model is more accurate than the Curran one and it was taken from the reference “*L. J. Williams, Estimated Aerodynamics of All-Body Hypersonic Aircraft Configurations, National Aeronautics and Space Administration, Moffett Field, California, March 1971*” [3]. It only refers to a representative family of all-body hypersonic aircraft: the configuration is a delta planform with an elliptical cone forebody and an elliptical cross-section afterbody that forms a smooth transition surface from the end of the forebody to a straight-line trailing edge.

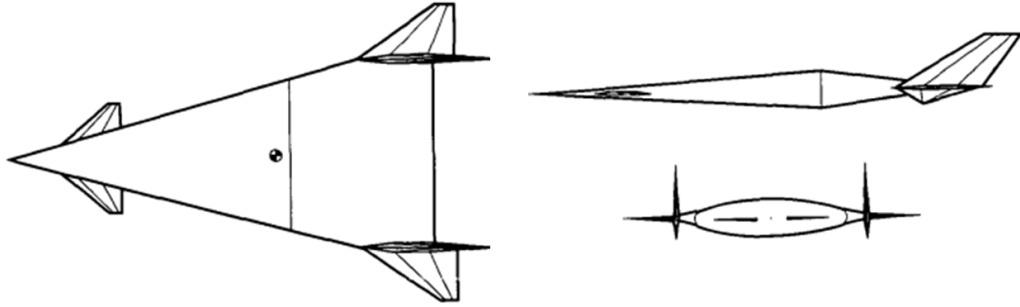


Figure 2.2. Model II - nominal configuration [3]

The geometry of the basic configuration (fig.2.2) is defined by three independent shape parameters:

- The leading-edge sweep angle Λ ;
- The position of the breakpoint between the forebody and afterbody, defined as the breakpoint length ratio $\frac{l_\pi}{l}$, where l is the total body length;
- The ratio of the maximum cross-section area S_{max} to the total planform area S_{Plan} defined as the fatness ratio $\frac{S_{max}}{S_{Plan}}$;

Using these three configurational parameters, it is possible to define the forebody cross-section ellipse ratio (eq.2.7):

$$\frac{a}{b} = \frac{\pi \left(\frac{l_\pi}{l} \right)^2 \cot \Lambda}{S_{max}/S_{Plan}} \quad (2.7)$$

As can be seen, for constant fatness ratio, the forebody ellipse ratio is proportional to the square of the breakpoint length ratio and the cotangent of the leading-edge sweep angle.

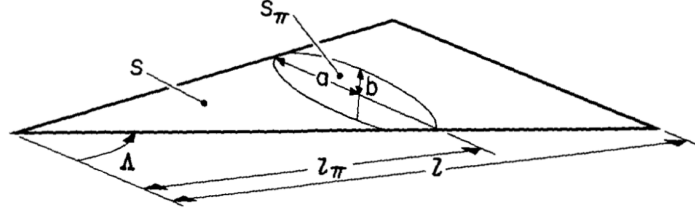


Figure 2.3. Model II - configurational parameters [3]

In the following lines, all the equations used for the Lift coefficient and Drag coefficient estimation are shown. The model is simplified for a preliminary design level and allows to take into account not only the wing contribution but also the fins one (Vertical tail, Horizontal tail and Canard).

- **Lift Coefficient**

The lift equations for the basic configuration described previously were estimated by means of nonlinear relations, developed by curve fitting data for low aspect ratio delta wings from various references. The coefficients used in these equations were modified to account for the rounded leading edge of the all-body configuration, which causes linear subsonic variation of the lift coefficient in contrast to the significant nonlinear variation present for the sharp leading edge of a delta wing.

The equations used for the lift coefficient estimation depend only on planform shape, therefore, the effect of the thickness distribution on the lift curve is neglected.

$$C_L = C_1 \sin(\alpha) + C_2 \sin^2(\alpha) \quad (2.8)$$

where C_1 and C_2 coefficients are evaluated differently depending on the flight regime:

$$\begin{aligned} & - \text{if } M \leq 1 \\ & \quad \begin{cases} C_1 = \frac{\pi \cdot AR}{2} - 0.355 \cdot \beta^{0.45} \cdot AR^{1.45} \\ C_2 = 0 \end{cases} \end{aligned} \quad (2.9)$$

$$\begin{aligned} & - \text{if } M > 1, \beta < \frac{4}{AR} \\ & \quad \begin{cases} C_1 = \frac{\pi \cdot AR}{2} - 0.153 \cdot \beta \cdot AR^2 \\ C_2 = \text{linear interpolation with respect to } \beta \text{ from} \\ \quad C_2 = 0 \text{ at } \beta = 0 \text{ to} \\ \quad C_2 = e^{0.955 - (4.35/M)} \text{ at } \beta = \frac{4}{AR} \end{cases} \end{aligned} \quad (2.10)$$

– if $M > 1, \beta \geq \frac{4}{AR}$

$$\begin{cases} C_1 = \frac{4.17}{\beta} - 0.13 \\ C_2 = e^{0.955 - (4.35/M)} \end{cases} \quad (2.11)$$

• **Drag Coefficient**

The total Drag Coefficient is given by the sum of the Zero Lift Drag and the Induced Drag (eq. 2.12)

$$C_D = C_{D_0} + C_{Di}; \quad (2.12)$$

– ***Induced Drag***

$$C_{Di} = K_m \cdot C_L \cdot \tan(\alpha); \quad (2.13)$$

The coefficient K_m allows the equation for the sharp leading edge of the delta wing to be modified taking into account the rounded leading edge of the all-body configuration:

$$\begin{cases} K_m = 0.25 \cdot (1 + M) & \text{if } M < 3 \\ K_m = 1.0 & \text{if } M \geq 3 \end{cases} \quad (2.14)$$

– ***Zero-Lift (Parasite) Drag***

Zero-Lift Drag is obtained adding the Body contribution and the Fins one:

$$C_{D_0} = C_{DB_0} + C_{DF_0} \quad (2.15)$$

1. Zero-Lift Body Drag

The Body contribution consists of three components, which are the Pressure (or wave) Drag C_{DB_p} , the Skin friction Drag C_{DB_f} and the nose Bluntness Drag C_{DB_b} , as can be seen in the eq. 2.16.

$$C_{DB_0} = C_{DB_p} + C_{DB_f} + C_{DB_b} \quad (2.16)$$

1a. Body Pressure Drag

For an aircraft with a configuration such as the one examined, this contribution can be considered zero.

$$C_{DB_p} = 0 \quad (2.17)$$

1b. Body Friction Drag

The Friction Drag of the body was calculated using a relation based on turbulent boundary layer, flat-plate skin friction and contains an empirical correction for thickness induced pressure fields (eq.2.18).

$$C_{D_{Bf}} = 0.455 \cdot \frac{\left[1 + 2 \left(\frac{t}{c} \right)_{body} \right] \cdot \left(\frac{S_{Wet}}{S_{Plan}} \right)}{(\log_{10} Re_{body})^{2.58} \cdot \left(1 + \frac{\gamma-1}{2} M_0^2 \right)^{0.467}} \quad (2.18)$$

S_{Wet} is the wetted surface, S_{Plan} is the planform area, Re_{body} is the body Reynolds number (eq.2.19) and $\left(\frac{t}{c} \right)_{body}$ is the body thickness ratio (eq.2.20).

$$Re_{body} = \rho_0 \cdot M_0 \cdot a_0 \cdot \frac{MAC_{body}}{\mu_0} \quad (2.19)$$

$$\left(\frac{t}{c} \right)_{body} = \frac{2 \frac{l\pi}{l}}{\frac{a}{b} \cdot \tan \Lambda} \quad (2.20)$$

1c. Body Bluntness Drag

This contribution is proportional to the nose radius (eq.2.23) evaluated, in the supersonic regime, for a given maximum radiation equilibrium temperature T_{le} and for a given emissivity of the skin ε_{Skin} (eq.2.24). The Body Bluntness Drag can be neglected in the subsonic regime while in the transonic one it is calculated as a linear interpolation between the other two regimes.

– if $M \leq 0.8$

$$\left\{ C_{D_{Bb}} = 0 \right. \quad (2.21)$$

– if $0.8 < M < 1.0$

$$\left\{ \begin{array}{l} C_{D_{Bb}} = \text{linear interpolation with respect to } M \text{ from} \\ C_{D_{Bb}} = 0 \text{ at } M = 0.8 \text{ to} \\ C_{D_{Bb}} = C_{D_{Bb}} \text{ at } M = 1 \end{array} \right. \quad (2.22)$$

– if $M \geq 1.0$

$$\left\{ C_{D_{Bb}} = \frac{\pi * r_{nose}^2}{S_{Plan}} \right. \quad (2.23)$$

where:

$$r_{nose}^{0.5} = \frac{1820 \cdot \left(\frac{\rho}{\rho_{sl}}\right)^{1/2} \cdot (M_{Max} \cdot a \cdot 10^{-4})^{3.15}}{\varepsilon_{Skin} \cdot \left(\frac{T_{le}}{1000}\right)^4} \quad (2.24)$$

2. Zero-Lift Fin Drag

The Zero-Lift Fin Drag is added to the body one, in order to obtain the total vehicle Zero-Lift Drag coefficient. Like in the previous case, the Zero-Lift Fin Drag always consists of the three contributions: Pressure (or wave) Drag $C_{D_{Fp}}$, the Skin friction Drag $C_{D_{Ff}}$ and the Fin leading-edge Bluntness Drag $C_{D_{Fb}}$ (eq.2.25).

$$C_{D_{F0}} = C_{D_{Fp}} + C_{D_{Ff}} + C_{D_{Fb}} \quad (2.25)$$

2a. Fin Pressure Drag

The Pressure Drag of each Fin (horizontal tail, vertical tail, and canard) is calculated using the same set of equations. Subsonically, it is assumed zero whereas for a $M = 1$ it is estimated using an empirical equation (eq.2.28). At Mach number equal or greater than the shock attachment Mach number M_{SA} , the wave drag is estimated by linear supersonic theory (eq.2.30). In the intermediate flight regimes, the Fin Pressure Drag is calculated by linear interpolation with respect to M (eq.2.27, eq.2.29).

– if $M \leq 0.8$

$$\left\{ C_{D_{Fp}} = 0 \right. \quad (2.26)$$

– if $0.8 < M < 1.0$

$$\left\{ \begin{array}{l} C_{D_{Fp}} = \text{linear interpolation with respect to } M \text{ from} \\ C_{D_{Fp}} = 0 \text{ at } M = 0.8 \text{ to} \\ C_{D_{Fp}} = C_{D_{Fp}} \text{ at } M = 1 \end{array} \right. \quad (2.27)$$

– if $M = 1.0$

$$\left\{ C_{D_{Fp}} = 3.4 \cdot \left(\frac{t}{c}\right)_{Fin}^{\frac{5}{3}} \cdot \frac{S_{Fin}}{S_{Plan}} \cdot \cos^2(\Lambda_{Fin}) \right. \quad (2.28)$$

– if $1.0 < M < M_{SA}$

$$\left\{ \begin{array}{l} C_{D_{Fp}} = \text{linear interpolation with respect to } M \text{ from} \\ C_{D_{Fp}} = 0 \text{ at } M = 1.0 \text{ to} \\ C_{D_{Fp}} = C_{D_{Fp}} \text{ at } M = M_{SA} \end{array} \right. \quad (2.29)$$

– if $M \geq M_{SA}$

$$\left\{ C_{D_{Fp}} = 6 \cdot \left(\frac{t}{c} \right)_{Fin}^2 \cdot \frac{1}{\beta} \cdot \frac{S_{Fin}}{S_{Plan}} \right. \quad (2.30)$$

2b. Fin Friction Drag

This contribution is evaluated in exactly the same way as the Body Friction Drag (eq.2.35). the only difference is the Reynolds number, which is calculated with the mean aerodynamic chord of the fin under consideration (eq.2.32).

$$C_{D_{Ff}} = 0.455 \cdot \frac{\left[1 + 2 \left(\frac{t}{c} \right)_{Fin} \right] \cdot \left(\frac{(S_{WET})_{Fin}}{S_{Plan}} \right)}{(\log_{10} Re_{Fin})^{2.58} \cdot \left(1 + \frac{\gamma-1}{2} M_0^2 \right)^{0.467}} \quad (2.31)$$

where:

$$Re_{Fin} = \rho_0 \cdot M_0 \cdot a_0 \cdot \frac{MAC_{Fin}}{\mu_0} \quad (2.32)$$

2c. Fin Bluntness Drag

The Fin leading-edge is considered cylindrical, with the radius calculated for a nominal radiation equilibrium temperature at the specified leading-edge sweep angle Λ_{Fin} (eq.2.36). The Fin Bluntness Drag is considered equal to zero in the subsonic regime while in the supersonic regime it is evaluated with the equation 2.35. Transonically, it is assumed to vary linearly, with respect to Mach number.

– if $M \leq 0.8$

$$\left\{ C_{D_{Fb}} = 0 \right. \quad (2.33)$$

– if $0.8 < M < 1.0$

$$\left\{ \begin{array}{l} C_{D_{Fb}} = \text{linear interpolation with respect to } M \text{ from} \\ C_{D_{Fb}} = 0 \text{ at } M = 0.8 \text{ to} \\ C_{D_{Fb}} = C_{D_{Fb}} \text{ at } M = 1 \end{array} \right. \quad (2.34)$$

– if $M \geq 1.0$

$$\left\{ C_{D_{Fb}} = \frac{8}{3} \cdot \frac{r_{le_{Fin}} \cdot b_{Fin}}{S_{Plan}} \cdot \cos^2(\Lambda_{Fin}) \right. \quad (2.35)$$

where:

$$r_{le_{Fin}} = (0.725 \cdot \cos^{1.2}(\Lambda_{Fin}))^2 \cdot r_{Nose} \quad (2.36)$$

In conclusion, it's possible to say that although the Model is simplified for a preliminary design phase, it allows to consider the contribution of the main parts of the aircraft, including the tail planes and canard. Another positive aspect is that the outputs are function not only of the Mach number, like the Curran Model, but also of the angle of attack. The drawbacks are that it refers to the specific configuration described above and that it requires a high number of inputs as can be seen in the table below (2.2).

The speed range in which the model can be applied, as can be seen in the mathematical equations above, includes a subsonic flight regime up to hypersonic flight regime.

INPUT		<i>UoM</i>
Mach number	M	none
Planform surface	S_{plan}	$[m^2]$
Wetted surface	S_{wet}	$[m^2]$
Wing span	$span$	$[m]$
Fuselage length	$l_{fuselage}$	$[m]$
Maximum cross-sectional area	S_{max}	$[m^2]$
Distance from nose to maximum cross-sectional point	$l_{S_{max}}$	$[m]$
Mean aerodynamic chord of the body	MAC_{body}	$[m]$
Leading edge sweep angle of the wing	λ	$[^\circ]$
Horizontal tail thickness ratio	$(t/c)_{Htail}$	none
Horizontal tail surface	S_{Htail}	$[m^2]$
Leading edge sweep angle of the Horizontal tail	λ_{Htail}	$[^\circ]$
Horizontal tail span	b_{Htail}	$[m]$
Vertical tail thickness ratio	$(t/c)_{Vtail}$	none
Vertical tail surface	S_{Vtail}	$[m^2]$
Leading edge sweep angle of the Vertical tail	λ_{Vtail}	$[^\circ]$
Vertical tail span	b_{Vtail}	$[m]$
Canard thickness ratio	$(t/c)_{Canard}$	none
Canard surface	S_{Canard}	$[m^2]$
Leading edge sweep angle of the Canard	λ_{Canard}	$[^\circ]$
Canard span	b_{Canard}	$[m]$
OUTPUT		
$C_L = f(M, \alpha)$		
$C_D = f(M, \alpha)$		
$E = f(M, \alpha)$		

Table 2.2. Model II - Input and Output

2.3 Model III (Raymer Model)

This third aerodynamic Model, unlike the all-body hypersonic Model, refers to a generic high speed aircraft configuration with a clear distinction between fuselage and delta wing (fig.2.4).

The delta wing is able to fly successfully, producing enough lift, up to angles of attack higher than conventional wings: this phenomenon is called vortex lift. As the angle of attack increases (at slower speeds), the delta wing creates larger vortices which slowly move forward along the leading edge, eventually enveloping the whole upper surface of the wing: the suction and therefore the lift are increased. The airspeed in the vortex is high, and so the pressure on the upper surface is lower than the undersurface.

This is the most complete method of those analysed: it allows to consider the contributions of the main parts of the aircraft, such as the wing, fuselage and tail planes, but also the air intakes, engine nacelles and others. This complexity is reflected in a very high number of inputs, which is the downside of this analysis.

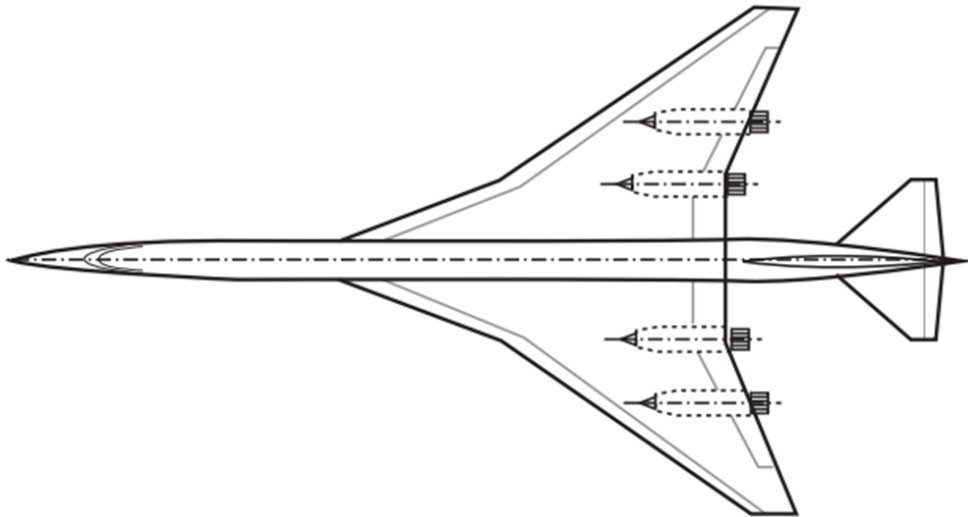


Figure 2.4. Model III - nominal configuration[4]

In the following pages, all the equations of this Model are given, whose reference is "*Raymer, Daniel. Aircraft design: a conceptual approach*" [4].

- **Lift Coefficient**

Given that the slope of the lift curve as a function of the angle of attack is essentially linear except near the stall angle, it is possible to calculate the lift coefficient under stall simply as the slope of the lift curve C_{L_α} multiplied by

the angle of attack α (eq.2.37).

$$C_L = C_{L_\alpha} \alpha \quad (2.37)$$

where C_{L_α} is evaluated differently depending on the flight regime:

– ***Subsonic regime***

The equation used for the slope of the complete wing lift curve is a semi-empirical formula (eq.2.38) that is reasonably accurate down to $M = 1$ for a swept wing (like a delta wing).

$$C_{L_\alpha} = \frac{2\pi AR}{2 + \sqrt{4 + \frac{AR^2 \beta^2}{\eta^2} \cdot \left(1 + \frac{\tan^2 \Lambda}{\beta^2}\right)}} \cdot \left(\frac{S_{exposed}}{S_{ref}}\right) \cdot F \quad (2.38)$$

where Λ is the wing leading-edge sweep angle; η is the airfoil efficiency which indicates how close the actual airfoil lift-slope curve is to the theoretical one (eq.2.40): if the airfoil lift-slope curve is unknown, the airfoil efficiency can be approximated as about 0.95; $S_{exposed}$ is the planform area less the part of the wing covered by the fuselage; F is the fuselage lift factor and takes into account the fuselage contribute in the lift generation ("d" is the fuselage diameter) (eq.2.41); AR is the aspect ratio of the wing and β is the Prandtl-Glauert correction factor (eq.2.39).

$$\beta = \sqrt{1 - M^2} \quad (2.39)$$

$$\eta = \frac{C_{L_\alpha}}{2\pi/\beta} \quad (2.40)$$

$$F = 1.07 \cdot \left(1 + \frac{d}{span_{wing}}\right)^2 \quad (2.41)$$

– ***Supersonic regime***

In this flight regime, the lift coefficient of a purely supersonic delta wing can be reliably approximated with the equation shown (eq.2.42). A wing is considered to be in a purely supersonic flow when the Mach cone angle is greater than the leading-edge sweep angle.

$$C_{L_\alpha} = \frac{4}{\beta \cdot C_{L_\alpha}} \quad (2.42)$$

- **Drag Coefficient**

In order to estimate the Total Drag Coefficient it's necessary to evaluate the Zero Lift (Parasite) Drag, the Induced Drag and add them together (eq.2.43), both for the subsonic and the supersonic flight regime.

$$C_D = C_{D0} + C_{D_i} \quad (2.43)$$

- ***Subsonic regime***

- 1. *Subsonic Zero Lift (Parasite) Drag*

The Subsonic Zero Lift Drag is assessed using a component build-up method, which consist of estimating the Zero Lift Drag of each vehicle component and summing them, taking into account the interference effects. The Parasite Drag is composed by three components, which are the Skin Friction Drag C_{D_f} , the Miscellaneous Drag $C_{D_{misc}}$ and the Leakage and Protuberance Drag $C_{D_{L\&P}}$ (eq.2.44).

$$C_{D0_{Subsonic}} = \frac{\sum(C_{f_c} \cdot FF_c \cdot Q_c \cdot S_{wetC})}{S_{plan}} + C_{D_{misc}} + C_{D_{L\&P}} \quad (2.44)$$

- 1a. *Skin Friction Drag*

When the aircraft moves through an air-flow, the molecules closest to the vehicle skin are stuck to it, while those more distant slip over them. In a real flow, in which viscosity is present, there is a resistance to this slippage, resulting in the creation of the boundary layer, which must be accelerated along with the aircraft: this additional force is called Skin Friction Drag. The flat-plate skin friction coefficient C_f depends on the Reynolds number Re (eq.2.47), the skin roughness k and the Mach number M . As can be seen, the equation is different depending on whether the flow is laminar (eq.2.45) or turbulent (eq.2.46). The first condition can be maintained for a local Reynolds number below approximately half a million and for a very smooth skin. A typical aircraft might have laminar flow on perhaps 10-20% of the wings and tails, and no laminar flow on the fuselage: in most cases, infact, turbulent flow covers the entire aircraft [4]. However, for a preliminary analysis, it is possible to consider *laminar flow* if $Re < 5 * 10^5$ and *turbulent flow* if $Re \geq 5 * 10^5$.

$$C_{f_{laminar}} = 1.328/\sqrt{Re} \quad (2.45)$$

$$C_{f_{turbolent}} = \frac{0.455}{(\log_{10} Re)^{2.58}(1 + 0.144M^2)^{0.65}} \quad (2.46)$$

$$Re = \frac{\rho V l}{\mu} \quad (2.47)$$

When the surface is relatively rough, the friction coefficient can be higher than the one just analysed. In this situation, it is possible to account for it thanks to the cut-off Reynolds number (eq.2.48). The lower of the actual Reynolds number and the cut-off one should be used in the C_f evaluation.

$$Re_{cutoff,sub} = 38.21(l/k)^{1.053} \quad (2.48)$$

Flow separation leads to an increase of the skin friction drag and it is closely dependent on the curvature and the shape of the aircraft. The form factor accounts for it and it is calculated differently depending on the part of the aircraft under consideration, as shown in the equation 2.49.

$$FF = \begin{cases} \left[1 + \frac{0.6}{(x/c)_m} \left(\frac{t}{c} \right) + \left(\frac{t}{c} \right)^4 \right] \left[1.34M^{0.18}(\cos \Lambda)^{0.28} \right] & \text{Wing, Tail} \\ \left(1 + \frac{60}{f^3} + \frac{f}{400} \right) & \text{Fuselage} \\ 1 + \left(\frac{0.35}{f} \right) & \text{Nacelle} \\ 1 + f & \text{Inlet} \end{cases} \quad (2.49)$$

where:

$$f = \frac{l}{d} \quad (2.50)$$

Interference drag is the increase in the drag of the various aircraft components due to the change in the airflow caused by the other components (eq.2.51).

$$Q = \begin{cases} 1 & \text{Wing, Fuselage, Inlet} \\ 1.04 & \text{Tail} \\ 1.5 & \text{Nacelle} \end{cases} \quad (2.51)$$

1b. Miscellaneous Drag

This component is the drag for special features of an aircraft such as flaps, un-retracted landing gear or an upswept aft fuselage. During a preliminary aerodynamic study, these contributions could be neglected; however, in order to be as accurate as possible, two of them can be considered, which are the Flaps one and the Base Area one. The flap contribution to parasite

drag is caused by the separated flow above the component, and can be roughly estimated using eq. 2.52.

$$C_{D0_{flap}} = 0.0023 \frac{flapspan}{wingspan} \cdot \delta_{flap} \quad (2.52)$$

where δ_{flap} is the flap deflection, in deg. The Base Area contribution is the one of any place where the aft fuselage angle to the freestream is higher than about 20 deg (eq.2.53).

$$C_{D0_{base,sub}} = [0.139 + 0.419(M - 0.161)^2]A_{base} \quad (2.53)$$

1c. Leakage and Protuberance Drag

Leakage Drag considers momentum loss and additional airflow separations, caused respectively by the tendency of an aircraft to inhale air in the high-pressure zone of the surface and to exhale air in the low-pressure zone. Protuberance Drag considers the negative contribute due flow deflection near lights, antennas and others. This is difficult to evaluate but, in a first approximation, it's possible to do it taking into account a percent of the total parasite drag (eq.2.54).

$$C_{D_{L\&P}} = \begin{cases} 2 - 5\% & \text{of parasite drag} & \text{Jet Transport or Bomber;} \\ 5 - 10\% & \text{of parasite drag} & \text{Propeller Aircraft;} \\ 10 - 15\% & \text{of parasite drag} & \text{Current Design-Fighter;} \end{cases} \quad (2.54)$$

2. Subsonic Drag due to Lift (Induced Drag)

The Induced Drag Coefficient, for a moderate angle of attack, may be evaluated as the product between the square of the lift coefficient and the drag due to lift factor K_i (eq.2.55). The latter, for a 3-D wing, is evaluated using the classical Oswald method (eq.2.56) where e is the Oswald factor which takes into account the extra drag due to the non-elliptical lift distribution and the flow separation that a real wing is affected by.

$$C_{D_i} = K_i \cdot C_L^2 \quad (2.55)$$

$$K_i = \frac{1}{\pi \cdot AR \cdot e} \quad (2.56)$$

The Oswald factor can be evaluated in three different ways, depending on

to the leading-edge sweep angle, as reported in the eq.2.57.

$$\begin{cases} e = 1.78 \cdot (1 - 0.045 \cdot AR^{0.68}) - 0.64; & \Lambda \geq 2^\circ \\ e = 4.61 \cdot (1 - 0.045 \cdot AR^{0.68}) \cdot (\cos\Lambda)^{0.15} - 3.1 & \Lambda \geq 30^\circ \\ e = \text{linear interpolation between the previous equations} & 2^\circ < \Lambda < 30^\circ \end{cases} \quad (2.57)$$

– **Supersonic regime**

1. *Supersonic Zero Lift (Parasite) Drag*

The supersonic Zero Lift Drag is evaluated in the same way as in the subsonic regime, with two exceptions (2.58): the first is that there is a new term, the Wave Drag, which takes into account the pressure drag due to the shock formation. Secondly, it's possible to see that the skin friction drag does not include the form and the interference factor: these contributes are included in the wave drag term.

$$C_{D0_{Supersonic}} = \frac{\sum(C_{f_c} \cdot S_{wetC})}{S_{plan}} + C_{D_{misc}} + C_{D_{L\&P}} + C_{D_{wave}} \quad (2.58)$$

All the terms described in the subsonic regime are the same, except for the flat-plate skin friction coefficient, that in the supersonic flight is:

$$Re_{cutoff,sup} = 44.62(l/k)^{1.053} M^{1.16} \quad (2.59)$$

And the Base Drag Area:

$$C_{D0_{base,sup}} = [0.064 + 0.042(M - 3.84)^2] A_{base} \quad (2.60)$$

1a. *Wave Drag*

The Wave Drag, that in supersonic regime will often be greater than all the other drag put together, is the pressure drag due to shock and it is a result of the vehicle's volume distribution, i.e the way that the cross-sectional area varies longitudinally. The body with the perfect distribution of the volume is the Sears-Haack one (eq.2.61), which permits to obtain the lowest possible wave drag value for a closed-end geometry.

$$\left(\frac{D}{q}\right)_{S-H} = \frac{9 * \pi i}{2} \cdot \left(\frac{A_{max}}{l_{fuselage}}\right)^2 \quad (2.61)$$

Unfortunately, no real aircraft has a geometry identical to that of the perfect body, due to problems with the internal volume being too small and unsuitable for passengers or any other type of payload. However, reasonable results can be achieved with a good design of the volume distribution. Thanks to the Sears-Haack body wave drag, it's possible to evaluate the realistic aircraft one (eq.2.62):

$$C_{D_{wave}} = \frac{E_{WD} \cdot \left[1 - 0.386 \cdot (M - 1.2)^{0.57} \cdot \left(1 - \frac{\pi \cdot \Lambda_{(deg)}^{0.77}}{100} \right) \right] \cdot \left(\frac{D}{q} \right)_{S-H}}{S_{plan}} \quad (2.62)$$

where E_{WD} is an empirical wave-drag efficiency factor and is the ratio between the actual wave drag and the perfect body one (eq.2.63):

$$E_{WD} = \begin{cases} 1.2 & \text{Blended delta wing or very smooth vehicle} \\ 1.4 - 2 & \text{Supersonic fighter, bomber, SSt design} \\ 2 - 3 & \text{Poor supersonic design, bumpy volume distribution} \end{cases} \quad (2.63)$$

2. Supersonic Drag due to Lift (Induced Drag)

In the supersonic flight, the Induced Drag is evaluated in exactly the same way as in the previous case (eq.2.55). In this regime, the drag-due-to-lift factor K_i increases substantially and the Oswald factor, e , is reduced to approximately 0.3 – 0.5 at $M = 1.2$. Thanks to the eq.2.64 it's possible to quickly estimate K_i at a supersonic speed.

$$K_i = \frac{AR \cdot (M^2 - 1)}{4 \cdot AR \cdot \sqrt{M^2 - 1} - 2} \cdot \cos \Lambda \quad (2.64)$$

In conclusion, this is undoubtedly the most complete method: it contains many more drag contributions than previous models, thanks to which it's possible to take into account practically all the main parts of the aircraft, despite the fact that it is only a preliminary estimate. This third model is reliable for both supersonic and subsonic flight and allows obtain the aerodynamic coefficients as a function of both the angle of attack and the Mach number. In addition, thanks to the drag build-up method, it is possible to "model" the configuration of the aircraft to be analysed. On the other hand, due to its complexity, it requires a large number of inputs, as can be seen in the table below (tab.2.3).

in terms of applicability, this model should not be reliable for a blended-body geometry, as it refers to a more generic configuration with a clear distinction between fuselage and wing. The speed range in which the model is reliable includes a subsonic flight regime up to a supersonic flight regime.

INPUT		UoM
Mach number	M	none
Planform surface	S_{plan}	$[m^2]$
Wetted surface	S_{wet}	$[m^2]$
Exposed surface	$S_{Exposed}$	$[m^2]$
Wing span	$span$	$[m]$
Fuselage length	$l_{fuselage}$	$[m]$
Fuselage diameter	$d_{fuselage}$	$[m]$
Maximum cross-sectional area	S_{max}	$[m^2]$
Mean aerodynamic chord of the wing	MAC_{wing}	$[m]$
Leading edge sweep angle of the wing	λ_w	$[^\circ]$
Wing thickness ratio	$(t/c)_{wing}$	none
Nacelle length	$l_{nacelle}$	$[m]$
Nacelle diameter	$d_{nacelle}$	$[m]$
Inlet length	l_{Inlet}	$[m]$
Inlet diameter	d_{Inlet}	$[m]$
Flap span	$Flap_{span}$	$[m]$
Flap deflection	$delta_{flap}$	$[^\circ]$
Horizontal tail thickness ratio	$(t/c)_{Htail}$	none
Horizontal tail surface	S_{Htail}	$[m^2]$
Leading edge sweep angle of the Horizontal tail	λ_{Htail}	$[^\circ]$
Mean aerodynamic chord of the Horizontal tail	MAC_{Htail}	$[m]$
Vertical tail thickness ratio	$(t/c)_{Vtail}$	none
Vertical tail surface	S_{Vtail}	$[m^2]$
Leading edge sweep angle of the Vertical tail	λ_{Vtail}	$[^\circ]$
Mean aerodynamic chord of the Vertical tail	MAC_{Vtail}	$[m]$
Canard thickness ratio	$(t/c)_{Canard}$	none
Canard surface	S_{Canard}	$[m^2]$
Leading edge sweep angle of the Canard	λ_{Canard}	$[^\circ]$
Mean aerodynamic chord of Canard	MAC_{Canard}	$[m]$
OUTPUT		
$C_L = f(M, \alpha)$		
$C_D = f(M, \alpha)$		
$E = f(M, \alpha)$		

Table 2.3. Model III - Input and Output

2.4 Model IV (Torenbeek Model)

This last aerodynamic model is a little less complete than the Raymer model, but it allows to evaluate the aerodynamic coefficients for a generic high speed aircraft configuration with a delta wing, a generic high speed aircraft configuration with an arrow wing and a blended wing body configuration. In the following lines, all the mathematical details are described, depending on which of the above configurations is being analysed. The reference of this analysis is "*Egbert Torenbeek, Essentials of Supersonic Commercial Aircraft Conceptual Design*" [5].

- ***Lift Coefficient***

In order to evaluate the Lift Coefficient, the same considerations are made for both delta and arrow wing. These slender geometries are the best application for high-speed vehicles and allow to obtain excellent aerodynamic properties for both transonic and supersonic speeds.

The flow through the wing is characterized by the leading-edge flow parameter (eq.2.65) which allow to distinguish between subsonic ($m < 1$) and supersonic ($m > 1$) leading-edge condition.

$$m = \frac{\tan \gamma}{\tan \mu} = \beta \cdot \cot \Lambda \quad (2.65)$$

γ is the complement of the leading-edge sweep angle Λ whereas μ is the Mach angle, as depicted in the figure 2.5:

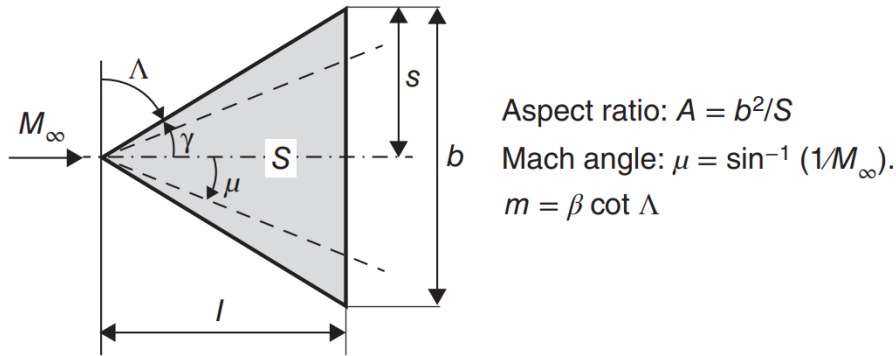


Figure 2.5. Basic wing geometry and definitions of flow parameters [5]

In order to calculate the Lift Coefficient it is possible to multiply the slope of the lift curve C_{L_α} by the angle of attack α (eq.2.66), where C_{L_α} is evaluated according to the leading-edge condition.

$$C_L = C_{L_\alpha} \cdot \alpha \quad (2.66)$$

– *Subsonic Leading Edge, $m < 1$*

When a slender wing is placed in a lower-supersonic airflow, the Mach angle increases: if the speed become low enough to make the Mach angle μ larger than γ , the flow parameter m is lower than 1 and the entire wing is inside the Mach cone; in this situation, the leading-edge is subsonic and the trailing-edge is supersonic: the lift gradient is evaluated from slender wing theory eq.(2.67) [5].

$$C_{L\alpha} = \frac{2\pi m}{E'(m)\beta} \quad (2.67)$$

where:

$$E'(m) = 1 + (\pi/2 - 1)m^\eta \quad (2.68)$$

$$\eta = 1.226 + 0.15\pi(1 - \sqrt{m}) \quad (2.69)$$

– *Supersonic Leading Edge, $m > 1$*

Contrary to the previous case, when a slender wing is placed in a higher-supersonic airflow, the Mach angle decreases until it became lower than γ : the flow parameter is now higher than 1 and both the leading-edge and the trailing-edge are in a supersonic condition.

$$C_{L\alpha} = \frac{4}{\sqrt{M^2 - 1}} = \frac{4}{\beta} \quad (2.70)$$

• **Drag Coefficient**

In general, as well as the models previously analysed, the Total Drag coefficient is obtained by adding the Parasite (or zero lift) Drag and the Induced Drag (eq.2.71).

$$C_D = C_{D_0} + C_{D_i} \quad (2.71)$$

The Parasite Drag consisting of the Skin Friction Drag C_{D_F} and the Wave Drag due to Volume $C_{D_{WV}}$ (eq.2.72):

$$C_{D_0} = C_{D_F} + C_{D_{WV}} \quad (2.72)$$

the Induced Drag (or Drag due to Lift) summarizes the Wave Drag due to Lift $C_{D_{WL}}$ and the Vortex-Induced Drag $C_{D_{VL}}$ (eq.2.73):

$$C_{D_i} = C_{D_{VL}} + C_{D_{WL}} \quad (2.73)$$

These four contributions are representative for the early design stages of an high-speed vehicle, as all other minor components cannot be analysed until much more data is available. In the following lines, these main contributions are analysed, taking into account their variation, depending on whether the configuration is a delta wing, arrow wing or blended body one.

– ***Delta Wing***

Delta wing configuration is the classical planform applied to supersonic aircraft, thanks to its acceptable aerodynamic properties at high Mach numbers as well as in subsonic flight. A triangular wing like this, typically, has a low Aspect Ratio AR , between 1 and 3.

1a. Skin Friction Drag

The Skin Friction Drag is generated by the presence of viscosity in a real flow, which opposes sliding between air molecules facing the surface of the aircraft. This contribution depends on the surface roughness, laminar or turbulent flow and kinetic heating due to stagnation of the boundary layer. In order to predict this Parasite Drag component in a conceptual design stage, it is possible to apply the flat-plate analogy: each component exposed to the flow is represented by a smooth flat plate with same length and area exposed to the air, situated in undisturbed flow at the same Reynolds number (eq.2.74) [5].

$$C_{D_F} = \frac{\sum(C_F \cdot K_F \cdot S_{wet})}{S_{plan}} \quad (2.74)$$

C_F is the skin friction coefficient, S_{wet} is the wetted surface of the aircraft, S_{plan} is the reference area and K_F accounts for non-ideal drag due to imperfections which can be evaluated as reported (eq.2.75):

$$K_F = \begin{cases} 1 & \text{Wing} \\ 1.05 & \text{Fuselage} \\ 1.15 & \text{Vertical and Horizontal tail, Canard} \end{cases} \quad (2.75)$$

Talking about the skin friction coefficient C_F , it is possible to apply the classical Prandtl–Schlichting formula (eq.2.76) which is reliable for a turbulent boundary layer:

$$C_F = \frac{0.455}{r_T} \cdot (\log_{10} Re - 2.8 \log_{10} r_T)^{-2.58} \quad (2.76)$$

where the factor r_T accounts for the kinetic heating due to stagnation of the boundary layer (eq.2.77) and P_r is the Prandtl number which expresses the ratio of kinematic diffusivity to thermal diffusivity, in first

approximation equal to 0.71.

$$r_T = 1 + P_r^{(1/3)} \cdot \frac{\gamma - 1}{2} M^2 \quad (2.77)$$

1b. Wave Drag due to Volume

The Wave Drag due to Volume is the contribution caused by the presence, in the supersonic regime, of shock waves and it is a direct result to the vehicle volume distribution. In the case of a slender wing, it is possible to evaluate this contribution starting from the wave drag of the perfect body, called Sears-Haack body. Therefore, the formula used for a delta wing is the one reported below (eq.2.78):

$$C_{D_{WV}} = K_{WV} \cdot A_W \left(\frac{t}{c} \right)^2 \quad (2.78)$$

where K_{WV} is evaluated with the eq. 2.79 and K_{SH} is the Sears-Haack body factor (eq.2.80)

$$K_{WV} = 2.2 \cdot K_{SH} \quad (2.79)$$

$$K_{SH} = 1.17 \cdot \frac{1 + 1.5\beta \cdot \cot \Lambda}{1 + 4\beta \cdot \cot \Lambda} \quad (2.80)$$

In addition to the wing's contribution, it is important to take into account also the fuselage one (eq.2.81), where d_f is the fuselage diameter, l_n is the nose length and l_t il the tail length.

$$C_{D_{WV_{fuselage}}} = \frac{\frac{\pi}{4} \cdot d_f^2 \cdot [(d_f/l_n)^2 + (d_f/l_t)^2]}{S_{plan}} \quad (2.81)$$

2a. Vortex Induced Drag

The Vortex Induced Drag is caused by the circulation about the airfoil that, for a three-dimensional wing, produces vortices in the airflow behind the wing itself. The minimum value of this contribution is the one of an elliptical lift distribution (ideal condition). According to linearized theory, the induced drag of a delta wing amounts to eq. 2.82, where the factor K_{VL} accounts for non-elliptical distribution of a real wing. A realistic assumption for an early design stage is $K_{VL} = 1.15$.

$$C_{D_{VL}} = K_{VL} \cdot \frac{C_L^2}{\pi AR} \quad (2.82)$$

2b. Wave Drag due to Lift

When a wing is immersed in a flow with a low angle of attack, it experiences a lift-dependent drag associated with shock and expansion waves, called Wave Drag due to Lift (eq.2.83); the factor K_{WL} accounts for non-elliptical distribution of a real wing and for an early design stage $K_{WL} = 1.15$.

$$C_{D_{WL}} = K_{WL} \cdot \frac{\beta^2 C_L^2 AR}{8\pi} \quad (2.83)$$

As can be seen from the equation above, this contribution is proportional to the Aspect Ratio of the wing AR and the Mach number (β).

– **Arrow Wing**

It is possible to obtain the arrow wing geometry modifying the delta wing one, as follow: the center-line section remains at a fixed location and the tips are relocated in downstream direction parallel to the center-line, so that the wing span remains constant. The planform area S_{Plan} , the aspect ratio AR , and the volume are equal to the previous geometry (fig.2.6).

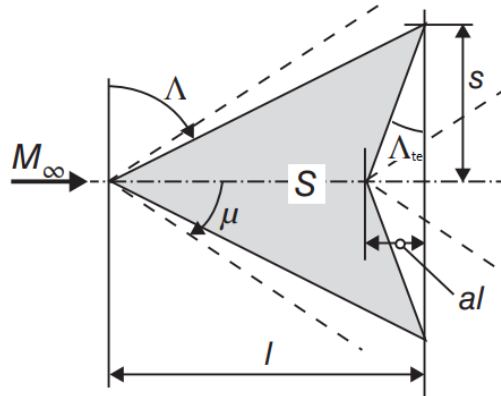


Figure 2.6. Arrow wing geometry [5]

This configuration is defined by the *notch ratio* (eq. 2.84) that basically indicates how large the trailing-edge sweep angle is.

$$a = \cot \Lambda / \cot \Lambda_{te} \quad (2.84)$$

As can be deduced, the arrow wing is more slender than a delta wing with the same volume: this has a significant effect on the wave drag due to volume and on the wave drag due to lift, with a consequent decrease of the total drag and an increase of the aerodynamic efficiency. Although the larger the notch the greater the efficiency, it is also important to take

into account some drawbacks, such as the subsonic aerodynamic performance reduction and the degradation of structural efficiency as trailing-edge sweep increases. In order to obtain an acceptable aerodynamic design, a trailing edge sweep angle higher 30 deg is suggested [5].

1a. Skin Friction Drag

This contribution is evaluated in exactly the same way as the previous configuration (eq.2.74), except for the calculation of the Reynolds number: the reference length is now $MAC_{arrow} = MAC_{delta}(1 - a)$.

1b. Wave Drag due to Volume

All the considerations made for the previous geometry are still valid, except for the equation 2.78, now corrected by the factor $(1 - a)$ to account for the $C_{D_{WV}}$ reduction caused by the overall wing length increment (eq.2.85).

$$C_{D_{WV}} = K_{WV} \cdot A_W \cdot \left(\left(\frac{t}{c} \right) (1 - a) \right)^2 \quad (2.85)$$

There is no difference for the evaluation of the fuselage contribution.

2a. Vortex Induced Drag

Considering that the resulting arrow wing has the same aspect ratio as the previous configuration and that the lift coefficient is evaluated in the same way (eq.2.66), it's possible to calculate the Vortex Induced Drag equally to the delta wing (eq.2.82).

2b. Wave Drag due to Lift

As in the case of the wave drag due to volume, it is necessary to take into account the correction by the factor $(1 - a)^2$, in order to consider the slenderness increment of the arrow geometry.

$$C_{D_{WL}} = K_{WL} \cdot \frac{\beta^2 \cdot C_L^2 \cdot AR(1 - a)^2}{8 \cdot \pi} \quad (2.86)$$

– ***Blended Body***

The last configuration analysed is a blended all-wing one, where the volume is spread out in longitudinal as well as lateral directions (fig.2.7).

The result is a reduction of the total wetted area and consequently a reduction of the skin friction drag; moreover, the leading edges of this concept are swept far behind the Mach cone and consequently a lower wave drag due to volume is obtained.

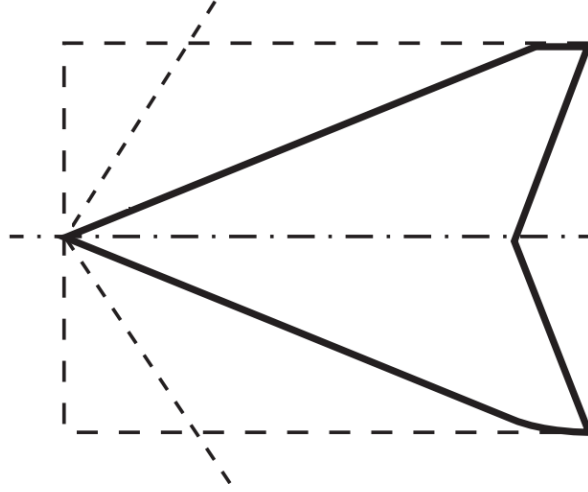


Figure 2.7. Blended-body geometry [5]

Despite the advantage of an higher aerodynamic efficiency, the main drawback is that this highly integrated configuration has an unfavorable utilization of the internal volume which is useful for the payload accomodation. With regard to the calculation of the all drag components, the only difference is the wave drag due to volume: since there is no longer a clear distinction between fuselage and wings, the only contribution of the total body is considered, evaluated as reported in the equation 2.87.

$$C_{D_{wv}} = r_S K_{SH} \frac{128\tau^2 \cdot (s/l)}{\pi} \quad (2.87)$$

where r_S is the area ratio (2.88) and τ is the equivalent thickness ratio (2.89).

$$r_S = \frac{S_{plan}}{2 \cdot span \cdot l_{wing}} \quad (2.88)$$

$$\tau = \frac{wing_{volume}}{S_{plan} \cdot l_{wing}} \quad (2.89)$$

In conclusion, therefore, it is possible to say that this model is advantageous in that there are no configurational restrictions but it allows to obtain the aerodynamic coefficients for three different configurations, requiring not too many inputs. It also allows to consider the contribution of the tail planes, in addition to the wings, providing results as a function of both Mach number and angle of attack. On the other hand, it is only applicable for a supersonic flight regime with speeds from

$M = 1.2$ up to $M = 5$, where the air can be treated as a calorific perfect gas with constant values of the specific heat [5].

All the input and output are reported on the table (2.4)

INPUT		<i>UoM</i>
Mach number	M	none
Total Volume	V_{tot}	$[m^3]$
Planform surface	S_{plan}	$[m^2]$
Wetted surface	S_{wet}	$[m^2]$
Wing span	$span$	$[m]$
Wing length	l_{wing}	$[m]$
Mean aerodynamic chord of the wing	MAC_{wing}	$[m]$
Wing thickness ratio	$(t/c)_{wing}$	none
Leading edge sweep angle of the wing	λ	$[^\circ]$
Trailing edge sweep angle of the wing	Λ_{te}	$[^\circ]$
Fuselage length	$l_{fuselage}$	$[m]$
Fuselage diameter	$d_{fuselage}$	$[m]$
Nose length	l_{nose}	$[m]$
Tail length	l_{tail}	$[m]$
Maximum cross-sectional area	S_{max}	$[m^2]$
Horizontal tail surface	S_{Htail}	$[m^2]$
Mean aerodynamic chord of the Horizontal tail	MAC_{Htail}	$[m]$
Vertical tail surface	S_{Vtail}	$[m^2]$
Mean aerodynamic chord of the Vertical tail	MAC_{Vtail}	$[m]$
Canard surface	S_{Canard}	$[m^2]$
Mean aerodynamic chord of Canard	MAC_{Canard}	$[m]$
OUTPUT		
	$C_L = f(M, \alpha)$	
	$C_D = f(M, \alpha)$	
	$E = f(M, \alpha)$	

Table 2.4. Model IV - Input and Output

Chapter 3

Final Aerodynamic Models

In the previous chapter, four preliminary aerodynamic estimation models taken from the literature have been described: their main theoretical aspects, limitations and capabilities have been listed. The next step in this work is to implement them in Matlab, test them with existing aircraft whose main geometric characteristics are known, and compare the results obtained with the available aerodynamic coefficients. Then, in order to better estimate the aerodynamic behaviour of the aircraft under consideration for the entire mission profile, corrective coefficients are added into the basic models.

It is important to remember that the final goal is to provide a useful tool for a preliminary design phase, where the geometric data of the aircraft are limited: it is very difficult to predict with high precision the aerodynamic behaviour during the flight. However, thanks to these corrective coefficients, it is possible to obtain acceptable results when compared to the reference aerodynamic characteristics, both in numerical terms and curve trends.

In order to obtain an aerodynamic estimation routine as complete as possible and capable of supporting a wide range of users and aircraft configurations, eight different high-speed vehicles are used for the models validation. These are grouped into four different configurational families, based on their geometric concept, taking into account that aircraft of the same family have very similar aerodynamic characteristics. The classification is made on the basis of the correlation between τ and K_w (introduced in the Curran Model chapter 2.1) and it is possible to refer to the figure 3.1, taken from [1]: it shows the range of these two parameters for a number of families of hypersonic configuration concepts appropriate for launchers. The vehicles of interest are the combined cycle engine launchers (which include hypersonic cruise aircraft), powered by air-breathing propulsion over all or part of their flight mission:

- Waverider configuration;
- Blended Body configuration;

- Wing Body configuration;
- Cylinder Wing configuration.

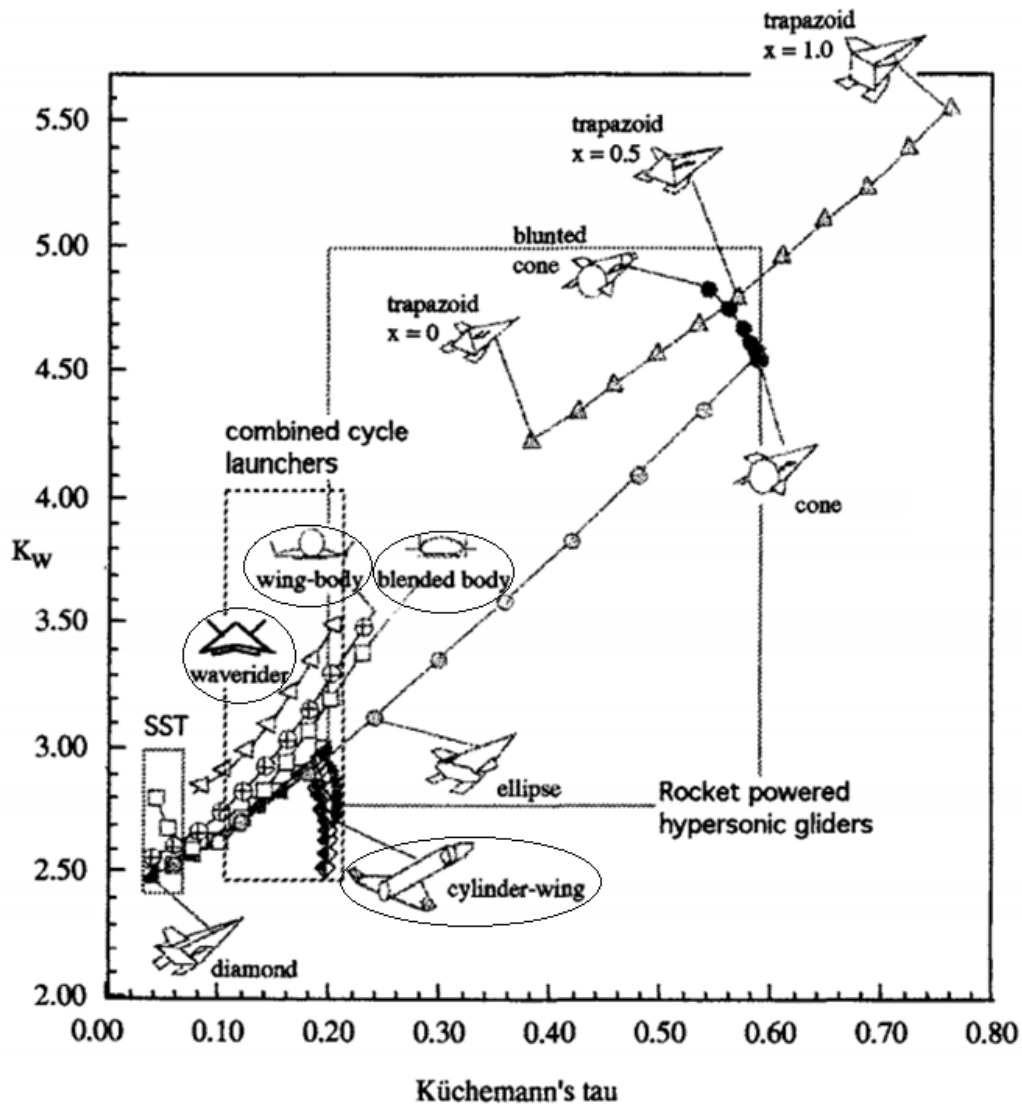


Figure 3.1. Surface and Volume Characteristics of Hypersonic Configuration Concepts [1]

In the following pages of this thesis, all the families listed above are analysed. For each of them, it is specified which vehicles were tested and the most important geometric data entered as input for the models validation. Finally, the basic models are modified by means of corrective coefficients, used to improve the curves trend.

3.1 Dorsal Waverider Configuration

This first configurational family being analysed is the best in terms of aerodynamics efficiency for supersonic and hypersonic flight. Before listing the the key points of this concept and its performances, it is interesting to have a look at the main characteristics of a hypersonic aircraft in general, which are [7]:

- Very small frontal area and highly streamlined shape to minimize total surface area;
- Little wing area, but the fuselage is often shaped to generate additional lift;
- Propulsion highly integrated into the vehicle;

Based on these features, it is possible to verify how waveriders represent optimum shapes and maximize the overall performances.

The most critical effect found in hypersonic flight is the decrease in aerodynamic efficiency which can be attributed to the strong shock wave drag effects and the high skin friction ones that vehicles suffer. In order to counteract these negative effects, however, it is possible to follow the three key aspects described above, thus achieving good performance even for these flight regimes. The first two points are linked together with the aim to conceive a vehicle as slender as possible, capable of remaining within the Mach cone generated by the nose of the aircraft, reducing the total drag. The last point is also essential, to prevent the shock wave from one component of the aircraft produce negative interferences with other components: shock interactions and ideal engine operation require the propulsion system to be integrated into the overall airframe design.

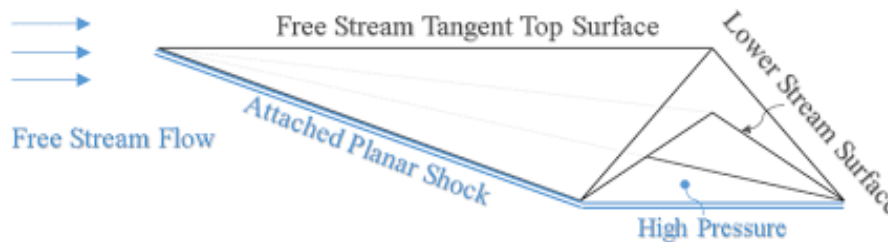


Figure 3.2. Nonweiler (Caret) Waverider showing the attached shock [6]

Waverider is any supersonic or hypersonic lifting body conceived from a known flowfield and designed such that the bow shock generated by the shape is attached along its leading edge, at the design flight condition. The first waverider concept was generated by Terence Nonweiler, starting from the flowfield behind a planar oblique shock and used the stream surfaces behind the wave to generate a body

shape: the result is the *"Nonweiler Waverider"*, also known as *"Caret Waverider"* (fig. 3.2). As can be seen, the body seems to ride on top of the shock wave, with two main advantages: firstly, the shock attached to the leading edge prevents the flow spillage from the lower to upper surface; secondly, the flow under the vehicle is at high pressure due to the shock compression. This results in the compression lift generation phenomenon on the lower surfaces, which is the major contribution to the high supersonic and hypersonic efficiency of this configurational concept. Similar to the caret wing, more complicated flow fields can also be used to generate hypersonic bodies, like the conical ones [6].

Depending on the location of the propulsion unit with respect to the central body, it is possible to make a distinction within this configurational family: Dorsal waverider and Ventral waverider. The first subfamily to be analysed is the dorsal one, in which the propulsion unit is installed in the upper part of the aircraft, as the name suggests, and embedded into the airframe. This geometry brings some advantages: first of all, it allows to maximize the available under surface for lift generation without additional drag penalties; secondly, it allows to optimize the internal volume and to expand the exhausted flow without large external nozzle, which would lead to an extra pressure drag.

In the following subsections, the Stratofly MR3 dorsal waverider vehicle is presented, including details of configuration, geometrical data and the aerodynamic database description, used for the Models validation.

3.1.1 STRATOFLY MR3 project

The STRATOFLY MR3 vehicle was designed under the STRATOFLY project (STRATOspheric FLYing opportunities for high-speed propulsion concepts), which has been funded by the European Commission, under the framework of Horizon 2020 research and innovation programme [8]. The project stems from the worldwide incentive to reconsider commercial high-speed transport in order to cope with the worrying increase in the number of civil aviation passengers expected in the coming years. As its name suggests, it focuses on the investigation and feasibility analysis of high-speed civil passenger stratospheric flight opportunities. In particular, the objective is to review and improve the LAPCAT MR2 vehicle, taken as a starting point, considering technical, environmental and economic viability in combination with human factors, social acceptance, implementation and operational aspects.

This vehicle concepts flight along unexploited routes in the stratosphere, offering a solution to the presently congested flight paths while ensuring a minimum environmental impact in terms of emitted noise and green-house gasses, particularly during the stratospheric hypersonic cruise phase [9]. In conclusion, it is possible to summarise the main objectives and requirements of this project:

- To drastically decrease the transfer time of long range civil flights;

- To perform an antipodal civil passenger transport mission, flying at Mach number of 8 above 30 km of altitude;
- To reduce the impact on existing on-ground infrastructures in compliance with environmental compatibility and safety issues;
- To evaluate the sustainability of the future operability of hypersonic vehicles from an economical and also environmental point of view;

Vehicle Configuration

The STRATOFLY MR3 configuration is a waverider concept (fig.3.3) with a dorsal engine located on top of the vehicle, able to maximize the lift-to-drag ratio (L/D) during cruise. This shape has been obtained following several iterations and it is able to guarantee an L/D of about 7 at its Mach 8 design point. In addition, this concept allows to optimize the internal volume, making it suitable for civil transportation and to reduce the wetted surface.

The aircraft has a an integrated cabin accommodating 300 passengers, located in the ventral part of the vehicle. This position confers some advantages, including a greater safety due to the better location of the compartment in relation to other subsystems and the organisation of boarding and evacuation procedures.



Figure 3.3. STRATOFLY MR3 Vehicle [29]

The air-breathing propulsive subsystem is able to accelerate the vehicle up to Mach 8 and it is highly integrated in the dorsal part of the concept. It consists of [10]:

- 6 Air Turbo Rocket engines (ATR), which operates at Mach numbers from 0 up to 4-4.5. This flight range include take-off, subsonic and supersonic acceleration, and the final approach and landing at the end of the mission.
- Dual Mode Ramjet (DMR), which cover the hypersonic flight conditions operating from M=4-4.5 up to M=8 in order to power the aircraft during hypersonic acceleration and cruise.

Liquid hydrogen has been chosen as the propellant, due to its high energy content. However, this presents a number of problems such as larger tanks due to lower density and extremely low storage temperatures, which require thick layers of insulation. In order to counter this negative effects, the 200 tons of LH2 are stored in cryogenic bubble tanks, which maximise fuel storage capacity and minimise weight. talking about the Flight Control Subsystem (FCS), it aims to guarantee the stability and controllability in both low-speed and high-speed regime and it is constituted of 2 rudders and 4 elevons, as can be seen in the figure (3.3).

In conclusion, the main dimensions are the total length of 94 m , the wing span of 41 m , the total volume of about 10000 m^3 , the reference surface of 2365 m^2 and all the other geometrical data are reported in the table (3.1).

GEOMETRICAL DATA		Value
Total volume	V_{tot}	10000 [m^3]
Reference surface	S_{plan}	2365 [m^2]
Wetted surface	S_{wet}	5422 [m^2]
Exposed surface	$S_{Exposed}$	1265 [m^2]
Wing span	$span$	41 [m]
Wing length	l_{wing}	70 [m]
Fuselage length	$l_{fuselage}$	94 [m]
Fuselage diameter	$d_{fuselage}$	11 [m]
Nose length	l_{nose}	12.5 [m]
Tail length	l_{tail}	7.35 [m]
Maximum cross-sectional area	S_{max}	210 [m^2]
Mean aerodynamic chord of the wing	MAC_{wing}	14 [m]
Leading edge sweep angle of the wing	λ_w	81 [$^\circ$]
Trailing edge sweep angle of the wing	λ_{te}	0 [$^\circ$]
Wing thickness ratio	$(t/c)_{wing}$	0.22 none
Inlet length	l_{Inlet}	26 [m]
Inlet diameter	d_{Inlet}	8 [m]
Flap span	$Flap_{span}$	5.03 [m]
Vertical tail thickness ratio	$(t/c)_{Vtail}$	0.037 none
Vertical tail surface	S_{Vtail}	72.8 [m^2]
Vertical tail span	b_{Vtail}	8.5 [m]
Leading edge sweep angle of the Vertical tail	λ_{Vtail}	45 [$^\circ$]
Mean aerodynamic chord of the Vertical tail	MAC_{Vtail}	9.4 [m]
Vertical tail number	$Vtail_{number}$	2 none

Table 3.1. STRATOFly MR3 geometrical data

Aerodynamic Database

The aerodynamic database (*AEDB*) allows to describe the behaviour of the vehicle during its mission phases and it is extremely important for this thesis work. It is the starting point and allows to compare the outputs of the estimation models with the real behaviour of the aircraft under consideration.

This AEDB has been generated as a function of two independent variables which are the angle of attack (from $\alpha = -6^\circ$ to $\alpha = +6^\circ$) and the Mach number (from $M = 0.3$ to $M = 8$).

The STRATOFly MR3 aerodynamic database consists of the following three excel files:

- "*AEDB_Stratofly3_Clean*": it refers to the clean configuration, i.e. it does not take into account the canards contribution while the flaps one is considered for a zero deflection condition. In this file, the coefficients for both inviscid flow and viscous flow are reported. Another important feature of this AEDB file is that it reports the aerodynamic coefficients for two different conditions: the "*External*" condition which takes into account only the contribution of the external surface of the aircraft and the "*External+Internal*" condition which also considers the contribution of the air intake and the air duct located inside the fuselage.
- "*AEDB_Stratofly3_Flap*": this file structure is similar to the previous one. Inside the flaps contribution for different deflection is reported, ranging from -20° to $+20^\circ$, with a variation of 5° . All the aircraft flaps are considered to be deflected in the same way at the same time.
- "*AEDB_Stratofly3_Canard*": this file structure is exactly the same of the previous one. Also in this case, the canards contribution for different deflection is reported, ranging from -20° to $+20^\circ$, with a variation of 5° . All the aircraft canards are considered to be deflected in the same way at the same time.

In order to obtain the total aerodynamic coefficients, therefore, it is necessary to simply add the "clean" contribution with the flaps one and the canards one, for the angle of attack and the Mach number under consideration.

It is important to distinguish the condition in which the STRATOFly MR3 engines are switched on or off, as the aerodynamic behaviour is different. Below, it is explained how the coefficients are obtained in the two different operative conditions:

- "*ENGINE – ON Condition*"
In this case, the C_L coefficient is given from the "*External+Internal*" contribution from database while the C_D coefficient is given from the only "*External*" contribution. This occurs because of the propulsive database composition. In this case, in fact, the thrust is calculated as net thrust, so it already takes

into account the contribution to drag (and CD) due to the presence of the internal air duct. For this reason, the aerodynamic database does not take this contribution into account when the engines are active.

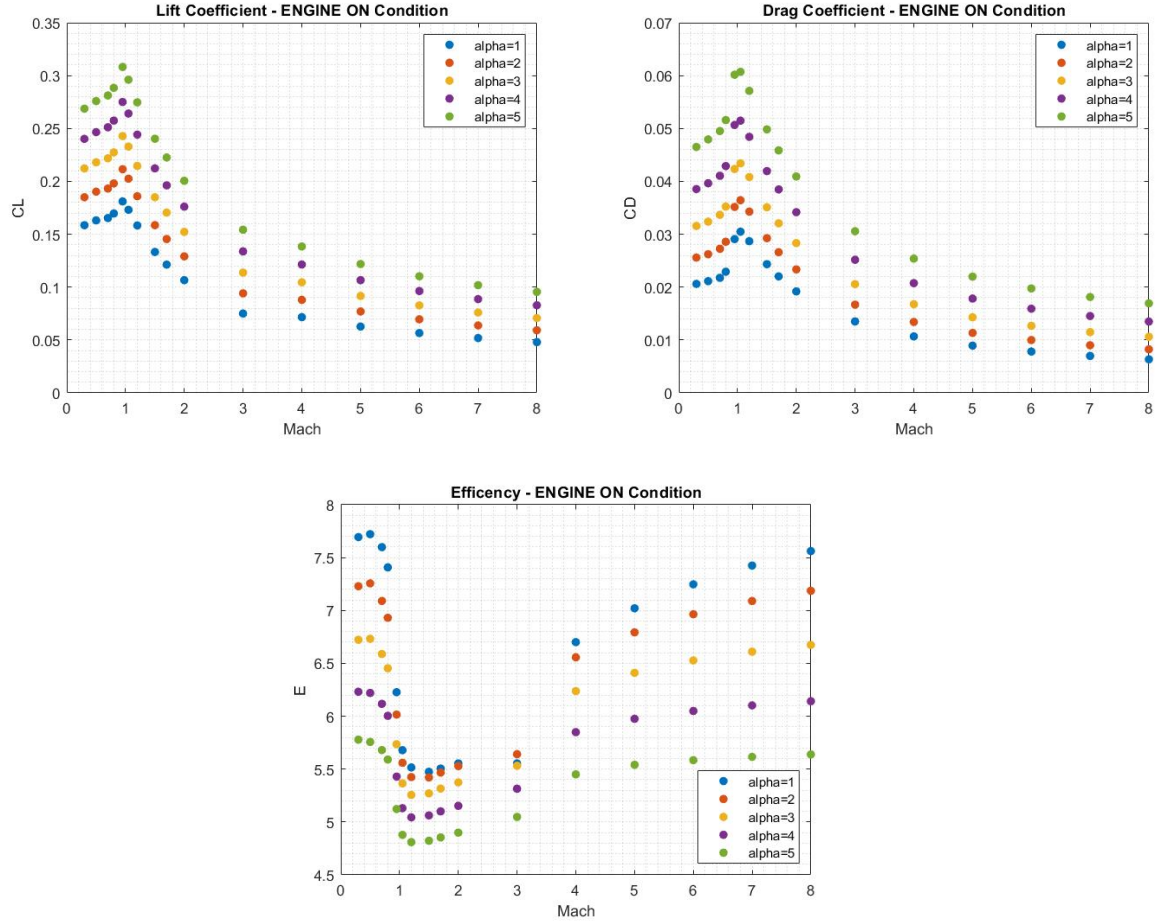


Figure 3.4. STRATOFLY MR3 aerodynamic coefficients for the engine operative condition

The STRATOFLY MR3 aerodynamic coefficients (zero deflection of canards and flaps) for the operative condition of the engine are reported in the figure (3.4), for an angle of attack range between $\alpha = 1^\circ$ to $\alpha = +5^\circ$. As can be seen, the drag coefficient presents the typical behaviour as a function of the Mach number: the CD increases in the subsonic regime until reaching a maximum in the transition phase, then it decreases in the hypersonic regime. Furthermore, the lower is the AoA the lower is the CD. The Lift coefficient behaviour as a function of the angle of attack is similar to the Drag coefficient one.

- *"ENGINE – OFF Condition"*

Unlike the previous case, in order to consider the condition in which the engines are switched off, it is necessary to take into account the *"External+Internal"* contribution from the database, for both the Lift coefficient and the Drag coefficient.

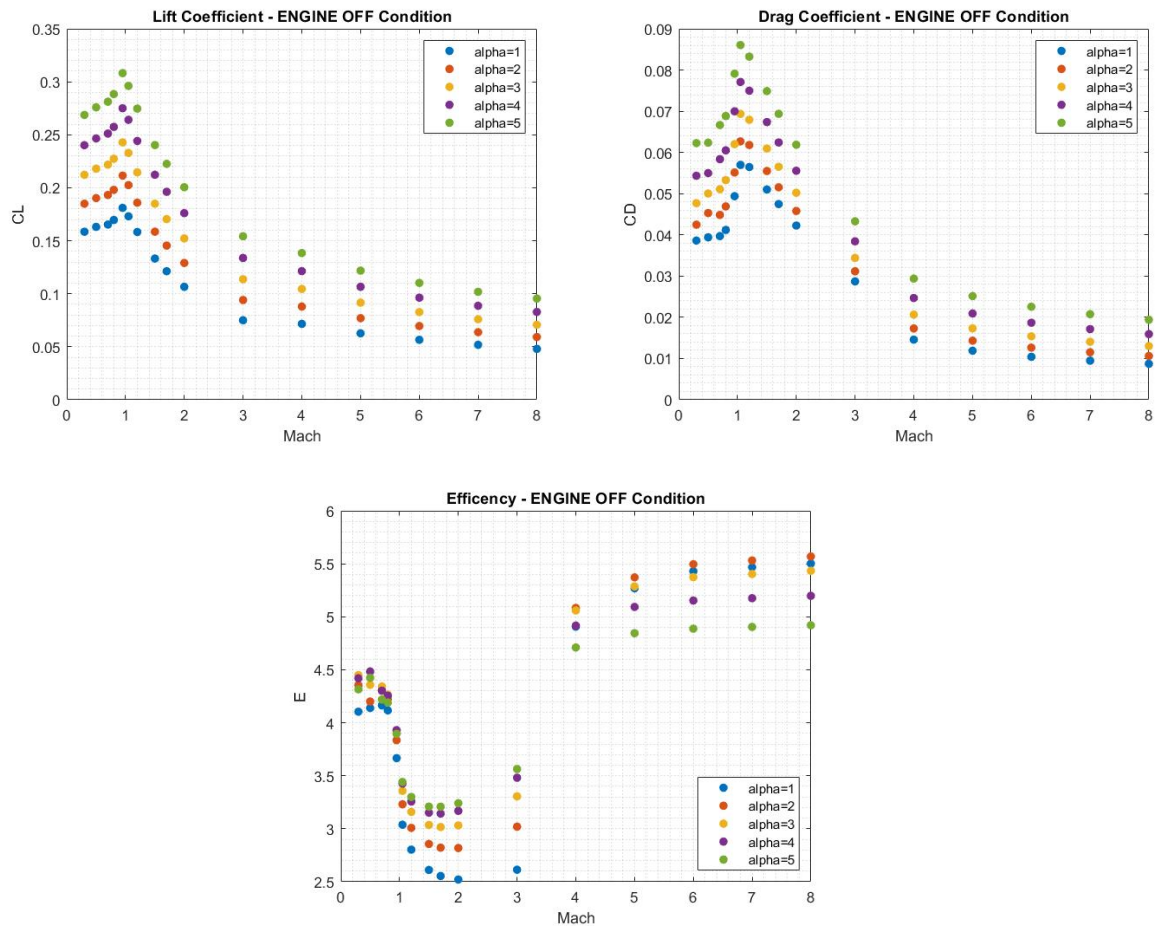


Figure 3.5. STRATOFLY MR3 aerodynamic coefficients for the engine off condition

In the figure (3.5) it is possible to see that the CD is higher with respect to the previous case and consequently the Efficiency is lower. This occurs because the air entering the central duct is impeded by the engine being switched off, the flow is not able to pass as in the operative engine condition and this generates a non-negligible increase of the Drag.

3.1.2 Curran Model Results

The first model tested and analysed is the simplest of all, the Curran one, introduced in the previous chapter. As explained before, it permits to estimate the aerodynamic coefficients of the vehicle under consideration requiring only three geometrical data as input: the total volume of the aircraft V_{tot} , the reference surface S_{plan} and the wetted surface S_{wet} . These values, in the case of the STRATOFLY MR3, are reported in the table (3.1).

The value of the two main configurational parameters of the model are $\tau = 0.0869$ and $K_w = 2.6926$, which are therefore in agreement with the classification made previously (fig. 3.1). The aerodynamic coefficient obtained for an Engine - ON condition are shown in the figure below (3.6) with the light blue curve.

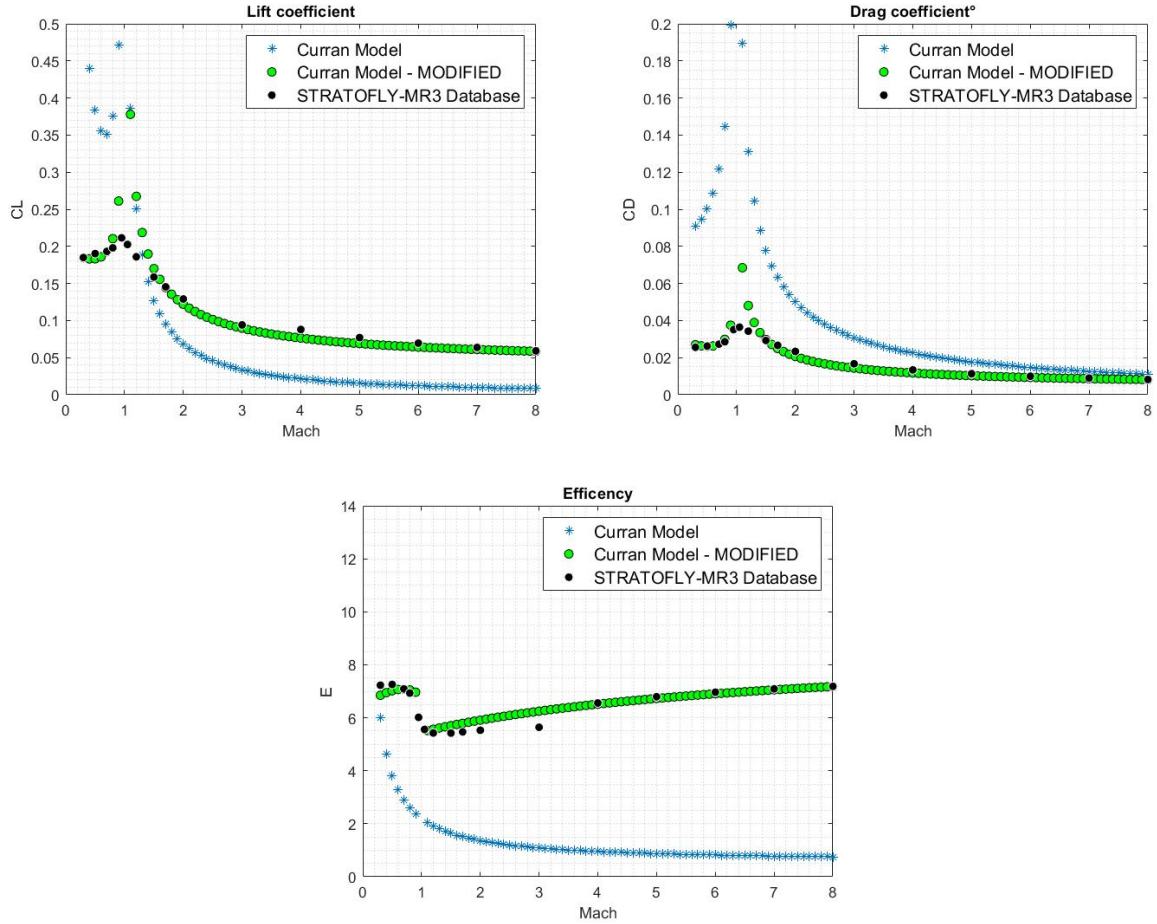


Figure 3.6. Aerodynamic coefficients of the basic Curran Model compared with the aerodynamic coefficients of the modified Curran Model

As can be seen, if the model outputs are compared with the STRATOFly aerodynamic database (black points), there is a clear discrepancy. In particular, it can be seen that there is an underestimation of the lift coefficient and an overestimation of the drag coefficient: the efficiency is consequently worse than in the real case. This discrepancy of the results can be attributed to the very small amount of input data useful for the characterisation of the aircraft being analysed. The model is too simple, so it is able to capture the trends in the Drag coefficient and Lift coefficient curves but cannot be sufficiently precise in numerical terms. Furthermore, as can be seen, the model fails to capture the increase in efficiency as Mach increases, a typical feature of the waverider configuration.

In order to improve the estimation of aerodynamic behaviour in the preliminary design phase, corrective coefficients were added, found with the help of the "Curve fitting" Matlab tool. Thanks to this application, it's possible to enter the CL and CD equation as a Mach number function, the database curve to be approximated, and appropriate corrections are automatically suggested. Subsequently, after several tests, the values were further improved: the all coefficients are reported in the table (3.2).

CURRAN MODEL		
α	Flight Regime	Corrective Coefficients
$\alpha = 1^\circ$	<i>Subsonic</i>	<ul style="list-style-type: none"> • CL: (eq.2.6)·(12.5 – 8.2 · M); • CD: (eq.2.4)·(0.29 – 0.165 · M);
$\alpha = 1^\circ$	<i>Supersonic</i>	<ul style="list-style-type: none"> • CL: (eq.2.6)·(M · 0.77); • CD: (eq.2.4)·(0.25 + M/21);
$\alpha = 2^\circ$	<i>Subsonic</i>	<ul style="list-style-type: none"> • CL: (eq.2.6)·(13.8 – 8.5 · M); • CD: (eq.2.4)·(0.35 – 0.18 · M);
$\alpha = 2^\circ$	<i>Supersonic</i>	<ul style="list-style-type: none"> • CL: (eq.2.6)·(M · 0.89); • CD: (eq.2.4)·(0.3 + M/18);
$\alpha = 3^\circ$	<i>Subsonic</i>	<ul style="list-style-type: none"> • CL: (eq.2.6)·(15 – 8.5 · M); • CD: (eq.2.4)·(0.4 – 0.18 · M);
$\alpha = 3^\circ$	<i>Supersonic</i>	<ul style="list-style-type: none"> • CL: (eq.2.6)·(M · 1.1); • CD: (eq.2.4)·(0.45 + M/16);

$\alpha = 4^\circ$	<i>Subsonic</i>	<ul style="list-style-type: none"> • CL: (eq.2.6)·(18 – 11 · M); • CD: (eq.2.4)·(0.48 – 0.18 · M);
$\alpha = 4^\circ$	<i>Supersonic</i>	<ul style="list-style-type: none"> • CL: (eq.2.6)·(M · 1.25); • CD: (eq.2.4)·(0.42 + M/9.5);
$\alpha = 5^\circ$	<i>Subsonic</i>	<ul style="list-style-type: none"> • CL: (eq.2.6)·(20 – 12.5 · M); • CD: (eq.2.4)·(0.55 – 0.18 · M);
$\alpha = 5^\circ$	<i>Supersonic</i>	<ul style="list-style-type: none"> • CL: (eq.2.6)·(M · 1.45); • CD: (eq.2.4)·(0.49 + M/7);

Table 3.2: Curran Model Corrective Coefficients for the all angles of attack analysed, Engine - ON condition

Thanks to the corrections, the results obtained are much better, as can be seen from the green curves in the figure (3.6): the Lift coefficient and the Drag coefficient are now reliable for both the subsonic and the supersonic regime, while there is a slight overestimation in the transonic regime. In addition, the efficiency curve now shows the correct trends and it is possible to capture the positive effect of this configuration for high Mach numbers. The results for the all angles of attack analysed are reported in the figures (3.11, 3.12) for the Engine - ON condition and in the figures (3.13, 3.14) for the Engine - OFF condition.

In conclusion, thanks to the "Curve fitting" Matlab tool it is possible to calculate confidence bounds for the corrective coefficients. The confidence bounds define the lower and upper values of the uncertainty range associated with the correction coefficients and define the width of the interval. The range width indicates how much uncertainty there is about the expected fit. The bounds can be defined with a specified level of certainty.

The figure (3.7) shows the prediction range with an accuracy of 95%, i.e. there is a 95% chance that the new observation is actually contained within the lower and upper limits of the interval. The upper limit is obtained with the corrective coefficient $(0.2+M/15)$ while the lower one is obtained with the corrective coefficient $(0.28 + M/27)$, suggested by the Matlab tool.

The accuracy of 95% is always used throughout the thesis work described in the following pages.

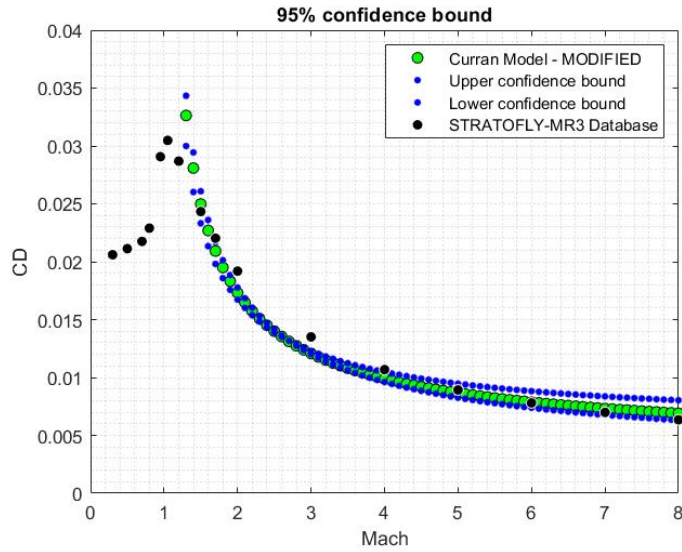


Figure 3.7. Confidence bound for the Curran Model supersonic Drag Coefficients, $\alpha = 1^\circ$

3.1.3 All-Body Hypersonic Aircraft Model Results

As introduced in the chapter (2.2), this model is more accurate than the Curran one. It only refers to a representative family of all-body hypersonic aircraft: the configuration is a delta planform with an elliptical cone forebody and an elliptical cross-section afterbody. The speed range in which the model can be applied includes a subsonic flight regime up to hypersonic flight regime.

The results obtained for the STRATOFLY MR3 vehicle (geometric data reported in the table 3.1) for an angle of attack equal to 4° and engine - ON condition are shown by the light blue curve in the figure (3.8).

The underestimation of the Lift coefficient can be attributed to the compression lift phenomenon which is characteristic of a waverider configuration but doesn't occur for a blended body concept. On the other hand, the latter geometry has a more smooth surface, as there is no clear distinction between fuselage and wings, which is reflected in a lower total drag. As can be seen from the yellow points in the figure (3.8), the aerodynamic coefficients of the modified all-body hypersonic aircraft model globally approximate the behaviour of the STRATOFLY MR3 (black points). In particular, the results are reliable for both the subsonic flight regime and the high supersonic one.

The Lift coefficient is linearised from the transonic Mach number up to high supersonic one, depending on the value of the aspect ratio of the aircraft under consideration. In the case of the STRATOFLY MR3, it is a slender vehicle, with a sweep angle equal to 81° and the AR is very low. This result in a range of linearity quite

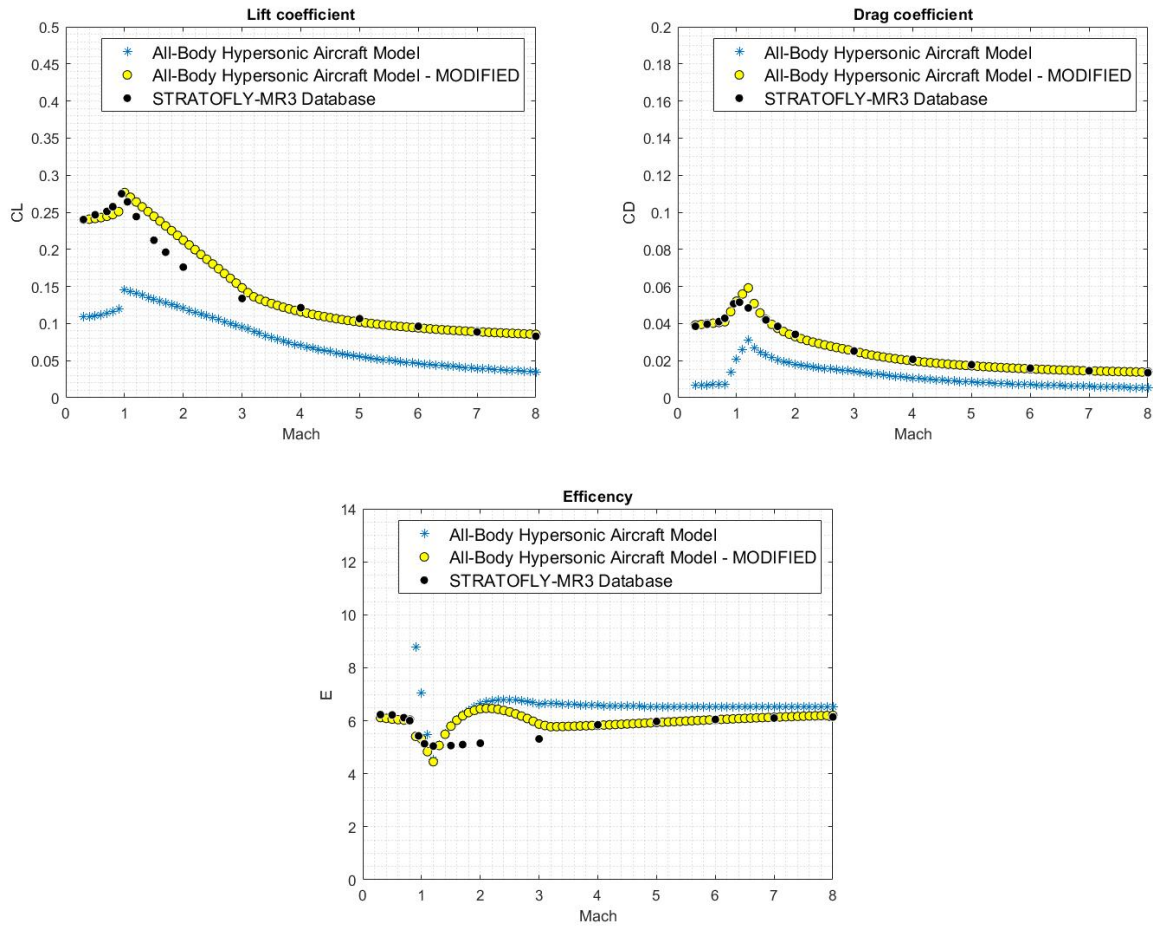


Figure 3.8. Aerodynamic coefficients of the basic All-Body Hypersonic Aircraft Model compared with the aerodynamic coefficients of the modified All-Body Hypersonic Aircraft Model

large and consequently in an unreliable efficiency trend for low supersonic speed. In conclusion, it is possible to affirm that this model is reliable for hypersonic flight regimes.

All the corrective coefficients are listed in the table below (3.3).

ALL - BODY HYPERSONIC AIRCRAFT MODEL		
α	Flight Regime	Corrective Coefficients
$\alpha = 1^\circ$	<i>Subsonic</i>	<ul style="list-style-type: none"> CL, (eq.2.9): $c_1 \cdot 4.7$; CD: (eq.2.12)+0.015;

$\alpha = 1^\circ$	<i>Supersonic</i>	<ul style="list-style-type: none"> • CL, (eq.2.11): $c_1 \cdot 2.84, c_2 \cdot 56$; • CD: (eq.2.12)·(0.9 + M/14.5);
$\alpha = 2^\circ$	<i>Subsonic</i>	<ul style="list-style-type: none"> • CL, (eq.2.9): $c_1 \cdot 2.8$; • CD: (eq.2.12)+0.018;
$\alpha = 2^\circ$	<i>Supersonic</i>	<ul style="list-style-type: none"> • CL, (eq.2.11): $c_1 \cdot 1.9, c_2 \cdot 17$; • CD: (eq.2.12)·(1.03 + M/18);
$\alpha = 3^\circ$	<i>Subsonic</i>	<ul style="list-style-type: none"> • CL, (eq.2.9): $c_1 \cdot 2.25$; • CD: (eq.2.12)+0.025;
$\alpha = 3^\circ$	<i>Supersonic</i>	<ul style="list-style-type: none"> • CL, (eq.2.11): $c_1 \cdot 1.5, c_2 \cdot 9$; • CD: (eq.2.12)·(0.93 + M/18);
$\alpha = 4^\circ$	<i>Subsonic</i>	<ul style="list-style-type: none"> • CL, (eq.2.9): $c_1 \cdot 1.9$; • CD: (eq.2.12)+0.03;
$\alpha = 4^\circ$	<i>Supersonic</i>	<ul style="list-style-type: none"> • CL, (eq.2.11): $c_1 \cdot 1.3, c_2 \cdot 6.4$; • CD: (eq.2.12)·(0.95 + M/25);
$\alpha = 5^\circ$	<i>Subsonic</i>	<ul style="list-style-type: none"> • CL, (eq.2.9): $c_1 \cdot 1.7$; • CD: (eq.2.12)+0.033;
$\alpha = 5^\circ$	<i>Supersonic</i>	<ul style="list-style-type: none"> • CL, (eq.2.11): $c_1 \cdot 1.15, c_2 \cdot 5$; • CD: (eq.2.12)·(0.95 + M/25);

Table 3.3: All-Body Hypersonic Aircraft Model Corrective Coefficients for the all angles of attack analysed, Engine - ON condition

The results for the all angles of attack analysed are shown in the figures (3.11, 3.12) for the Engine - ON condition and in the figures (3.13, 3.14) for the Engine - OFF condition.

3.1.4 Raymer Model Results

This third aerodynamic model is the most complete of those analysed: it allows to consider the contributions of the main parts of the aircraft, such as the wing, fuselage and tail planes, but also the air intakes, engine nacelles and others. This complexity is reflected in a very high number of inputs, which values, in the case of the STRATOFly MR3, are shown in the table (3.1).

The aerodynamic coefficients obtained by the basic Raymer model for an angle of attack equal to 4° and Engine - ON condition are represented by the light blue curve in the figure (3.9).

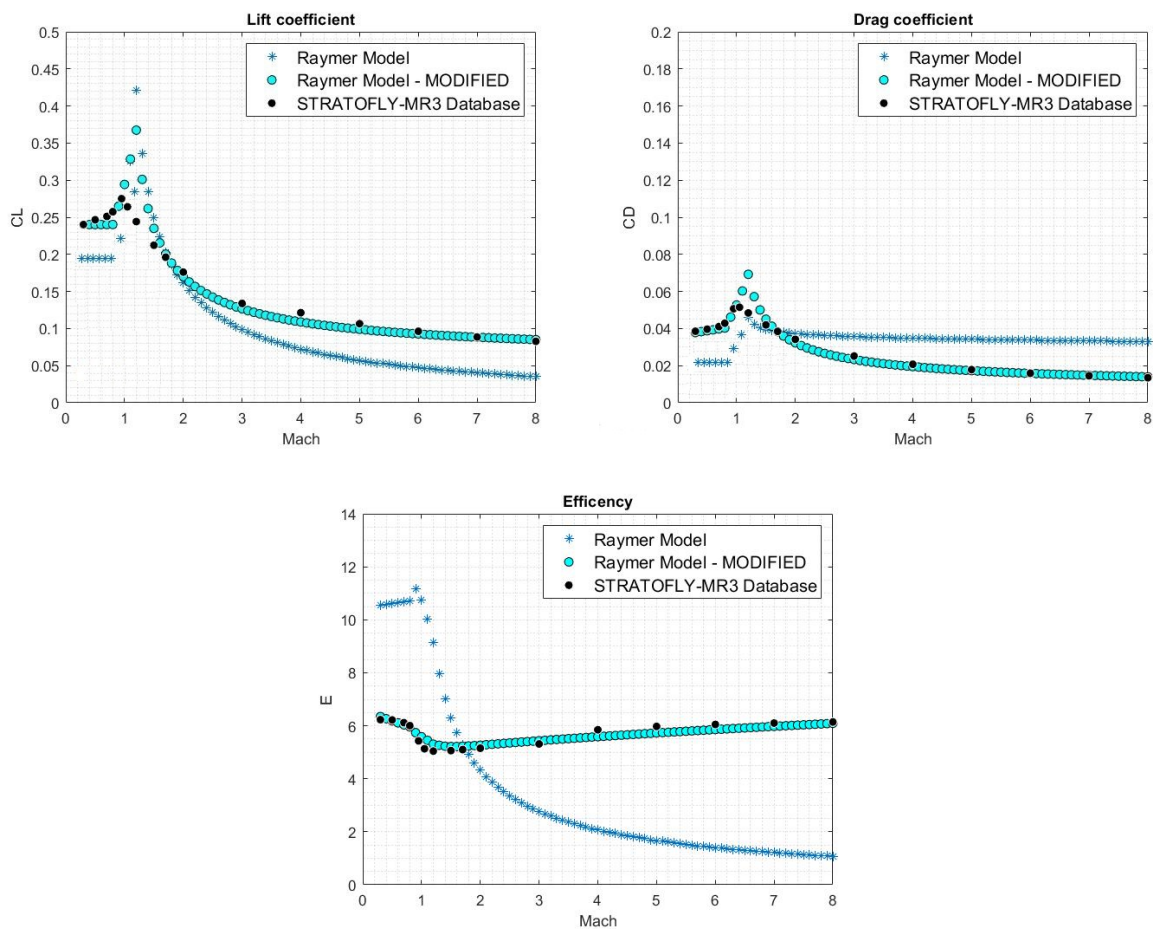


Figure 3.9. Aerodynamic coefficients of the basic Raymer Model compared with the aerodynamic coefficients of the modified Raymer Model

If these values are compared with the STRATOFly MR3 database, it's possible to see a different curve trend. Looking at the Subsonic regime, in fact, there is a clear underestimation of both C_L and C_D while in the supersonic regime the discrepancy

between the Model results and the experimental data (black points on the graph) increases as the Mach number increases. This discordance is due to the fact that this third aerodynamic Model refers to a generic high speed aircraft configuration with a clear distinction between fuselage and delta wing, totally different to the STRATOFly MR3 configuration. As introduced in the section (3.1) of this thesis, one of the main characteristic of a waverider vehicle is the compression lift that occurs as the Mach number increases. This phenomenon does not occur in the case of a classical configuration, so the Raymer Model does not take it into account and underestimates the lift of the aircraft under consideration. As far as the drag coefficient concerns, it is overestimated because a generic high speed aircraft with a clear distinction between fuselage and wing is certainly less slender than a waverider one and therefore the wave drag is higher.

As in the previous cases, in order to improve the curves trend, correction coefficients were obtained from the Matlab tool and added to the basic model, all of which are shown in the table below (3.4).

RAYMER MODEL		
α	Flight Regime	Corrective Coefficients
$\alpha = 1^\circ$	<i>Subsonic</i>	<ul style="list-style-type: none"> • CL: (eq.2.37)+0.15; • CD: (eq.2.43)·0.47;
$\alpha = 1^\circ$	<i>Supersonic</i>	<ul style="list-style-type: none"> • CL: (eq.2.37)·(1.6 + M/1.9); • CD: (eq.2.43)·(0.55/log(1.9 · M - 0.6));
$\alpha = 2^\circ$	<i>Subsonic</i>	<ul style="list-style-type: none"> • CL: (eq.2.37)+0.16; • CD: (eq.2.43)·0.44;
$\alpha = 2^\circ$	<i>Supersonic</i>	<ul style="list-style-type: none"> • CL: (eq.2.37)·(0.9 + M/3); • CD: (eq.2.43)·(0.7/log(1.9 · M - 0.5));
$\alpha = 3^\circ$	<i>Subsonic</i>	<ul style="list-style-type: none"> • CL: (eq.2.37)+0.18; • CD: (eq.2.43)·(0.4 + M/20);
$\alpha = 3^\circ$	<i>Supersonic</i>	<ul style="list-style-type: none"> • CL: (eq.2.37)·(0.6 + M/3.56); • CD: (eq.2.43)·(0.9/log(2 · M - 0.5));
$\alpha = 4^\circ$	<i>Subsonic</i>	<ul style="list-style-type: none"> • CL: (eq.2.37)+0.2; • CD: (eq.2.43)·(0.37 + M/20);

$\alpha = 4^\circ$	<i>Supersonic</i>	<ul style="list-style-type: none"> • CL: (eq.2.37)·(0.6 + M/4.4); • CD: (eq.2.43)·(1.1/log(2 · M - 0.4));
$\alpha = 5^\circ$	<i>Subsonic</i>	<ul style="list-style-type: none"> • CL: (eq.2.37)+0.22; • CD: (eq.2.43)·(0.35 + M/20);
$\alpha = 5^\circ$	<i>Supersonic</i>	<ul style="list-style-type: none"> • CL: (eq.2.37)·(0.55 + M/5); • CD: (eq.2.43)·(1.3/log(2 · M - 0.4));

Table 3.4: Raymer Model Corrective Coefficients for the all angles of attack analysed, Engine - ON condition

The results obtained, as can be seen from the cyan curves in the figure (3.9), are excellent and the estimation of the aerodynamic behaviour is reliable for the entire flight mission, from the subsonic to the supersonic regime, with a slight overestimation in the transonic regime. The positive effect of the compression lift is visible from the efficiency curve.

The results for the all angles of attack analysed are reported in the figures (3.11, 3.12) for the Engine - ON condition and in the figures (3.13, 3.14) for the Engine - OFF condition.

3.1.5 Torenbeek Model Results

This four model, as introduced in the chapter (2.4), is applicable only for a supersonic flight regime and allows to evaluate the aerodynamic behaviour of a generic high speed aircraft configuration with a delta wing, a generic high speed aircraft configuration with an arrow wing and a blended wing body configuration. Like the previous cases, this model has been tested with the STRATOFLY MR3 vehicle in order to verify its reliability for a waverider configuration.

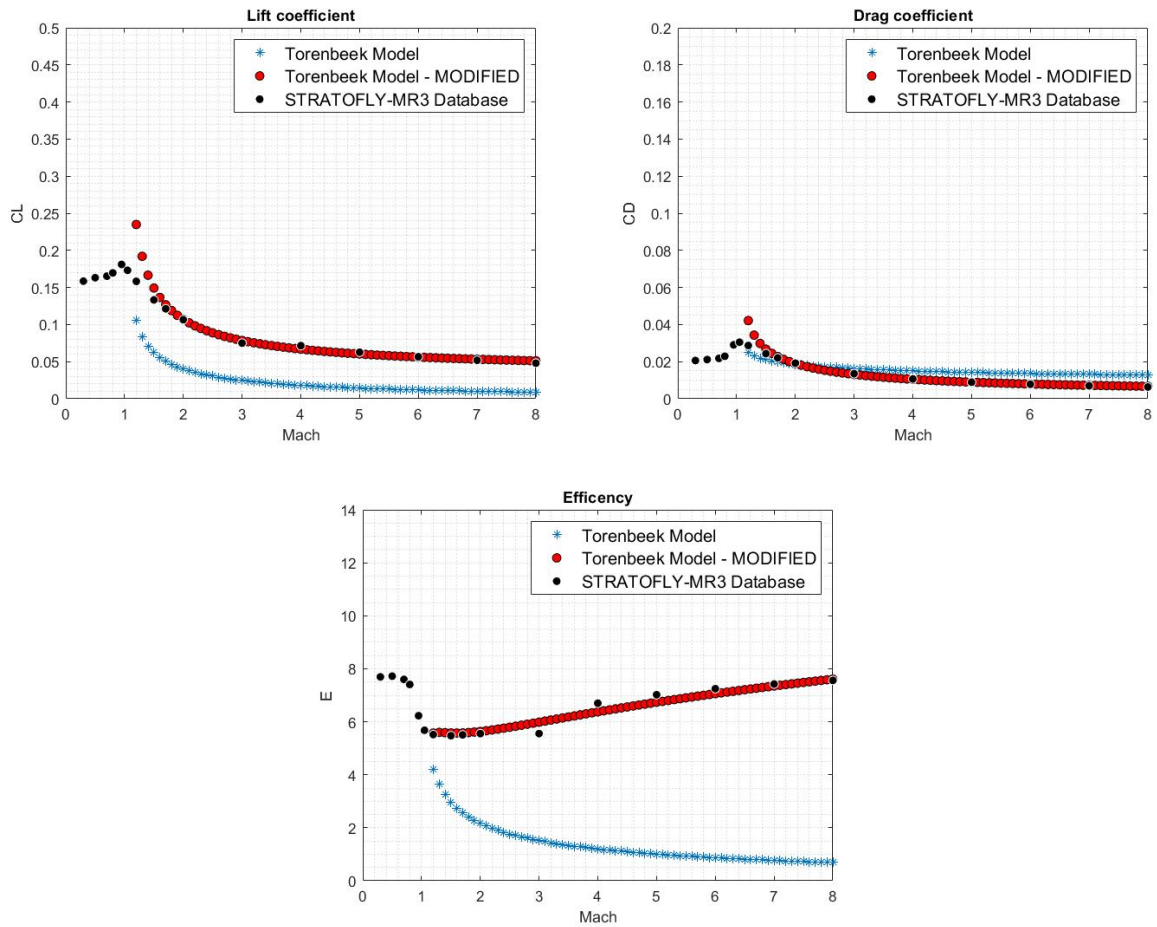


Figure 3.10. Aerodynamic coefficients of the basic Torenbeek Model compared with the aerodynamic coefficients of the modified Torenbeek Model

The geometrical input are reported in the table (3.1) and the results of the basic Torenbeek model for a blended body configuration are shown by the light blue curve in the figure (3.10). As can be seen, for an angle of attack equal to 1° and an Engine - ON condition there is an underestimation of the lift coefficient for all the supersonic flight regime while the drag coefficient represents quite closely the real

behaviour. The explanation is always the same: the model has been theorised for a blended body concept so it fails to capture the positive effects of the compression lift that a waverider configuration presents.

Thanks to the corrective coefficients shown in the table (3.5), the curve trends are improved and the final results are now much more reliable throughout the supersonic regime (red curves).

TORENBEEK MODEL		
α	Flight Regime	Corrective Coefficients
$\alpha = 1^\circ$	<i>Supersonic</i>	<ul style="list-style-type: none"> • CL: (eq.2.66)·(1.6 + $M/1.9$); • CD: (eq.2.71)·(1.15/$\log(1.2 \cdot M + 1.3)$);
$\alpha = 2^\circ$	<i>Supersonic</i>	<ul style="list-style-type: none"> • CL: (eq.2.66)·(0.95 + $M/3$); • CD: (eq.2.71)·(1.5/$\log(1.2 \cdot M + 2)$);
$\alpha = 3^\circ$	<i>Supersonic</i>	<ul style="list-style-type: none"> • CL: (eq.2.66)·(0.6 + $M/3.56$); • CD: (eq.2.71)·(2.1/$\log(1.8 \cdot M + 3)$);
$\alpha = 4^\circ$	<i>Supersonic</i>	<ul style="list-style-type: none"> • CL: (eq.2.66)·(0.6 + $M/4.4$); • CD: (eq.2.71)·(2.4/$\log(1.8 \cdot M + 3)$);
$\alpha = 5^\circ$	<i>Supersonic</i>	<ul style="list-style-type: none"> • CL: (eq.2.66)·(0.58 + $M/5$); • CD: (eq.2.71)·(2.8/$\log(1.8 \cdot M + 3)$);

Table 3.5: Torenbeek Model Corrective Coefficients for the all angles of attack analysed, Engine - ON condition

The curve trends for the all angles of attack analysed are reported in the figures (3.11, 3.12) for the Engine - ON condition and in the figures (3.13, 3.14) for the Engine - OFF condition.

3.1.6 Engine - ON Final Results

In the previous four chapters, the results of the aerodynamic models for the STRATOFly MR3 vehicle were analysed. The comparison was made with the AEDB values for the engine - ON condition. The procedure followed to derive the correction coefficients has been explained and all of them are reported for each model; however, only a few curves were presented as examples.

In the following figures (3.11, 3.12), it is possible to confirm that the results obtained in the engine - ON condition are reliable for the all angles of attack analysed, ranging from 1° to 5° .

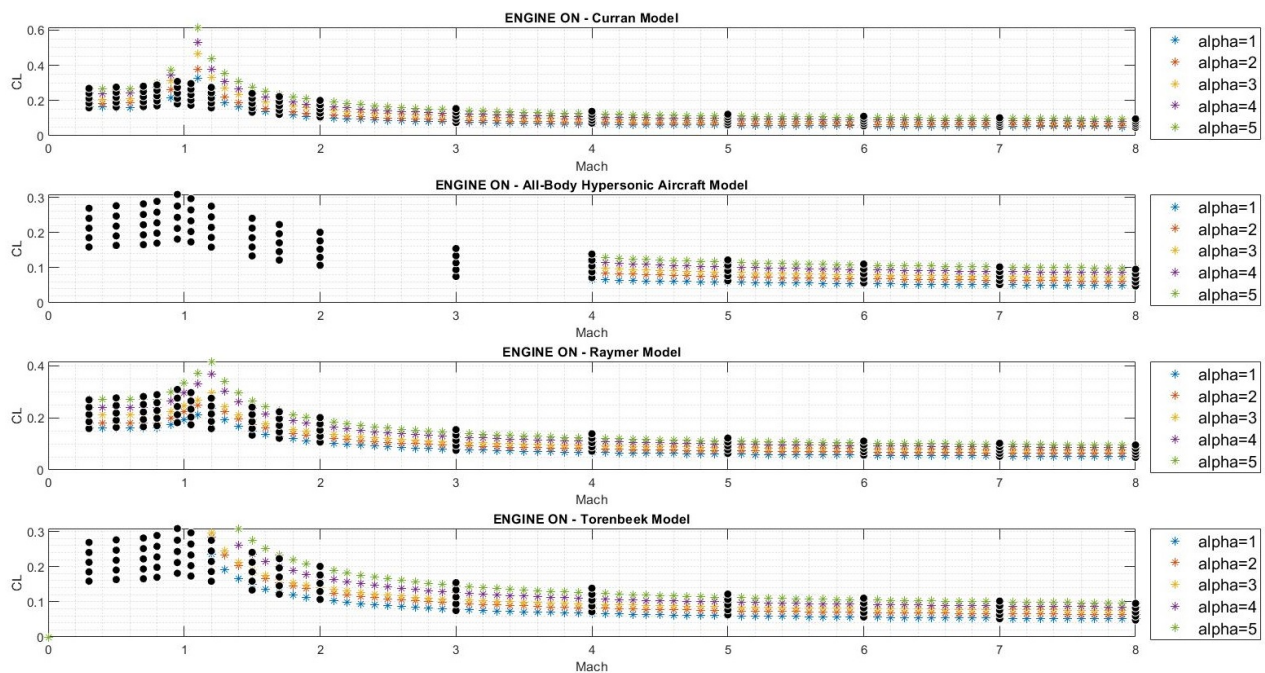


Figure 3.11. Lift Coefficient - Engine ON condition - Mach and Alpha variation

Thanks to the corrective coefficients, in a preliminary design phase it is therefore possible to estimate the aerodynamic behaviour of the STRATOFly MR3 with a good precision. In particular, the Curran Model and the Raymer Model allow the analysis for the all flight regimes, the Torenbeek model only for the supersonic regime and the All-Body Hypersonic Aircraft Model only for hypersonic flight regime.

Final Aerodynamic Models

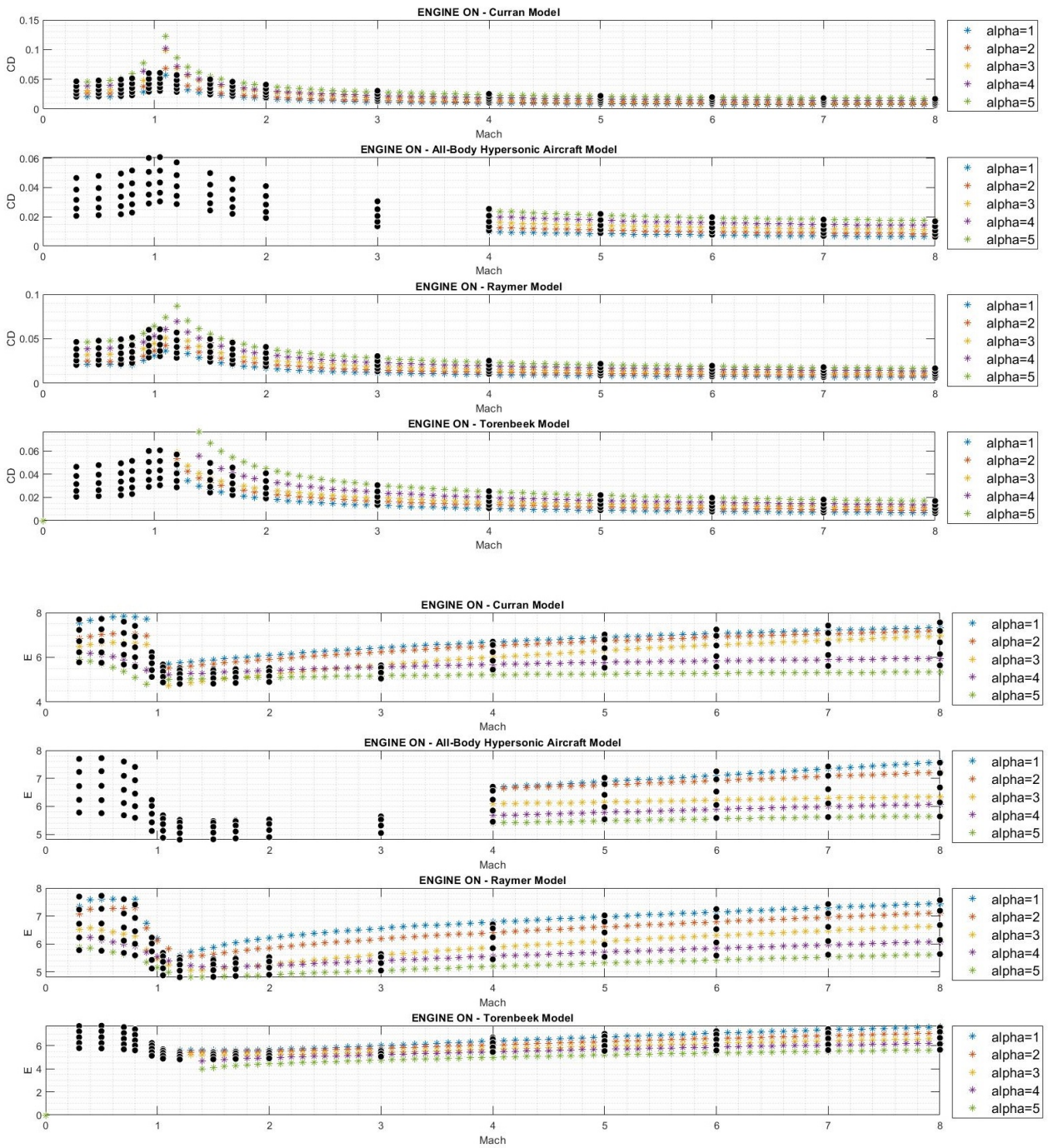


Figure 3.12. Drag Coefficient and Efficiency - Engine ON condition - Mach and Alpha variation

3.1.7 Engine - OFF Final Results

In conclusion, the models are also tested and validated for the case in which the engines are switched off. As explained in the chapter (3.1.1), the reference aerodynamic coefficients for this operating condition are taken from the AEDB, considering for both CL and CD the "External+Internal" contribution. It is therefore clear that the lift coefficient will be the same as in the engine - OFF condition, as can be seen in the graphs (3.4, 3.5): the corrective coefficients are the same. As far as drag is concerned, all the added coefficients are shown in the table below (3.6).

CURRAN MODEL		
α	Flight Regime	Corrective Coefficients
$\alpha = 1^\circ$	<i>Subsonic</i>	<ul style="list-style-type: none"> • CD: (eq.2.4)·(0.48 – 0.21 · M);
$\alpha = 1^\circ$	<i>Supersonic</i>	<ul style="list-style-type: none"> • CD: (eq.2.4)·(0.5 + M/24);
$\alpha = 2^\circ$	<i>Subsonic</i>	<ul style="list-style-type: none"> • CD: (eq.2.4)·(0.5 – 0.18 · M);
$\alpha = 2^\circ$	<i>Supersonic</i>	<ul style="list-style-type: none"> • CD: (eq.2.4)·(0.45 + M/15);
$\alpha = 3^\circ$	<i>Subsonic</i>	<ul style="list-style-type: none"> • CD: (eq.2.4)·(0.56 – 0.18 · M);
$\alpha = 3^\circ$	<i>Supersonic</i>	<ul style="list-style-type: none"> • CD: (eq.2.4)·(0.56 + M/13);
$\alpha = 4^\circ$	<i>Subsonic</i>	<ul style="list-style-type: none"> • CD: (eq.2.4)·(0.64 – 0.21 · M);
$\alpha = 4^\circ$	<i>Supersonic</i>	<ul style="list-style-type: none"> • CD: (eq.2.4)·(0.63 + M/10);
$\alpha = 5^\circ$	<i>Subsonic</i>	<ul style="list-style-type: none"> • CD: (eq.2.4)·(0.75 – 0.3 · M);
$\alpha = 5^\circ$	<i>Supersonic</i>	<ul style="list-style-type: none"> • CD: (eq.2.4)·(0.72 + M/7.5);
ALL - BODY HYPERSONIC AIRCRAFT MODEL		
$\alpha = 1^\circ$	<i>Subsonic</i>	<ul style="list-style-type: none"> • CD: (eq.2.12)+0.032;
$\alpha = 1^\circ$	<i>Supersonic</i>	<ul style="list-style-type: none"> • CD: (eq.2.12)·(0.9 + M/20);
$\alpha = 2^\circ$	<i>Subsonic</i>	<ul style="list-style-type: none"> • CD: (eq.2.12)+0.035;
$\alpha = 2^\circ$	<i>Supersonic</i>	<ul style="list-style-type: none"> • CD: (eq.2.12)·(0.95 + M/19);
$\alpha = 3^\circ$	<i>Subsonic</i>	<ul style="list-style-type: none"> • CD: (eq.2.12)+0.039;
$\alpha = 3^\circ$	<i>Supersonic</i>	<ul style="list-style-type: none"> • CD: (eq.2.12)·(0.97 + M/19);
$\alpha = 4^\circ$	<i>Subsonic</i>	<ul style="list-style-type: none"> • CD: (eq.2.12)+0.042;
$\alpha = 4^\circ$	<i>Supersonic</i>	<ul style="list-style-type: none"> • CD: (eq.2.12)·(0.98 + M/19);

$\alpha = 5^\circ$	<i>Subsonic</i>	<ul style="list-style-type: none"> • CD: (eq.2.12)+0.048;
$\alpha = 5^\circ$	<i>Supersonic</i>	<ul style="list-style-type: none"> • CD: (eq.2.12)·(1 + M/19);
RAYMER MODEL		
$\alpha = 1^\circ$	<i>Subsonic</i>	<ul style="list-style-type: none"> • CD: (eq.2.43)·0.89;
$\alpha = 1^\circ$	<i>Supersonic</i>	<ul style="list-style-type: none"> • CD: (eq.2.43)·(0.7/log(1.7 · M - 0.6));
$\alpha = 2^\circ$	<i>Subsonic</i>	<ul style="list-style-type: none"> • CD: (eq.2.43)·0.75;
$\alpha = 2^\circ$	<i>Supersonic</i>	<ul style="list-style-type: none"> • CD: (eq.2.43)·(0.82/log(1.65 · M - 0.5));
$\alpha = 3^\circ$	<i>Subsonic</i>	<ul style="list-style-type: none"> • CD: (eq.2.43)·0.65;
$\alpha = 3^\circ$	<i>Supersonic</i>	<ul style="list-style-type: none"> • CD: (eq.2.43)·(0.94/log(1.65 · M - 0.5));
$\alpha = 4^\circ$	<i>Subsonic</i>	<ul style="list-style-type: none"> • CD: (eq.2.43)·0.55;
$\alpha = 4^\circ$	<i>Supersonic</i>	<ul style="list-style-type: none"> • CD: (eq.2.43)·(1.15/log(1.65 · M - 0.5));
$\alpha = 5^\circ$	<i>Subsonic</i>	<ul style="list-style-type: none"> • CD: (eq.2.43)·0.50;
$\alpha = 5^\circ$	<i>Supersonic</i>	<ul style="list-style-type: none"> • CD: (eq.2.43)·(1.4/log(1.7 · M - 0.4));
TORENBEEK MODEL		
$\alpha = 1^\circ$	<i>Supersonic</i>	<ul style="list-style-type: none"> • CD: (eq.2.71)·(1.4/log(1.2 · M + 0.7));
$\alpha = 2^\circ$	<i>Supersonic</i>	<ul style="list-style-type: none"> • CD: (eq.2.71)·(1.65/log(1.2 · M + 0.7));
$\alpha = 3^\circ$	<i>Supersonic</i>	<ul style="list-style-type: none"> • CD: (eq.2.71)·(1.95/log(1.2 · M + 1.1));
$\alpha = 4^\circ$	<i>Supersonic</i>	<ul style="list-style-type: none"> • CD: (eq.2.71)·(2.35/log(1.2 · M + 2));
$\alpha = 5^\circ$	<i>Supersonic</i>	<ul style="list-style-type: none"> • CD: (eq.2.71)·(3.2/log(1.8 · M + 3));

Table 3.6: Corrective Coefficients for the all angles of attack analysed, Engine - OFF condition

How it's possible to see from the figure below (3.13, 3.14), even for this operative condition it is possible to have an accurate estimate in a preliminary design stage. the range of applicability of the models is the same as in the previous case: the Curran Model and the Raymer Model allow the analysis for the all flight regimes, the Torenbeek model only for the supersonic regime and the All-Body Hypersonic Aircraft Model only for hypersonic flight regime.

Final Aerodynamic Models

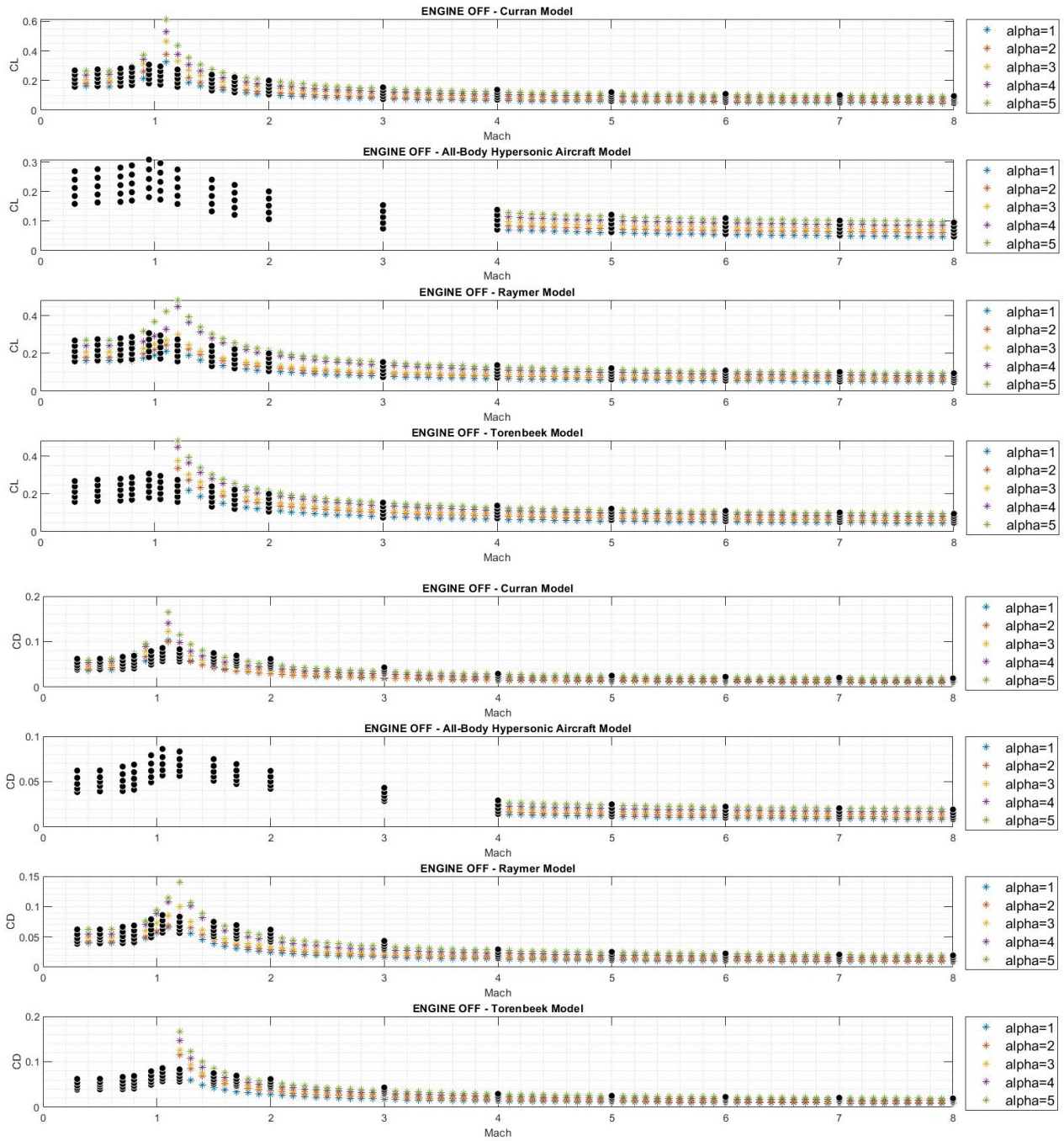


Figure 3.13. Lift Coefficient and Drag Coefficient - Engine OFF condition - Mach and Alpha variation

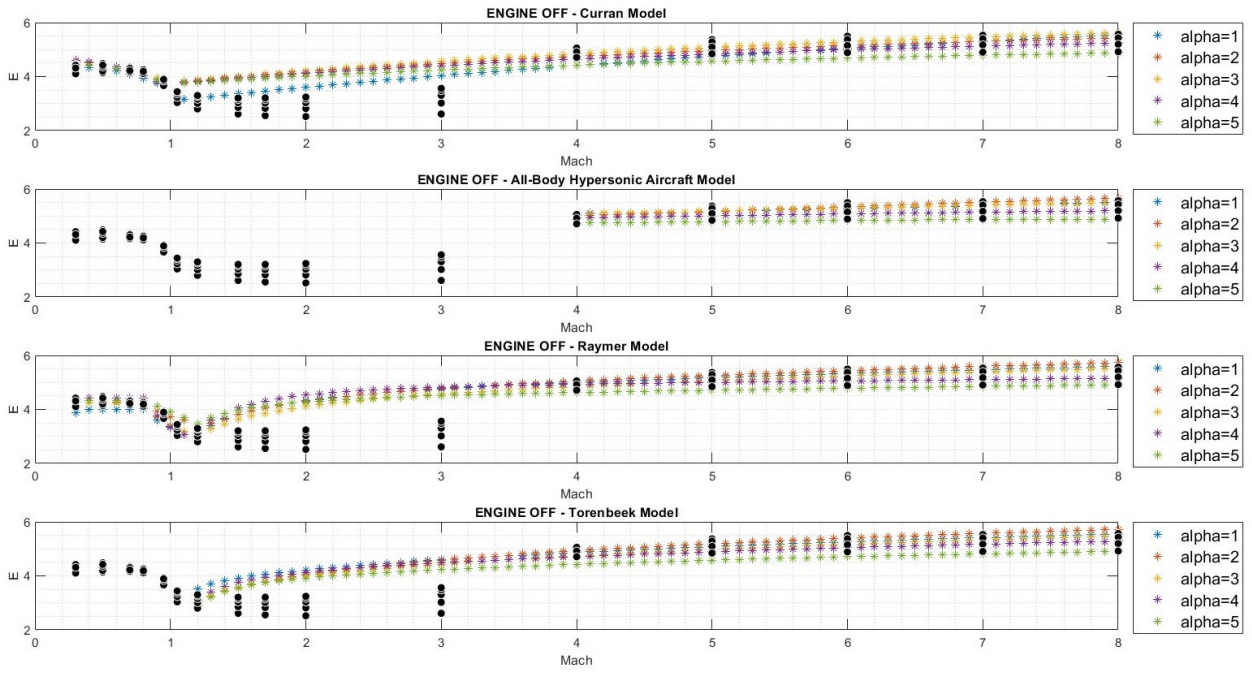


Figure 3.14. Efficiency - Engine OFF condition - Mach and Alpha variation

3.2 Ventral Waverider Configuration

In the previous section the Dorsal waverider configuration was analysed, thanks to the STRATOFly MR3 vehicle case study; the next subfamily is the ventral one, described below.

This configuration has the same basic characteristics as the previous one, with the main difference being the position of the propulsion system, which is installed in the lower part of the aircraft. Looking at the figure 3.15, where the X-43A vehicle is depicted, it's clear that this concept has some disadvantages. First of all, the engine is external to the main body and consequently represents an obstacle to the airflow: this avoids to maximize the available under surface for lift generation with additional drag penalties. Secondly, this leads to an increase in drag due to negative interference effects.

In order to reduce the size of the propulsion system package (including the inlet capture area) and all its disadvantages, forebody pre-compression is employed, achieved by an inclination of the undersurface ahead of the inlet. Another aspect to be considered for the propulsion package dimension is the exhaust nozzle: it requires a large area due to the high pressure ratio. However, a classical engine's bell cannot be utilized because it would be too large and consequently a high wave drag would appear. The way out is the employment of the rear undersurface, which essentially acts as an asymmetric external nozzle.

In the following pages, the Ventral waverider is analysed, thanks to the NASA X-43A vehicle case study.

3.2.1 NASA X-43A

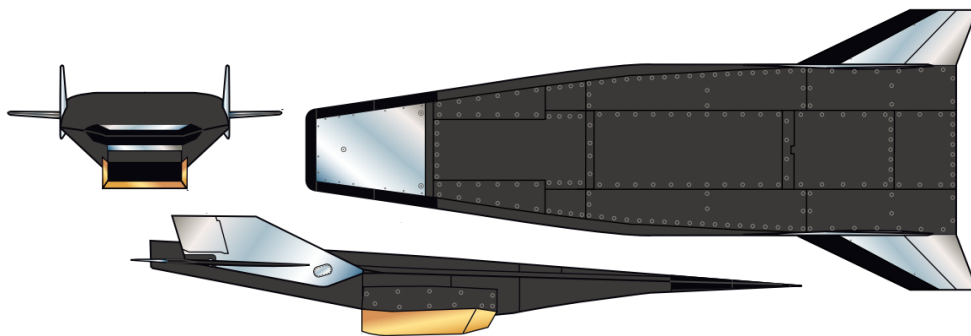


Figure 3.15. X-43A vehicle configuration [11]

In 1996 NASA launched the Hyper-X Program, a jointly conducted effort by the NASA Langley Research Center (LaRC) and the NASA Dryden Flight Research Center (DFRC), with the aim of moving scramjet research from the laboratory to the flight domain. In particular, the main objective was to demonstrate and

validate technologies, experimental techniques, methods and computational tools for the design and performance prediction of hypersonic aircraft with a scramjet propulsion system highly integrated into the airframe [13].

In order to accomplish this goal, it was necessary to develop an experimental research scramjet hypersonic aircraft called X-43A (also known as Hyper-x vehicle), whose concept is reported in the figure above (3.15). As can be seen, it consists of a waverider configuration with an highly integrated propulsion system, located in the undersurface of the vehicle, slightly aft the midbody. This solution makes it possible to use the lower part of the front body as compression surface and the lower part of the rear body as expansion surface for the scramjet exhaust flow.

GEOMETRICAL DATA		Value
Total volume	V_{tot}	0.267 [m ³]
Planform surface	S_{plan}	2.3 [m ²]
Wetted surface	S_{wet}	5.5 [m ²]
Exposed surface	$S_{Exposed}$	0.57 [m ²]
Wing span	$span$	1.52 [m]
Wing length	l_{wing}	1.93 [m]
Fuselage length	$l_{fuselage}$	3.66 [m]
Fuselage diameter	$d_{fuselage}$	0.2 [m]
Nose length	l_{nose}	0.7 [m]
Tail length	l_{tail}	0.94 [m]
Maximum cross-sectional area	S_{max}	0.3 [m ²]
Mean aerodynamic chord of the wing	MAC_{wing}	1.5 [m]
Leading edge sweep angle of the wing	λ_w	66 [°]
Trailing edge sweep angle of the wing	λ_{te}	5 [°]
Wing thickness ratio	$(t/c)_{wing}$	0.057 none
Nacelle length	$l_{nacelle}$	0.76 [m]
Nacelle diameter	$d_{nacelle}$	0.32 [m]
Vertical tail thickness ratio	$(t/c)_{Vtail}$	0.05 none
Vertical tail surface	S_{Vtail}	0.28 [m ²]
Vertical tail span	b_{Vtail}	0.35 [m]
Leading edge sweep angle of the Vertical tail	λ_{Vtail}	60 [°]
Mean aerodynamic chord of the Vertical tail	MAC_{Vtail}	0.8 [m]
Vertical tail number	$Vtail_{number}$	2 none

Table 3.7. X-43A geometrical data

The aircraft was approximately 3.66 meters long with a wing span of 1.52 m and a leading-edge sweep angle of 66° [11]. All the main geometrical specifications are reported in the table above (3.7).

During this programme, three X-43A vehicles were built: the first two were scheduled to fly at Mach 7 whereas the third was to reach a speed of Mach 10. In order

to achieve this ambitious goal, each of the three X-43A vehicles was individually boosted to the scramjet engine test points on a modified versions of the Pegasus Hybrid rocket first stage, which took the name of Hyper-X LaunchVehicle (HXLV). In conclusion, the Hyper-X programme was crucial for NASA to consolidate the knowledge acquired about scramjet technologies after decades of research, giving an important contribute for future developments.

In the following subsections, all the models' results are presented and compared to the aerodynamic data of the vehicle under consideration, taken from the references [12], [13].

3.2.2 Results

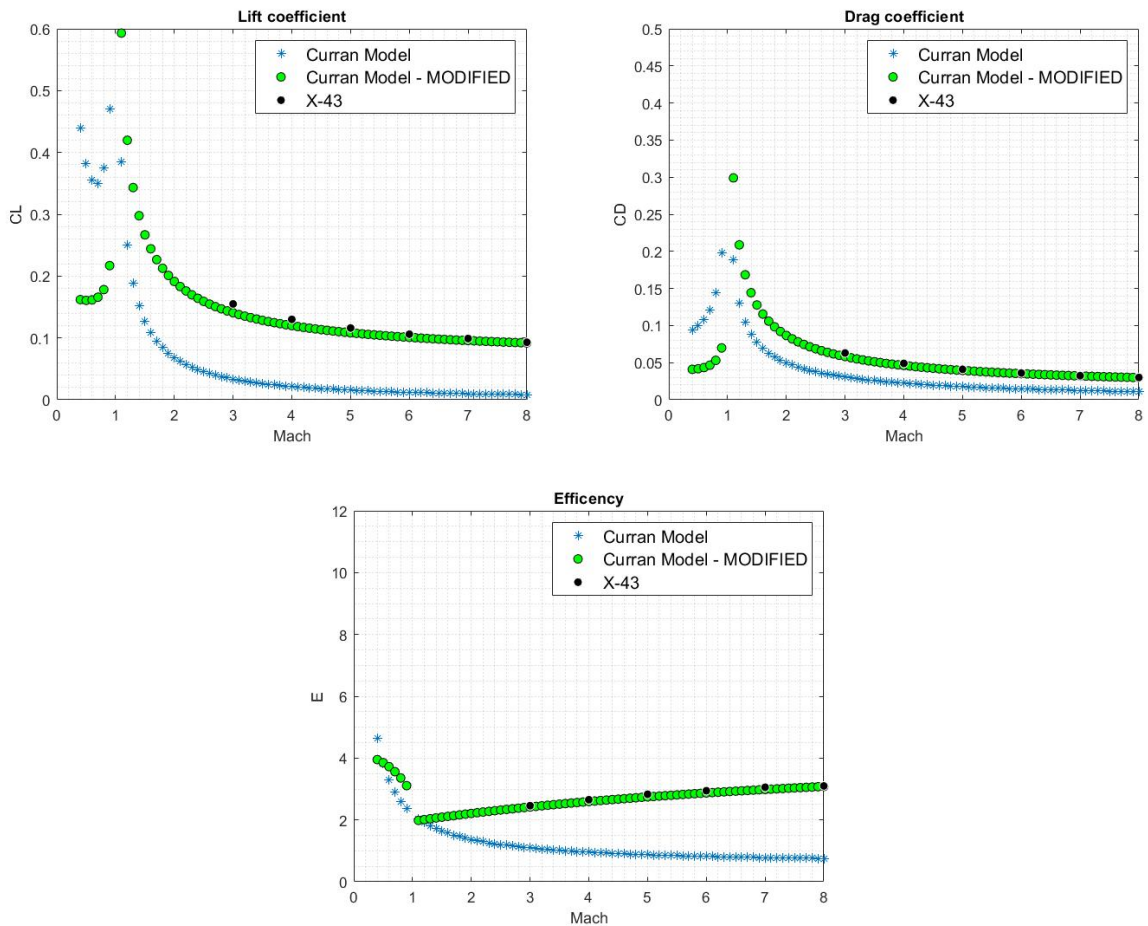


Figure 3.16. Aerodynamic coefficients of the basic Curran Model compared with the aerodynamic coefficients of the modified Curran Model for ventral waverider configuration

The Curran model is the first to be tested and analysed.

In the case of the X-43A vehicle, the Küchemann's τ is equal to 0.0765 and the wetted to planform surface ratio K_w is 2.4913. They are very similar to the STRATOFly parameters, because these vehicles are both classified as "waverider", in agreement with the graph 3.1 in the chapter 3.

The aerodynamic coefficients obtained for an angle of attack equal to 5° are shown in the figure 3.16. As can be seen, there is an underestimation of both the lift coefficient and the drag coefficient. This discrepancy of the results can be attributed to the very small amount of input data useful for the characterisation of the aircraft being analysed. Furthermore, the X-43A database is related to an angle of attack equal to 5° , so the coefficients values are high. However, the Curran model does not depend on this parameter, so the underestimation is also due to this fact.

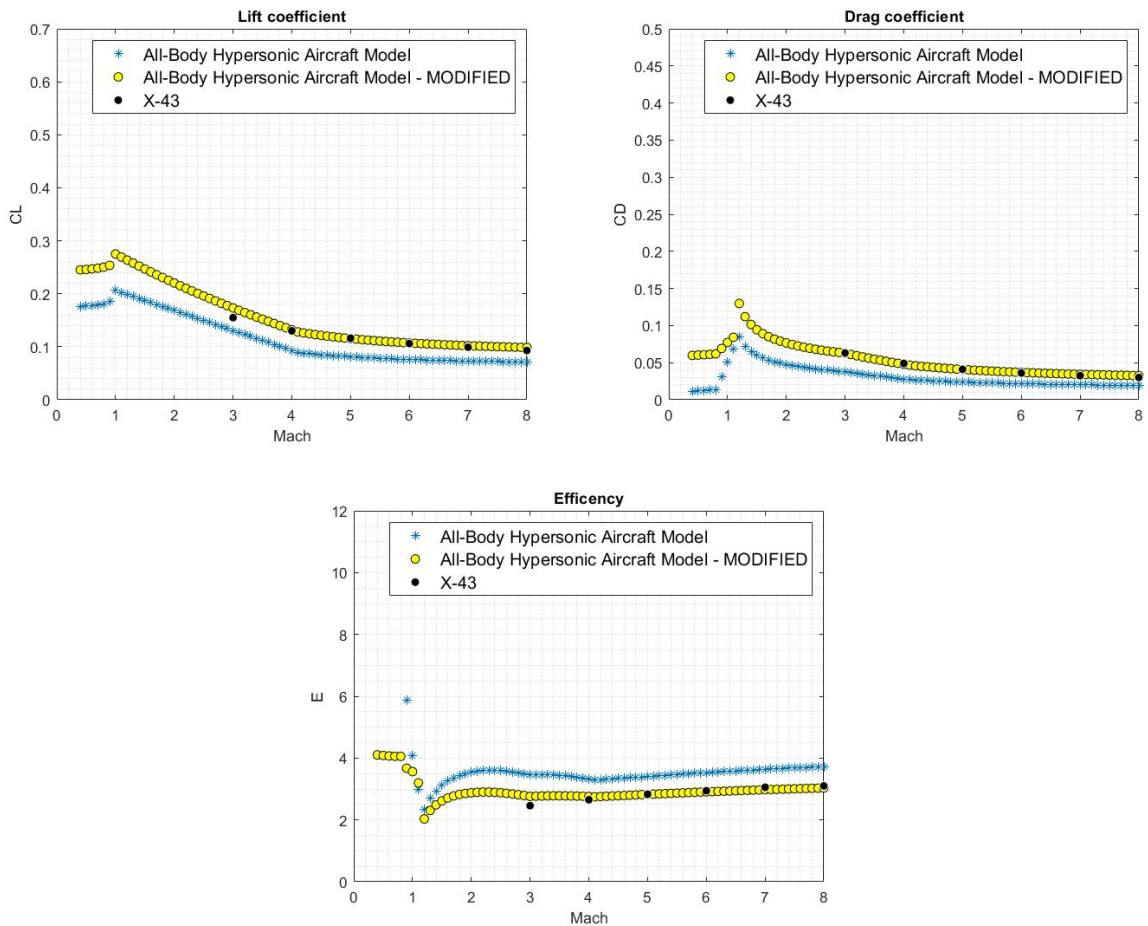


Figure 3.17. Aerodynamic coefficients of the basic All-Body Hypersonic Aircraft Model compared with the aerodynamic coefficients of the modified All-Body Hypersonic Aircraft Model for ventral waverider configuration

The All-Body Hypersonic Aircraft Model is the second to be analysed. It was theorised for a reference configuration which is quite close to the vehicle under study. Looking at the figure 3.15, in fact, it is possible to see that there is not a clear distinction between fuselage and wing, which are however small and installed in the rear position of the vehicle. Despite these aspects, the X-43A is a waverider concept, with all its benefits, like the compression lift.

The figure above (3.17) shows the results obtained with the geometrical data listed in the table 3.7. The underestimation of the Lift coefficient can be attributed to the compression lift phenomenon which is characteristic of this concept but doesn't occur for a blended body configuration.

Unlike the previous model, the Raymer one was generated for a conventional aircraft, with a clear distinction between fuselage and wings.

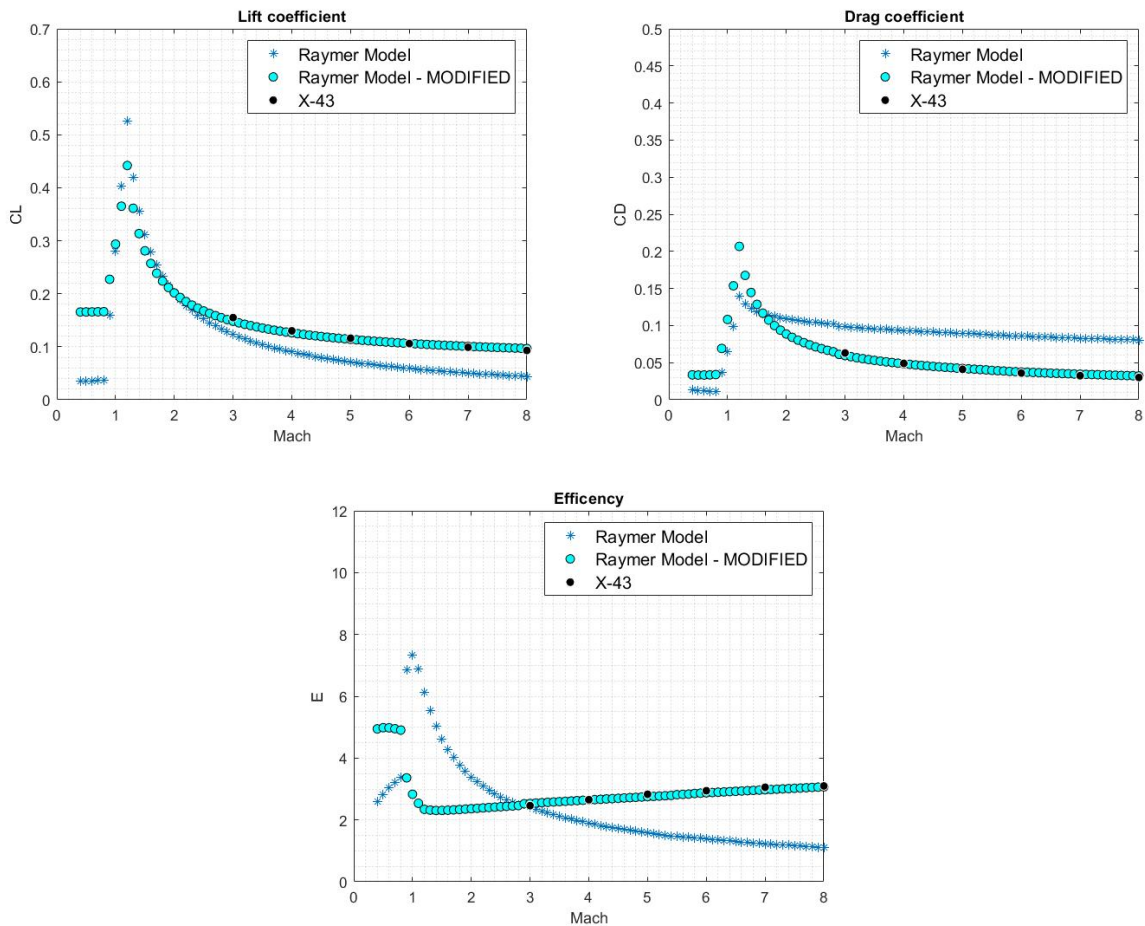


Figure 3.18. Aerodynamic coefficients of the basic Raymer Model compared with the aerodynamic coefficients of the modified Raymer Model for ventral waverider configuration

This concept is therefore totally different from the X-43A vehicle. As can be seen in the graphs above (fig. 3.18), the estimation of the aerodynamic coefficients reflects this aspects. In particular, the Drag coefficient is overestimated because the vehicle under study is more slender than a generic high speed aircraft with a clear distinction between fuselage and wing, and consequently the wave drag is lower. The lift is underestimated because the increment due to the compression lift phenomenon is not considered by this method. The observations made for the previous model are still valid for the Torenbeek one. The latter allows the estimation of the aerodynamic coefficients for a generic high speed aircraft configuration with a delta wing, a generic high speed aircraft configuration with an arrow wing and a blended wing body configuration.

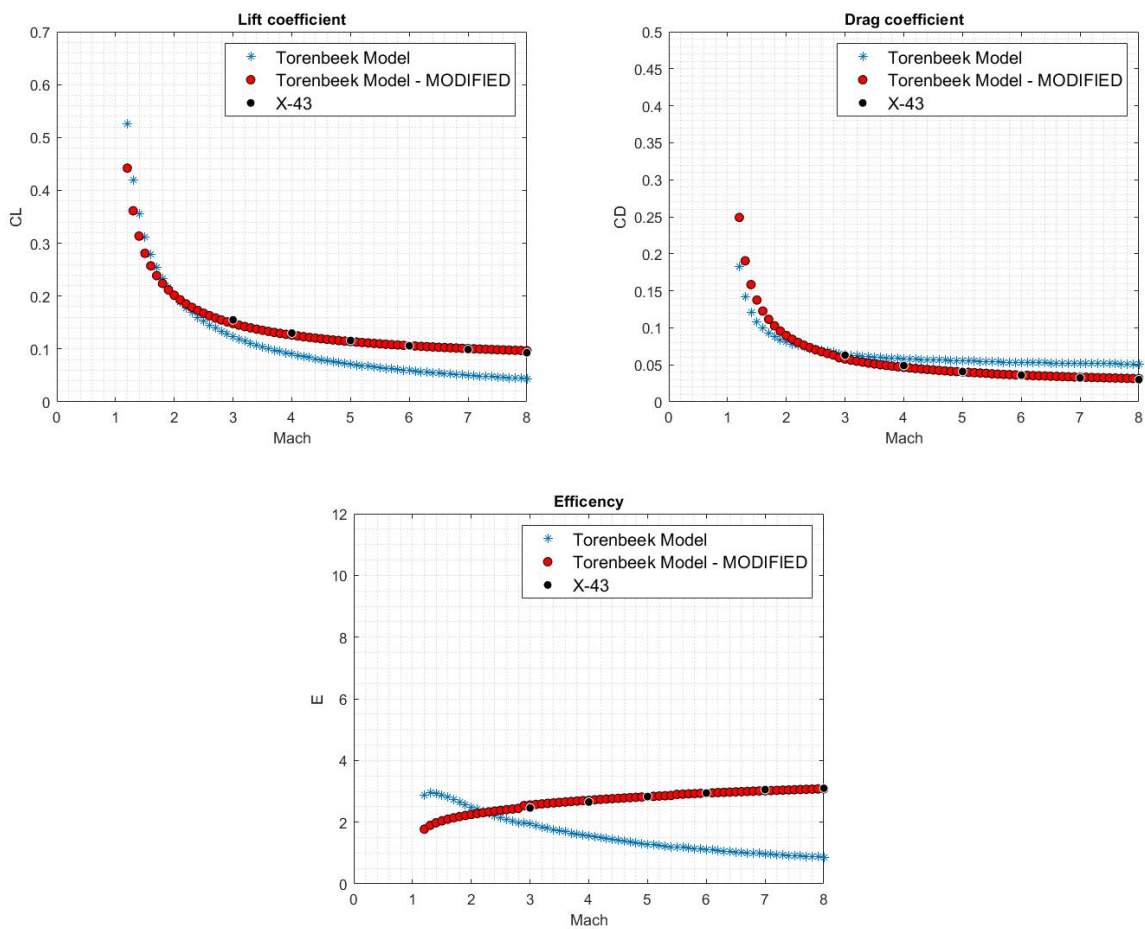


Figure 3.19. Aerodynamic coefficients of the basic Torenbeek Model compared with the aerodynamic coefficients of the modified Torenbeek Model for ventral waverider configuration

In this case, given the X-43A geometry, the results of the blended body concept

(the closest to a waverider) are shown in the figure 3.19 with the light blue curves. In order to improve the results, the corrective coefficients reported in the table below (3.8) were added to the basic models. the final curves trend is good, as can be seen in the figures 3.16, 3.17, 3.18, 3.19 with the green, yellow, cyan and red curves respectively. In particular it is possible to affirm that the Curran and Raymer model are applicable for the all flight regimes, the All-Body Hypersonic Aircraft model is reliable only for the subsonic regime and the high supersonic one and finally the Torenbeek model is valid for the supersonic flight regime.

CURRAN MODEL	
Flight Regime	Corrective Coefficients
<i>Subsonic</i>	<ul style="list-style-type: none"> • CL: (eq.2.6)·(12.5 – 8.2 · M); • CD: (eq.2.4)·(0.5 – 0.165 · M);
<i>Supersonic</i>	<ul style="list-style-type: none"> • CL: (eq.2.6)·M · 1.4; • CD: (eq.2.4)·(1.4 + M/6);
ALL BODY HYPERSONIC AIRCRAFT MODEL	
<i>Subsonic</i>	<ul style="list-style-type: none"> • CL, (eq.2.11): $c_1 \cdot 2$; • CD: (eq.2.12)+0.05;
<i>Supersonic</i>	<ul style="list-style-type: none"> • CL, (eq.2.11): $c_1 \cdot 1.15, c_2 \cdot 5$; • CD: (eq.2.12)·(2.2 + M/25);
RAYMER MODEL	
<i>Subsonic</i>	<ul style="list-style-type: none"> • CL: (eq.2.37)+0.13; • CD: (eq.2.43)·(1.15 + M/2);
<i>Supersonic</i>	<ul style="list-style-type: none"> • CL: (eq.2.37)·(0.6 + M/5); • CD: (eq.2.43)·(1.6/log(2 · M – 0.4));
TORENBEEK MODEL	
<i>Supersonic</i>	<ul style="list-style-type: none"> • CL: (eq.2.66)·(0.6 + M/5); • CD: (eq.2.71)·(1.7/(log(2 · M + 0.4)));

Table 3.8: Corrective coefficients for ventral waverider configuration

3.3 High - AR Wing Body Configuration

The Wing Body configuration is the most conventional of those analysed, with a clear distinction between fuselage and wings.

For high-speed aircraft, the appearance of shock waves can adversely affect both the lift and drag characteristics. In these cases, the flow speed can be higher than the speed of sound even when the aircraft is flying at subsonic regime. In order to minimize the shock wave effects, wings generally have a leading edge sweep angle, which allows the perpendicular component of the incoming flow to be reduced: higher flight speeds are achievable with delta wings. In addition, this concept allows to remain within the Mach cone generated from the nose, so that the wing does not penetrate this shock wave and develop a lower drag.

Given the clear distinction between the wings and the main body of the aircraft, there is a negative interference effect, which leads to greater drag. For this reason, lower efficiency is expected if compared to a waverider concept.

In the following pages, three vehicles are analysed. In order to improve the estimation, this configurational family can be divided into two subfamilies, depending on the aspect ratio. In particular, inside the High AR Wing-Body configuration are grouped the USV-FTB-1 and X-34, which have an aspect ratio greater than 2. Instead, in the Low AR Wing-Body configuration the HYPLANE is shown, due to its aspect ratio, which is lower than 2.

3.3.1 X-34

In 1996 NASA launched a new activity called Reusable Launch Vehicle (RLV) Technology Program, a partnership among NASA, the U.S. Air Force and private industry.

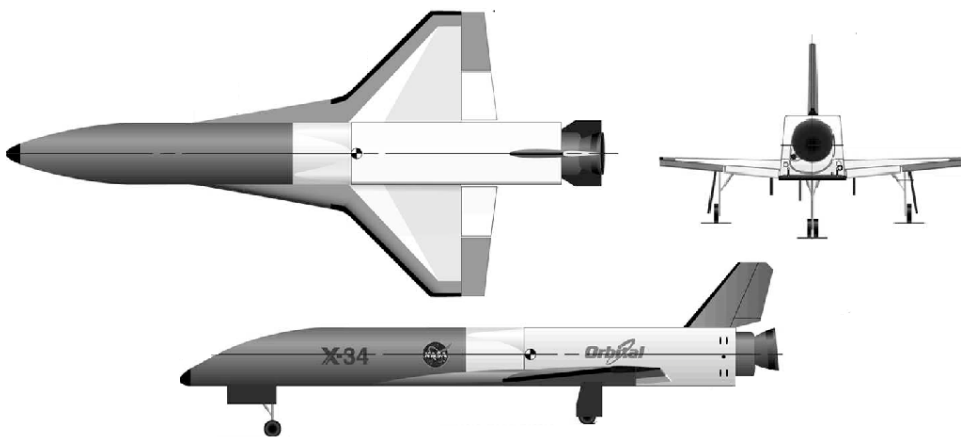


Figure 3.20. X-34 vehicle configuration

The main objective was to develop and test new concepts with three specific experimental vehicles, in order to significantly increase reliability and to lower the access to space costs. The intention was to prove the feasibility of the SSTO-RLV configurations and "advanced key technologies", necessary for the design and operation of a future reusable launch vehicle. One of these three experimental vehicles was the X-34A, developed by the Orbital Sciences Corporation [14].

As can be seen in the figure 3.20, it consists of an unmanned wing-body aircraft with a double delta wing (45° sweep of the main surface and a 80° of the leading edge strake), a wing span of 8.45 m, a total length of approximately 17 m, a reference surface of 33.2 m² and an Aspect Ratio of $AR = 2.15$. All the main X-34A geometrical specifications are reported in the table (3.9).

GEOMETRICAL DATA		Value
Total volume	V_{tot}	44 [m ³]
Reference surface	S_{plan}	33.2 [m ²]
Wetted surface	S_{wet}	106 [m ²]
Exposed surface	$S_{Exposed}$	19.9 [m ²]
Wing span	$span$	8.45 [m]
Fuselage length	$l_{fuselage}$	16.4 [m]
Fuselage diameter	$d_{fuselage}$	0.96 [m]
Nose length	l_{nose}	2.8 [m]
Tail length	l_{tail}	1.1 [m]
Maximum cross-sectional area	S_{max}	7 [m ²]
Mean aerodynamic chord of the wing	MAC_{wing}	5 [m]
Leading edge sweep angle of the wing	λ_w	65 [°]
Trailing edge sweep angle of the wing	λ_{te}	0 [°]
Wing thickness ratio	$(t/c)_{wing}$	0.096 none
Flap span	$Flap_{span}$	3.18 [m]
Vertical tail thickness ratio	$(t/c)_{Vtail}$	0.19 none
Vertical tail surface	S_{Vtail}	2.3 [m ²]
Vertical tail span	b_{Vtail}	1.9 [m]
Leading edge sweep angle of the Vertical tail	λ_{Vtail}	40 [°]
Mean aerodynamic chord of the Vertical tail	MAC_{Vtail}	1.6 [m]
Vertical tail number	$Vtail_{number}$	1 none

Table 3.9. X-34 geometrical data

It is designed to be launched from Orbital Sciences Corp.'s L-1011 (a specially modified commercial jetliner), ignite its engine and fly a pre-programmed profile reaching a speed of Mach number 8 and altitudes of approximately 50 miles. After that, it is able to do an automated approach and landing on a conventional runway.

The single stage vehicle used NASA's low cost Fastrac engine that burns a mixture of liquid oxygen and kerosene and is able to provide 267,000 N of thrust.

Key technologies planned for demonstration on the X-34 were many, including lightweight composite airframe structures that required little inspection; reusable composite propellant tanks; advanced thermal protection systems; integrated (built-in) low-cost avionics, including differential Global Positioning System and Inertial Navigation System; integrated automated vehicle health monitoring and others.

The reference database used to compare the models' results was obtained from investigations carried out in the wind tunnels at NASA Langley Research Centre [14].

3.3.2 PRORA USV-FTB-1

The Aerospace Research Program PRORA was launched in 2000 by Italy and entrusted to Italian Aerospace Research Center (CIRA), in order to improve the technology basis and the system cognitions about the transportation of space vehicles into Earth's orbits.

In this context, the Unmanned Space Vehicle (USV)-Flight Test Bed 1 (FTB-1) was developed, in order to perform many tasks, such as atmospheric re-entry, reusability and sustained hypersonic flight. During the missions, an aerostatic balloon brought the USV up to the desired altitude and then, after establishing a horizontal cruise trajectory, released it. At this point, the vehicle would begin its experimental flight along the programmed trajectory, in order to investigate many aspects like aerodynamics, structure and materials, autonomous guidance, navigation and control. The final landing was to be conducted by a parachute system either at sea or on ground [15].

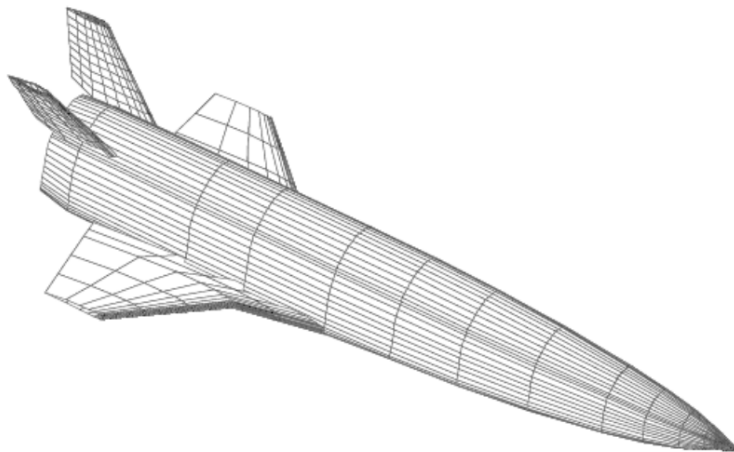


Figure 3.21. PRORA USV-FTB-1 vehicle configuration [16]

As can be seen in the figure 3.21, it consists of a winged body vehicle, with an overall length of about 8 m from the nose apex up to the base plate. The fuselage has a compact cross-section with a quasi-conical nose, a quasi-constant middle section and an afterbody which ends with a truncated base. The wing shape is a double delta one, with a sweep angle of 45 and 76 degrees whereas the trailing edge is characterized by a sweepforward angle of 6°. In order to improve control and directional stability, two vertical tails are installed on the rear part of the fuselage, with a dihedral angle of 40° and a leading-edge sweep angle of 45°. On the wing is installed an elevon which can operate as either an aileron for roll control and an elevator for pitch control. The Aspect Ratio is equal to $AR = 2.10$ and all the other main geometrical data are reported in the table below (3.10). The aerodynamic data for USV FTB-1 stem mainly from wind tunnel tests; In addition, a large number of CFD simulations has been performed in order to support the extrapolation to flight of wind tunnel measurements, and to fill gaps in experimental data [17].

GEOMETRICAL DATA		Value
Total volume	V_{tot}	3.2 [m ³]
Reference surface	S_{plan}	6 [m ²]
Wetted surface	S_{wet}	20 [m ²]
Exposed surface	$S_{Exposed}$	3.6 [m ²]
Wing span	$span$	3.5 [m]
Fuselage length	$l_{fuselage}$	7.8 [m]
Fuselage diameter	$d_{fuselage}$	0.47 [m]
Nose length	l_{nose}	4.2 [m]
Tail length	l_{tail}	1.3 [m]
Maximum cross-sectional area	S_{max}	1.5 [m ²]
Mean aerodynamic chord of the wing	MAC_{wing}	1.8 [m]
Leading edge sweep angle of the wing	λ_w	65 [°]
Trailing edge sweep angle of the wing	λ_{te}	6 [°]
Wing thickness ratio	$(t/c)_{wing}$	0.09 none
Flap span	$Flap_{span}$	1.1 [m]
Vertical tail thickness ratio	$(t/c)_{Vtail}$	0.125 none
Vertical tail surface	S_{Vtail}	0.67 [m ²]
Vertical tail span	b_{Vtail}	0.8 [m]
Leading edge sweep angle of the Vertical tail	λ_{Vtail}	45 [°]
Mean aerodynamic chord of the Vertical tail	MAC_{Vtail}	0.8 [m]
Vertical tail number	$Vtail_{number}$	2 none

Table 3.10. USV-FTB-1 geometrical data

In the following subsections, the results of the basic models for both USV-FTB-1 and X-34 vehicle are presented.

3.3.3 Results

The Curran Model is the simplest and the first to be analysed. As seen in the previous chapter, the two USV-FTB-1 and X-34 aircraft are of the same family and consequently have a very similar configuration and aerodynamic behaviour. The closeness of the geometry of these two vehicles is also visible from the two configurational parameters on which the entire model is based, τ and K_w . In the case of the USV-FTB-1, they are equal to $\tau = 0.2161$ and $K_w = 3.3167$, whereas in the case of X-34 they are equal to $\tau = 0.2302$ and $K_w = 3.1918$. This is in agreement with the figure 3.1 shown in chapter 3.

The graphs in next page (fig. 3.22) show the results of the basic model for an angle of attack equal to 5° (light blue curve), compared with the database of the two aircraft (black points). Starting from the top, the X-34 lift coefficients, the drag coefficients and the efficiency respectively are reported on the left, while the USV-FTB-1 results are reported on the right. The underestimation of both lift and drag coefficient is attributable to the simplicity of the Curran model. The three geometric data required as input do not allow an adequate modelling of the aircrafts and consequently the curves obtained do not follow the real behaviour with precision.

The All-Body Hypersonic Aircraft Model was theorized for a blended body configuration, which is very different from the one under consideration. Nevertheless, the model was analysed anyway and the response is good.

In fact, as can be seen in the figure 3.23, the prediction of the lift coefficient is very close to the real case (light blue curves compared with black points). This occurs because the two aircraft have efficient delta wings, a similar geometry to the blended body configuration for which the model was generated. On the other hand, the drag coefficient is underestimated: a blended body aircraft with an elliptical cross-section is very slender, with a smooth surface that allows to obtain a lower drag than a wing body aircraft, in which the fuselage and wings are distinct and there is a negative contribution due to interference.

Unlike the previous model, the Raymer one was generated for a conventional aircraft configuration with a clear distinction between fuselage and wings, like the USV-FTB-1 and the X-34 vehicles. In fact, As can be seen in the graphs below (fig. 3.24) the estimation of the aerodynamic coefficients is good, especially for the lift coefficient.

The Torenbeek model is the last to be analysed. As mentioned in the chapter 2.4, it allows to evaluate the aerodynamic coefficients for a generic high speed aircraft configuration with a delta wing, a generic high speed aircraft configuration with an arrow wing and a blended wing body configuration. In this case, given the wing

body geometry, the results of the delta wing are presented in the figure 3.25 with the light blue curves. The model responds very well even in the basic version: it is able to capture the aerodynamic behaviour of the aircraft quite accurately. In order to allow a more accurate estimation, corrective coefficients were added to the models; these are listed in the table 3.11. Having to fit the models for both USV-FTB-1 and X-34 vehicles and not just for one as in the previous case, the results are not of the same precision. The final aerodynamic coefficients for high aspect ratio wing body configuration are shown in the graphs below (fig. 3.22, 3.23, 3.24, 3.25), with the green, yellow, cyan and red curves respectively.

CURRAN MODEL	
Flight Regime	Corrective Coefficients
<i>Subsonic</i>	<ul style="list-style-type: none"> • CL: (eq.2.6)·(18 – 11 · M); • CD: (eq.2.4)·0.40;
<i>Supersonic</i>	<ul style="list-style-type: none"> • CL: (eq.2.6)·(0.6 + M/1.5); • CD: (eq.2.4)·(0.4 + M/3);
ALL BODY HYPERSONIC AIRCRAFT MODEL	
<i>Subsonic</i>	<ul style="list-style-type: none"> • CL, (eq.2.11): $c_1 \cdot 1.2$; • CD: (eq.2.12)+0.026;
<i>Supersonic</i>	<ul style="list-style-type: none"> • CL, (eq.2.11): $c_1 \cdot 0.9, c_2 \cdot 1.8$; • CD: (eq.2.12)·(1.25 + M/5);
RAYMER MODEL	
<i>Subsonic</i>	<ul style="list-style-type: none"> • CL: (eq.2.37)+0.14; • CD: (eq.2.43)·(1.6 + M/1.8);
<i>Supersonic</i>	<ul style="list-style-type: none"> • CL: (eq.2.37)·(0.7 + M/20); • CD: (eq.2.43)·(1.1/log(1.6 · M + 1));
TORENBEEK MODEL	
<i>Supersonic</i>	<ul style="list-style-type: none"> • CL: (eq.2.66)·(0.7 + M/15); • CD: (eq.2.71)·(3.2/log(10 · M + 3));

Table 3.11: Corrective coefficients for High AR wing-body configuration

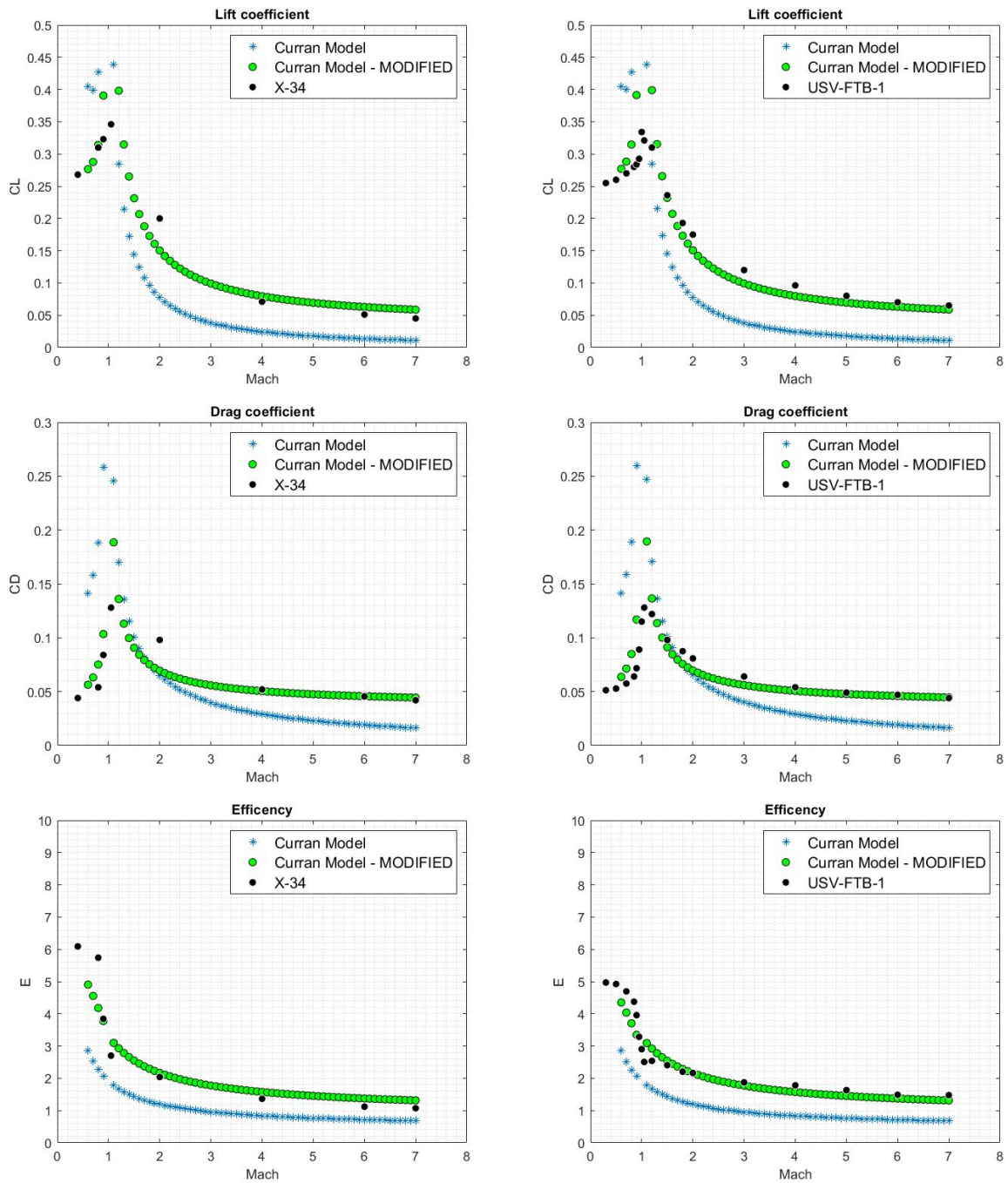


Figure 3.22. Aerodynamic coefficients of the basic Curran Model compared with the aerodynamic coefficients of the modified Curran Model for High AR Wing Body configuration

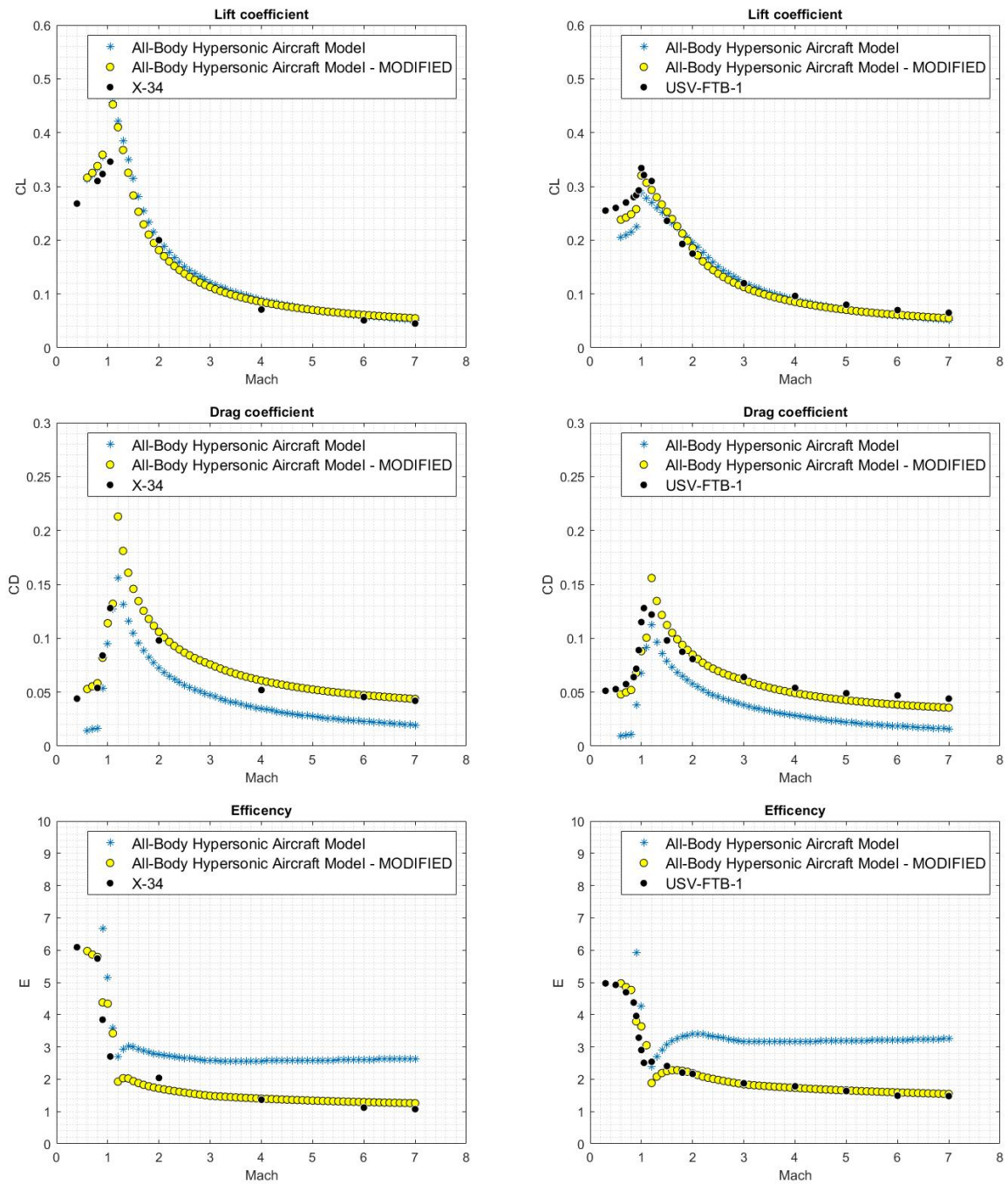


Figure 3.23. Aerodynamic coefficients of the basic All-Body Hypersonic Aircraft Model compared with the aerodynamic coefficients of the modified All-Body Hypersonic Aircraft Model for High AR Wing Body configuration

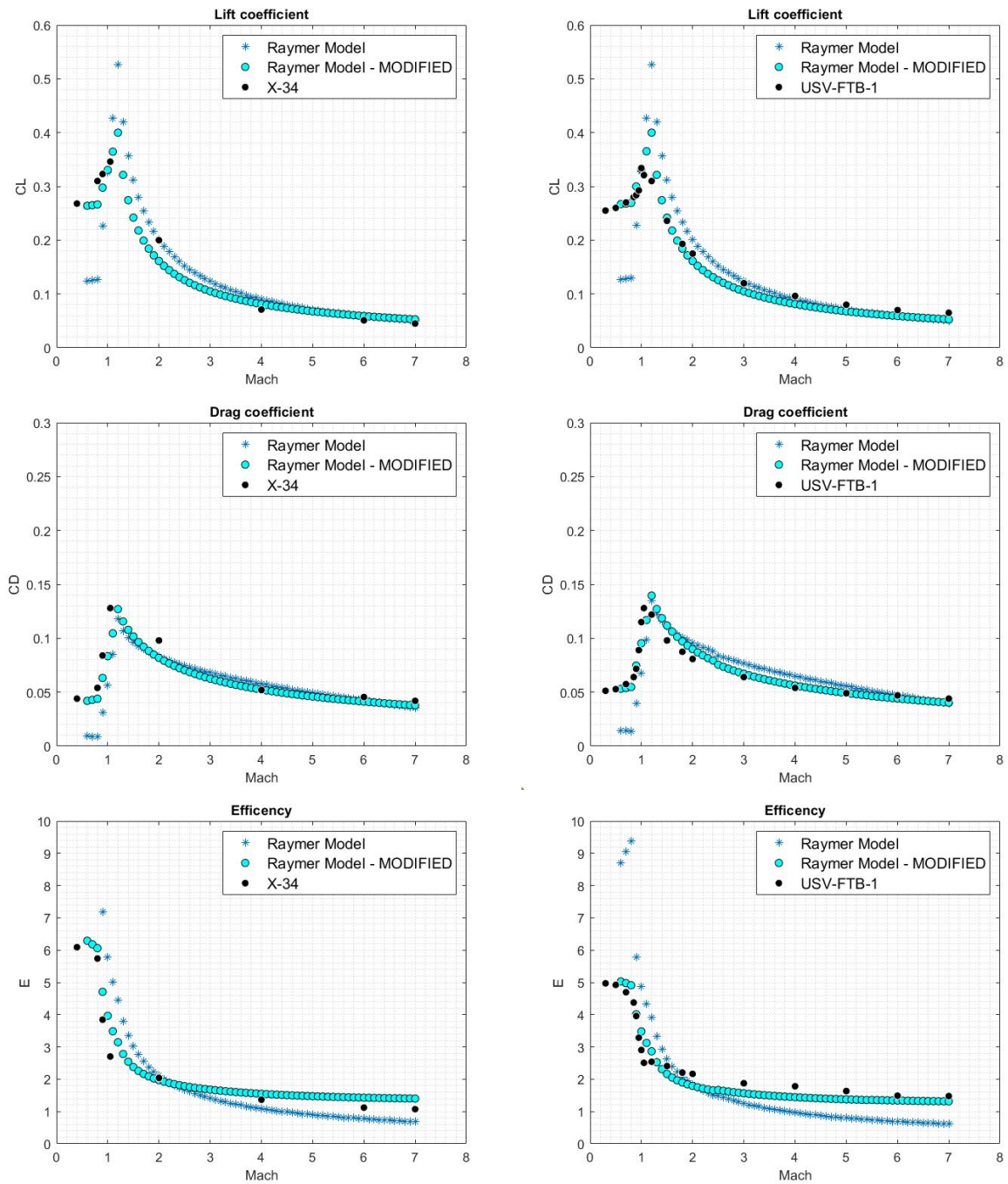


Figure 3.24. Aerodynamic coefficients of the Raymer Model compared with the aerodynamic coefficients of the modified Raymer Model for High AR Wing Body configuration

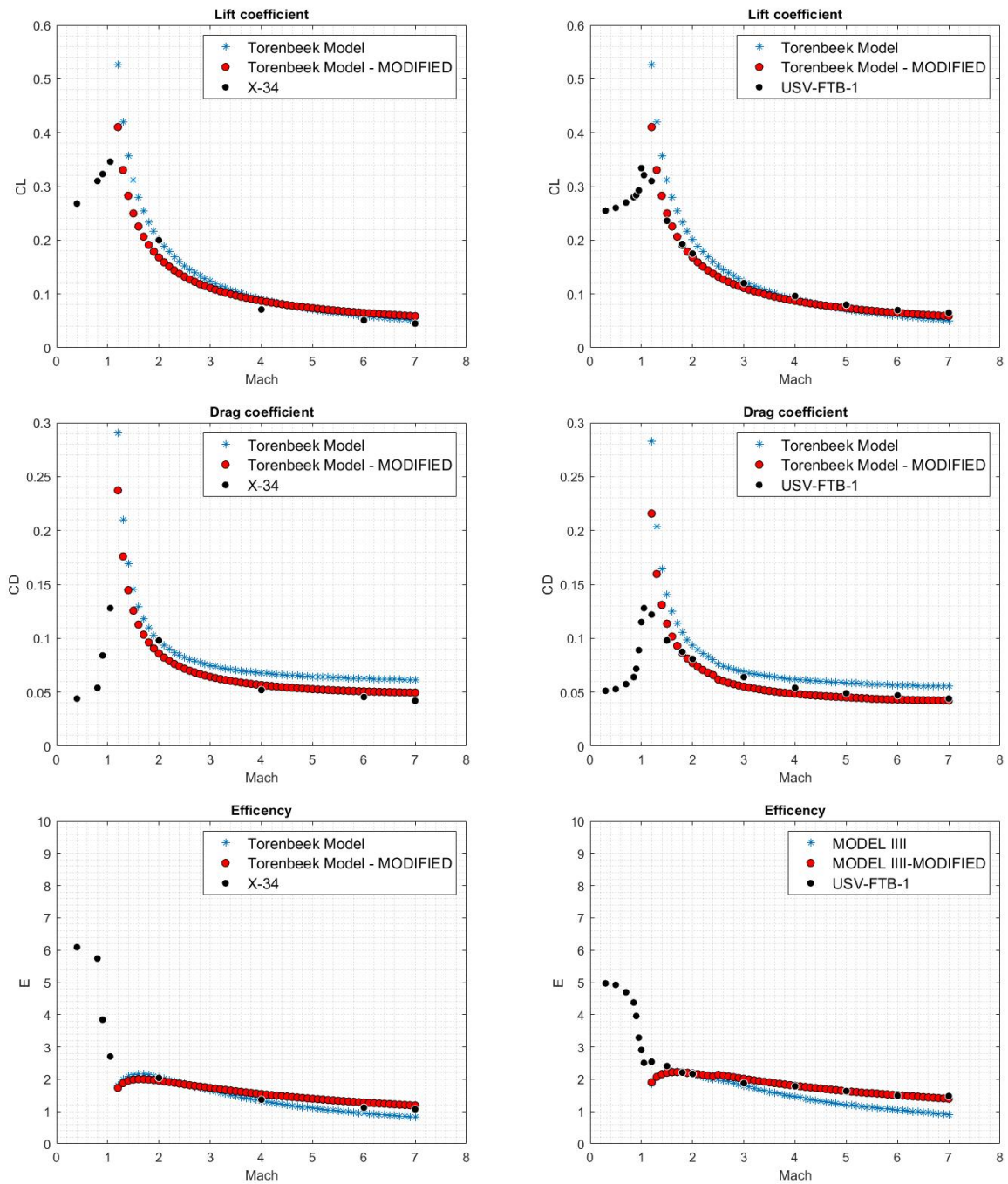


Figure 3.25. Aerodynamic coefficients of the Torenbeek Model compared with the aerodynamic coefficients of the modified Torenbeek Model for High AR Wing Body configuration

In conclusion, thanks to the corrective coefficients, it's possible to obtain a reliable estimate in a preliminary design stage. The Curran Model, All-Body Hypersonic Aircraft Model and the Raymer Model allow the analysis for the all flight regimes, from the subsonic one to the supersonic one, whereas the Torenbeek model is reliable only for the supersonic regime.

3.4 Low - AR Wing Body Configuration

In the previous section the Wing Body configuration with an aspect ratio higher than 2 was analysed, thanks to the USV-FTB-1 and X-34 case study. The next subfamily is the Low AR Wing-Body configuration, characterised by an aspect ratio lower than 2. All the main features mentioned before are still valid for the configuration analysed in this chapter, except for the AR, which is lower and consequently the response of the models is slightly different.

In the following pages, the HYPLANE vehicle is analysed and all the models' results are reported and discussed.

3.4.1 HYPLANE

In recent years some private enterprises have been approaching sub-orbital flights, which allow Space tourists to experiment microgravity conditions for a few minutes and to see a large area of the Earth, along with its curvature, from the stratosphere. In this scenario some small reusable airplane-like vehicles have been developed to perform sub-orbital missions, which could represent a first step towards a safer, less expensive and more comfortable access to Space in the near future [18].

An example is the HyPlane, represented in figure 3.26, whose project has been carried out within the University of Naples Federico II in Italy, in collaboration with the company Trans-Tech.



Figure 3.26. HYPLANE vehicle configuration [20]

This vehicle mission profile can be summarize with the following key points: horizontal take-off with engines operating in turbojet mode, subsonic ascent to altitudes between 5 and 10 km, acceleration through the transonic speed range and climbing with combined cycle engines until the achievement of an altitude of about 30 km

and a Mach number around 4, hypersonic cruise using ramjet engines (transcontinental range around 5000 km) or sequence of suborbital parabolas, descent and powered horizontal landing [19].

As can be seen in the figure above, the HYPLANE consists of a six-seat small-sized space-plane with a delta wing, four elevons for pitch and roll control if their deflection is symmetrical or asymmetrical respectively, and a vertical tail with a movable rudder for directional control. The vehicle is powered by two Turbine-Based Combined Cycle (TBCC) engines and a throttleable rocket. This concept is characterized by high aerodynamic efficiency that guarantees the maximization of the range with the minimum fuel consumption and also the minimization of the required thrust, so that the take-off propellant mass can be small.

GEOMETRICAL DATA		Value
Total volume	V_{tot}	280 [m ³]
Reference surface	S_{plan}	140 [m ²]
Wetted surface	S_{wet}	470 [m ²]
Exposed surface	$S_{Exposed}$	108.8 [m ²]
Wing span	$span$	13.5 [m]
Fuselage length	$l_{fuselage}$	23.6 [m]
Fuselage diameter	$d_{fuselage}$	2.6 [m]
Nose length	l_{nose}	7.8 [m]
Tail length	l_{tail}	4.7 [m]
Maximum cross-sectional area	S_{max}	8 [m ²]
Mean aerodynamic chord of the wing	MAC_{wing}	12 [m]
Leading edge sweep angle of the wing	λ_w	65 [°]
Trailing edge sweep angle of the wing	λ_{te}	0 [°]
Wing thickness ratio	$(t/c)_{wing}$	0.04 none
Inlet length	l_{Inlet}	6.5 [m]
Inlet diameter	d_{Inlet}	1.1 [m]
Vertical tail thickness ratio	$(t/c)_{Vtail}$	0.046 none
Vertical tail surface	S_{Vtail}	14 [m ²]
Vertical tail span	b_{Vtail}	3.6 [m]
Leading edge sweep angle of the Vertical tail	λ_{Vtail}	51 [°]
Mean aerodynamic chord of the Vertical tail	MAC_{Vtail}	4.3 [m]
Vertical tail number	$Vtail_{number}$	1 none

Table 3.12. HYPLANE geometrical data

The total length is about 23.6 m, the reference surface 140 m² and the Aspect Ratio is $AR = 1.30$; all the geometrical specifications are reported in the table 3.12.

In the following subsection, the results of the four aerodynamic models are presented and compared with the aerodynamic data of the HYPLANE vehicle. These, have

been evaluated both with Computational Fluid Dynamic (CFD) simulations and Missile DATCOM software, a semi-empirical aerodynamic prediction code which offers the possibility to quickly carry out aerodynamic performance analysis of conventional configurations of aircrafts [18].

3.4.2 Results

First of all, the Curran model is analysed. The characteristic parameters for the aircraft under consideration are $\tau = 0.1990$ and $K_w = 3.3571$. How it's possible to see, they are very similar to the USV-FTB-1 and X-34 vehicles (3.3.3), even if the τ is slightly lower because the HYPLANE is more slender: the lower is the τ the higher is the slenderness.

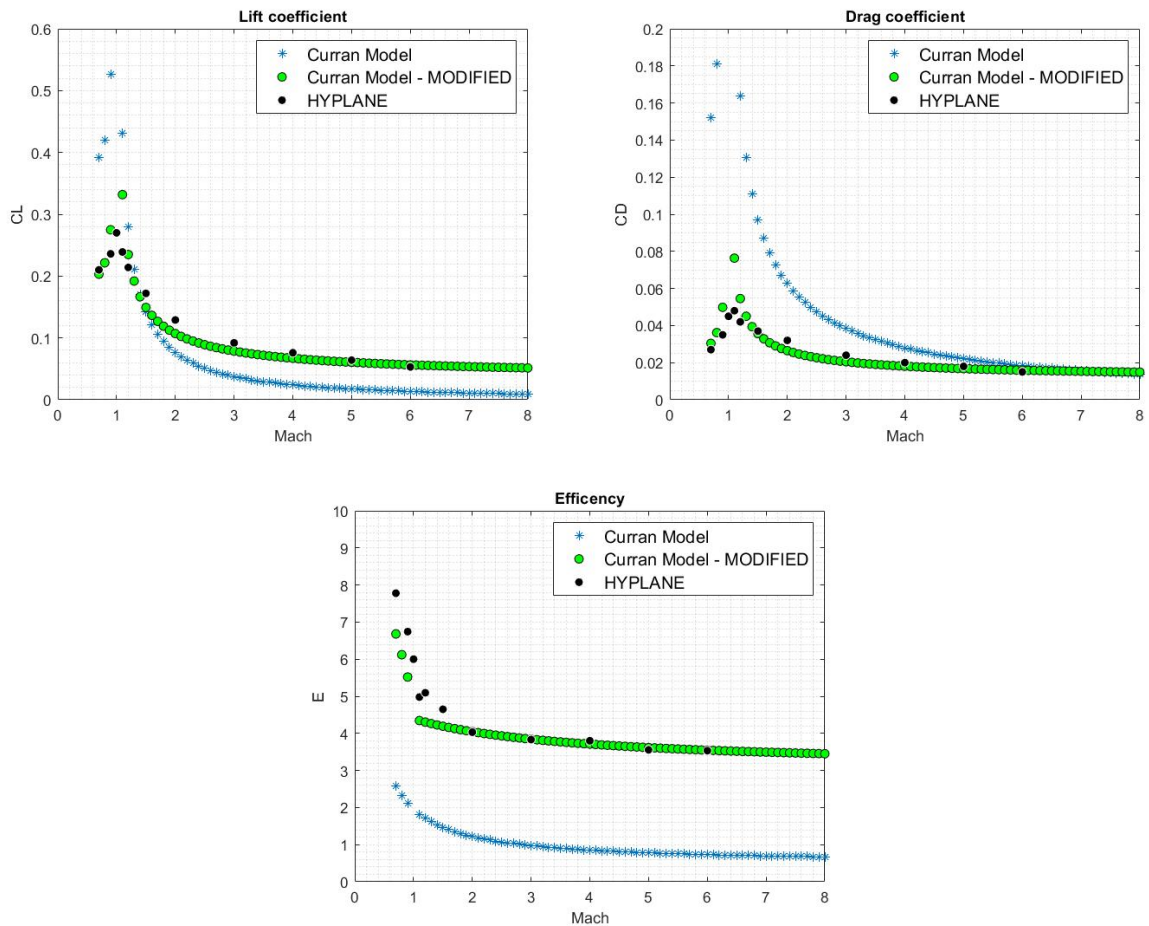


Figure 3.27. Aerodynamic coefficients of the basic Curran Model compared with the aerodynamic coefficients of the modified Curran Model for Low AR Wing Body configuration

The figure 3.27 shows the results of the basic Curran Model (light blue curve), compared with the database (black points) for an angle of attack equal to 5° . Given the closeness of the two characteristic parameters for all the wing body aircraft, the estimation of the aerodynamic coefficients is similar. In fact, it can be seen that there is an underestimation of the lift, as in the previous case, while drag is overestimated. This occurs because the HYPLANE is a more slender aircraft, capable of developing less drag, but the Curran Model is too simple and fails to capture this feature.

The All-Body Hypersonic Aircraft Model is the second to be analysed.

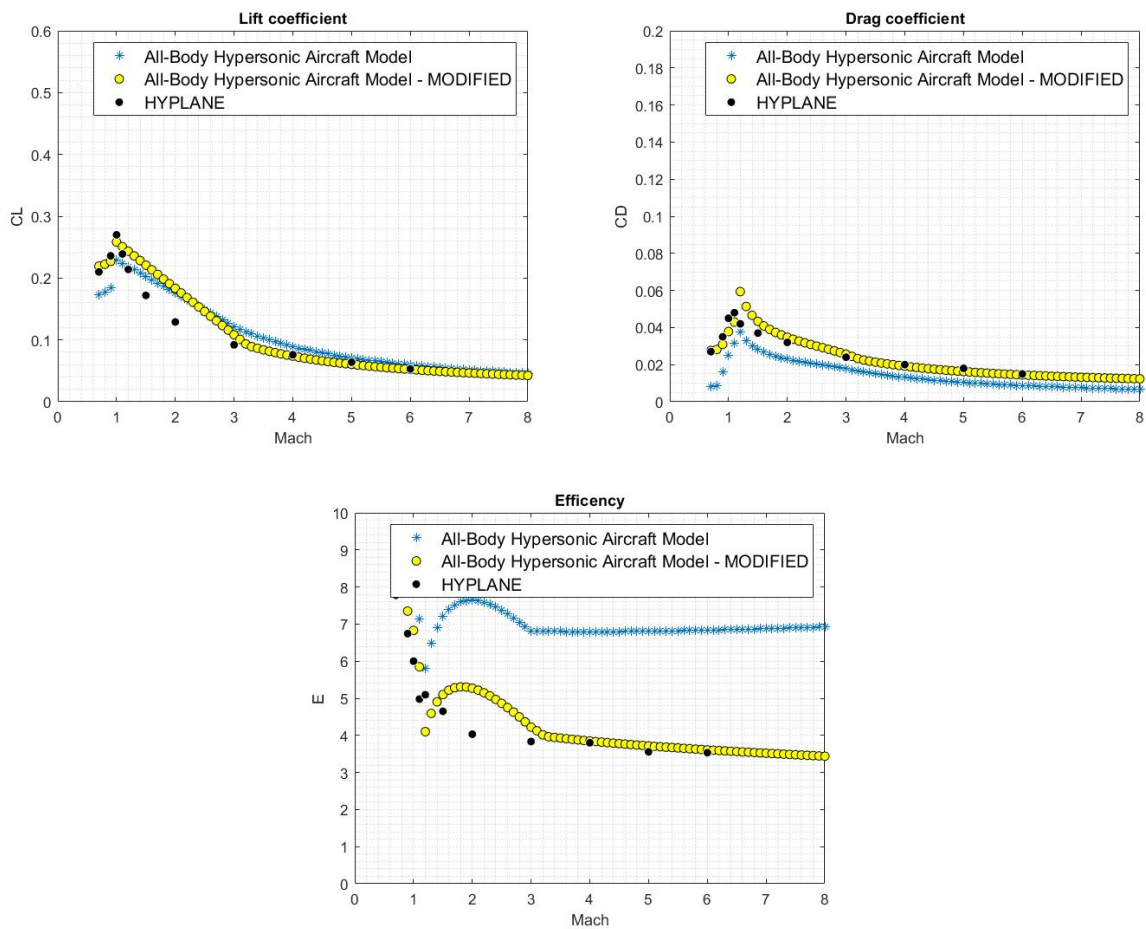


Figure 3.28. Aerodynamic coefficients of the basic All-Body Hypersonic Aircraft Model compared with the aerodynamic coefficients of the modified All-Body Hypersonic Aircraft Model for Low AR Wing Body configuration

In the case of the USV-FTB-1 and X-34 vehicles, there was a fairly evident underestimation of the drag coefficient, due to the fact that this model is theorised for a blended body aircraft, which is more slender and aerodynamically efficient.

However, in this case, it is possible to see that the drag curve is closer to the real one, (fig. 3.28) as the HYPLANE is more similar to the reference geometry (the wing surface is higher with respect to the fuselage dimension). The lift coefficient is close to the real case in both subsonic and high supersonic flight regime, while the approximation is less accurate for low supersonic speeds. The reason is the following: the lift is linearised from the transonic Mach number up to high supersonic one, depending on the value of the aspect ratio. In this case, the HYPLANE's aspect ratio is very low: the range of linearity is quite large and consequently the estimation is less precise.

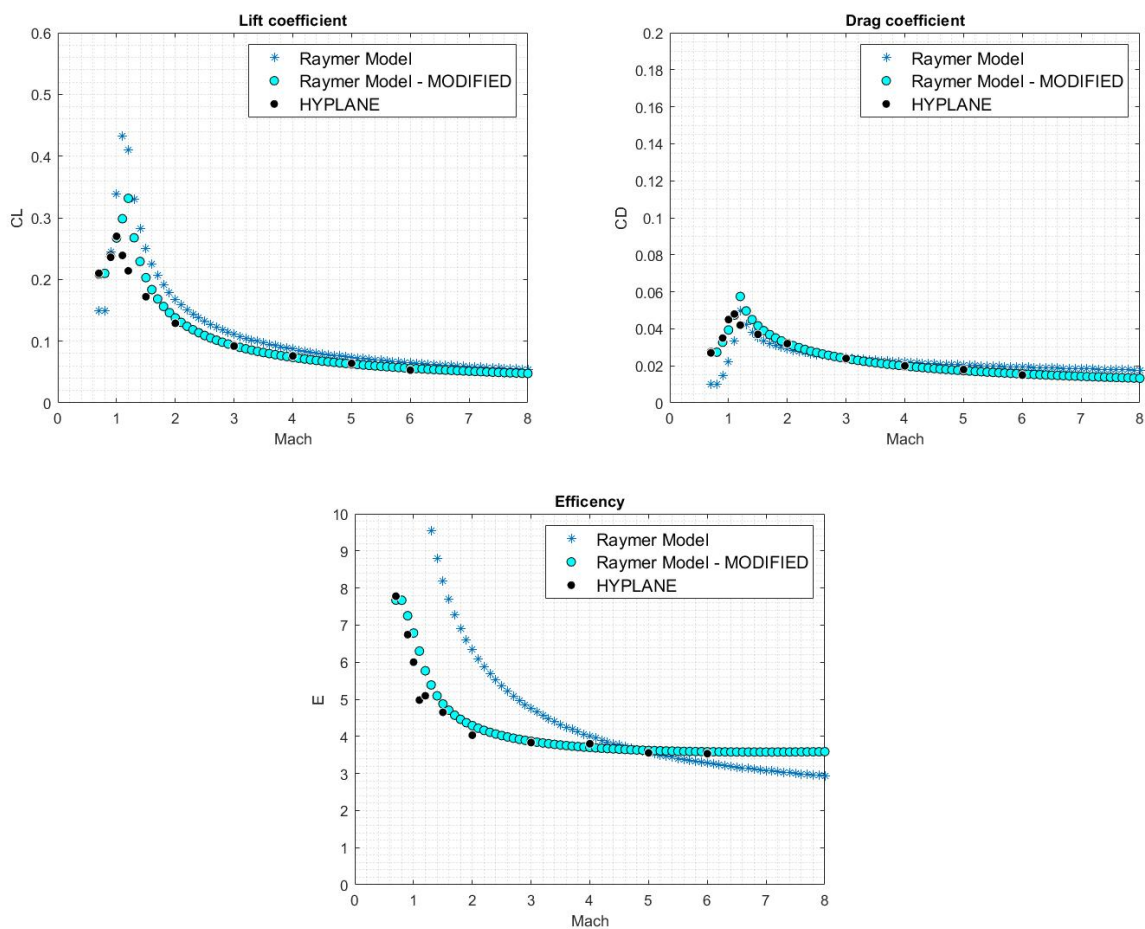


Figure 3.29. Aerodynamic coefficients of the basic Raymer Model compared with the aerodynamic coefficients of the modified Raymer Model for Low AR Wing Body configuration

The Raymer Model and the Torenbeek Model are the most suitable for this configurational family: the first was theorised for a concept of this type, in which there

is a clear distinction between wing and fuselage. Similarly, the second allows to predict the aerodynamic behaviour of a conventional delta-winged aircraft. The figures 3.29 and 3.30 show the results of the basic Raymer model and the basic Torenbeek model respectively (light blue curves). It can be seen that the coefficients are quite close to the real ones, especially with regard to drag, whereas the lift is slightly overestimated.

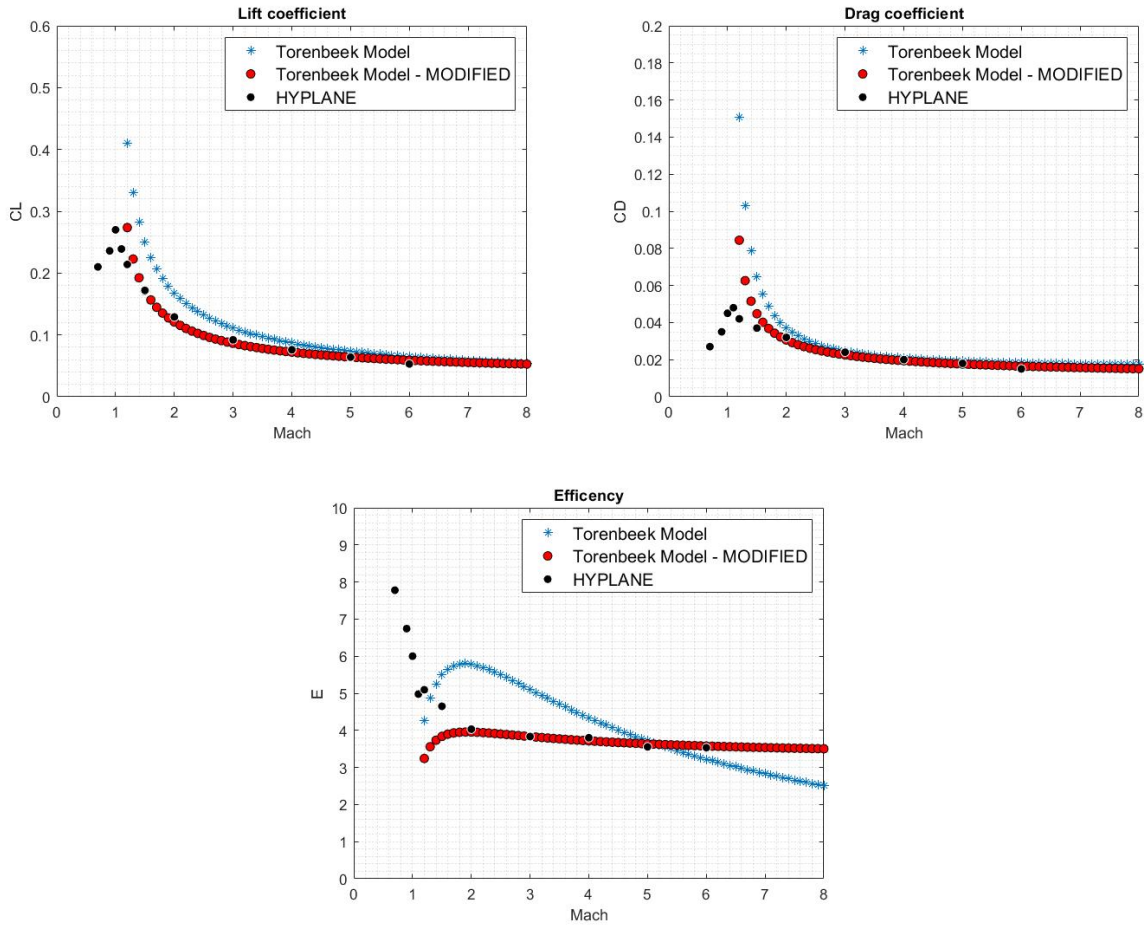


Figure 3.30. Aerodynamic coefficients of the basic Torenbeek Model compared with the aerodynamic coefficients of the modified Torenbeek Model for Low AR Wing Body configuration

In order to improve the precision, all the corrective coefficients listed in the table below (3.13) were added to the basic models.

Thanks to these, in a preliminary design phase it is therefore possible to estimate the aerodynamic behaviour of a wing body aircraft with a good reliability.

In particular, the Curran Model and the Raymer Model allow the analysis for all the flight regimes, the Torenbeek model only for the supersonic regime and the All-Body Hypersonic Aircraft Model it's reliable for subsonic and high supersonic flight regime.

CURRAN MODEL	
Flight Regime	Corrective Coefficients
<i>Subsonic</i>	<ul style="list-style-type: none"> • CL: (eq.2.6)·(13 – 8 · M); • CD: (eq.2.4)·0.20;
<i>Supersonic</i>	<ul style="list-style-type: none"> • CL: (eq.2.6)·M · 0.7; • CD: (eq.2.4)·(0.2 + M/9);
ALL BODY HYPERSONIC AIRCRAFT MODEL	
<i>Subsonic</i>	<ul style="list-style-type: none"> • CL, (eq.2.11): $c_1 \cdot 1.45$; • CD: (eq.2.12)+0.018;
<i>Supersonic</i>	<ul style="list-style-type: none"> • CL, (eq.2.11): $c_1 \cdot 0.8, c_2 \cdot 1.5$; • CD: (eq.2.12)·(1.15 + M/13);
RAYMER MODEL	
<i>Subsonic</i>	<ul style="list-style-type: none"> • CL: (eq.2.37)+0.06; • CD: (eq.2.43)·(0.55 + M/15);
<i>Supersonic</i>	<ul style="list-style-type: none"> • CL: (eq.2.37)·1.6; • CD: (eq.2.43)·(2.1/log(2 · M + 1));
TORENBEEK MODEL	
<i>Supersonic</i>	<ul style="list-style-type: none"> • CL: (eq.2.66)·(0.4 + M/10); • CD: (eq.2.71)·(4.5/log(3 · M + 10));

Table 3.13: Corrective coefficients for Low AR wing-body configuration

3.5 Cylinder Wing Configuration

The cylinder Wing configuration consists of a rather conventional missile-like vehicle, normally designed for a vertical take-off. In general, the aerodynamic configuration features a compact body with a circular fuselage cross-section and a delta planform wing as its basic shape.

The fuselage is large enough to accommodate the propulsion tanks and all necessary subsystems and has a flat bottom surface in order to increase the overall hypersonic performance of the vehicle. The circular cross section is constant up to the fuselage-wing interface, where the wing is blended into the fuselage to minimize wing-body interference heating. The forebody of the aircraft features a simple conical sphere configuration, with smooth streamlined surfaces in the upper and lower sides of the fuselage to avoid dangerous local overheating. The delta planform wing is swept enough to ensure the best performance with respect to supersonic drag and aerodynamic heating and is installed at the rear of the vehicle. In order to control the aircraft throughout the mission profile, the aerodynamic surfaces generally comprise one central vertical tail or two vertical tails with rudders, elevons and ailerons on the wings, and a body flap to improve the stability during the descent.

3.5.1 VTO-HOPPER

In 2003 the European Space Agency (ESA) started the Future Launchers Preparatory Programme (FLPP). It oversees system studies and research activities to foster new launcher technologies and architectures, capable of delivering performance and reliability coupled with reduced operational costs.

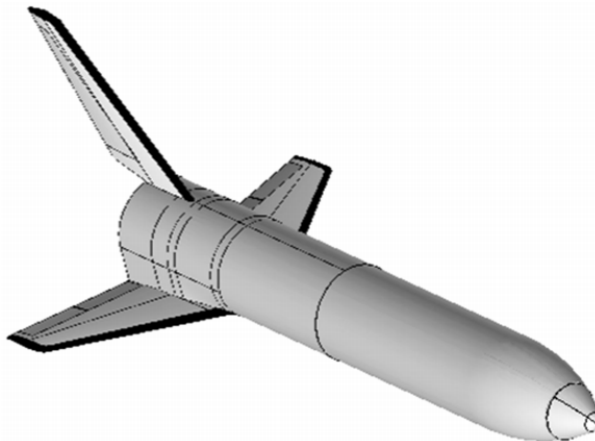


Figure 3.31. VTO-HOPPER reusable booster stage configuration [23]

Within this framework, the VTO-Hopper reusable launcher was investigated. It

consists of a winged sub-orbital vehicle designed for vertical take-off with an expendable upper stage and fully reusable lower stage (named booster), able to deliver a payload up to 8 Mg in geostationary transfer orbit. After separation from the payload, the reusable booster is designed to perform an unpowered ballistic arc, followed by a gliding downrange reentry flight to conclude the mission with a conventional horizontal landing [21], [22].

In the following lines, only the reusable stage is investigated and represented in the figure 3.31).

As can be seen, the booster features a rather conventional slender missilelike configuration layout: it consists of a circular cross section fuselage with delta planform wings in the rear position (45° leading-edge sweep angle), and a central vertical stabilizer. In order to reduce the interferences, the wing is blended into the fuselage.

GEOMETRICAL DATA		Value
Total volume	V_{tot}	1380 [m ³]
Planform surface	S_{plan}	349 [m ²]
Wetted surface	S_{wet}	869 [m ²]
Exposed surface	$S_{Exposed}$	193 [m ²]
Wing span	$span$	31.8 [m]
Fuselage length	$l_{fuselage}$	58.8 [m]
Fuselage diameter	$d_{fuselage}$	8.8 [m]
Nose length	l_{nose}	12.5 [m]
Tail length	l_{tail}	7.35 [m]
Maximum cross-sectional area	S_{max}	70 [m ²]
Mean aerodynamic chord of the wing	MAC_{wing}	12.6 [m]
Wing length	l_{wing}	17 [m]
Leading edge sweep angle of the wing	λ_w	45 [°]
Trailing edge sweep angle of the wing	λ_{te}	13 [°]
Wing thickness ratio	$(t/c)_{wing}$	0.075 none
Vertical tail thickness ratio	$(t/c)_{Vtail}$	0.09 none
Vertical tail surface	S_{Vtail}	36 [m ²]
Vertical tail span	b_{Vtail}	14 [m]
Leading edge sweep angle of the Vertical tail	λ_{Vtail}	46 [°]
Mean aerodynamic chord of the Vertical tail	MAC_{Vtail}	7.5 [m]
Vertical tail number	$Vtail_{number}$	2 none

Table 3.14. VTO - HOPPER geometrical data

The aerodynamic control surfaces comprise rudders on the vertical tail, elevons and ailerons on the wings, and a body flap underneath the main engines to provide maneuverability and longitudinal stability during the atmospheric descent [23].

The fuselage length is approximately 58 m with a delta wing surface equal to 193

m^2 and a wing leading/trailing edge sweep angle equal to $45^\circ / 13^\circ$. In the table 3.14 it's possible to see all the VTO-Hopper geometrical specifications.

The aerodynamic data used for the models adaptations were obtained by engineering methods and CFD computations [24]. In the next subsection, all the results of the basic models are shown, together with the corrective coefficients used to fit the models and the final curves.

3.5.2 Results

The characteristic parameters of the Curran model, in the case of this aircraft, are $\tau = 0.2117$ and $K_w = 2.4914$. Looking at the graphs 3.1 in the chapter 3, it is possible to see that these values fall within the Cylinder Wing configuration, which confirms the classification made.

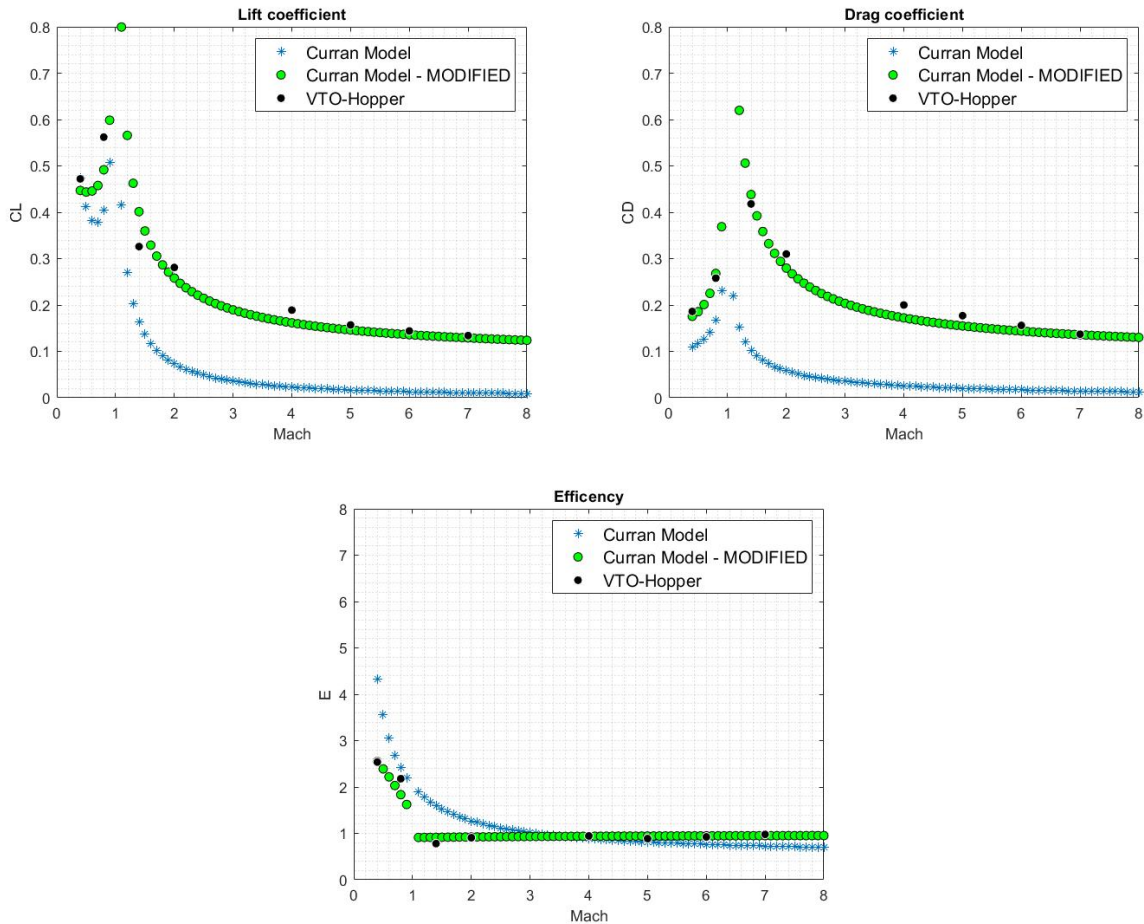


Figure 3.32. Aerodynamic coefficients of the basic Curran Model compared with the aerodynamic coefficients of the modified Curran Model for Cylinder Wing configuration

As can be seen from the light blue curve in the figure 3.33, this model does not approximate well the real values (black point). This graphs refer to an angle of attack equal to 5° and there is an underestimation of both lift and drag coefficients. This occurs because the values τ and k_w are those of a slender and aerodynamically-friendly aircraft. However, as mentioned before, this vehicle is not very performing: the three data required by the Curran model as input are not sufficient to adequately describe the geometry, so the estimation is too simplified and fails to capture these aspects.

The results of the All-Body Hypersonic Aircraft Model are shown in figure 3.33. It was theorized on the basis of a blended body configuration, which is totally different from the VTO-Hopper one. In fact, the latter has a clear distinction between fuselage and wing. Additionally, these are very small and located in the rear of the aircraft, with a low leading-edge sweep angle.

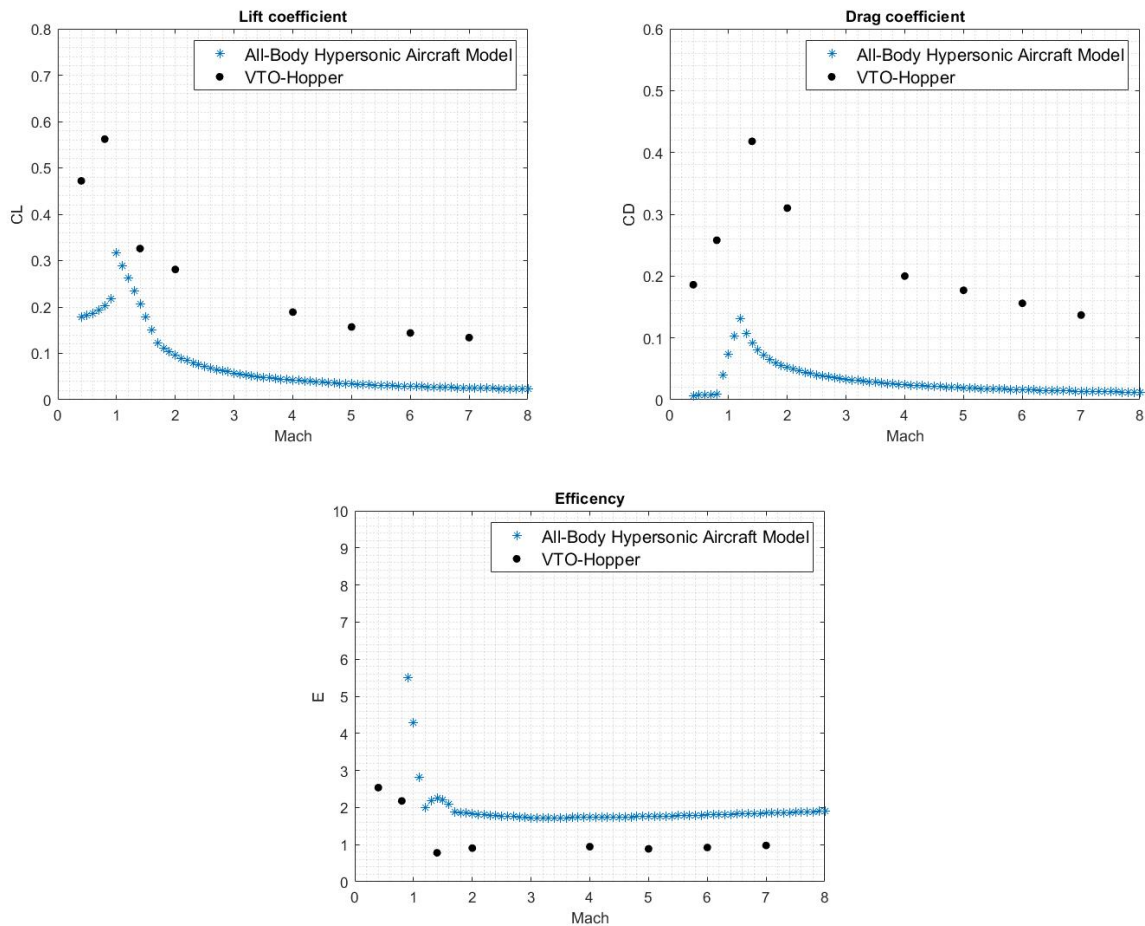


Figure 3.33. Aerodynamic coefficients of the basic All-Body Hypersonic Aircraft Model for Cylinder Wing configuration

The curves reflect this aspect and as can be seen, there is a clear discrepancy from the real case (black dots). In particular, the Drag coefficient is underestimated because the VTO-Hopper is less efficient than a blended body. For the reasons just described, no correction coefficients were introduced for this model, which is unreliable for all the flight conditions.

In contrast to the previous case, the reference configuration of the Raymer model is closer to the vehicle under consideration. In fact, it consists of an almost conventional geometry, despite the fact that the wings are very small if compared to the fuselage, which is very elongated.

These aspects are visible on the model's response, shown in the figure below (3.34).

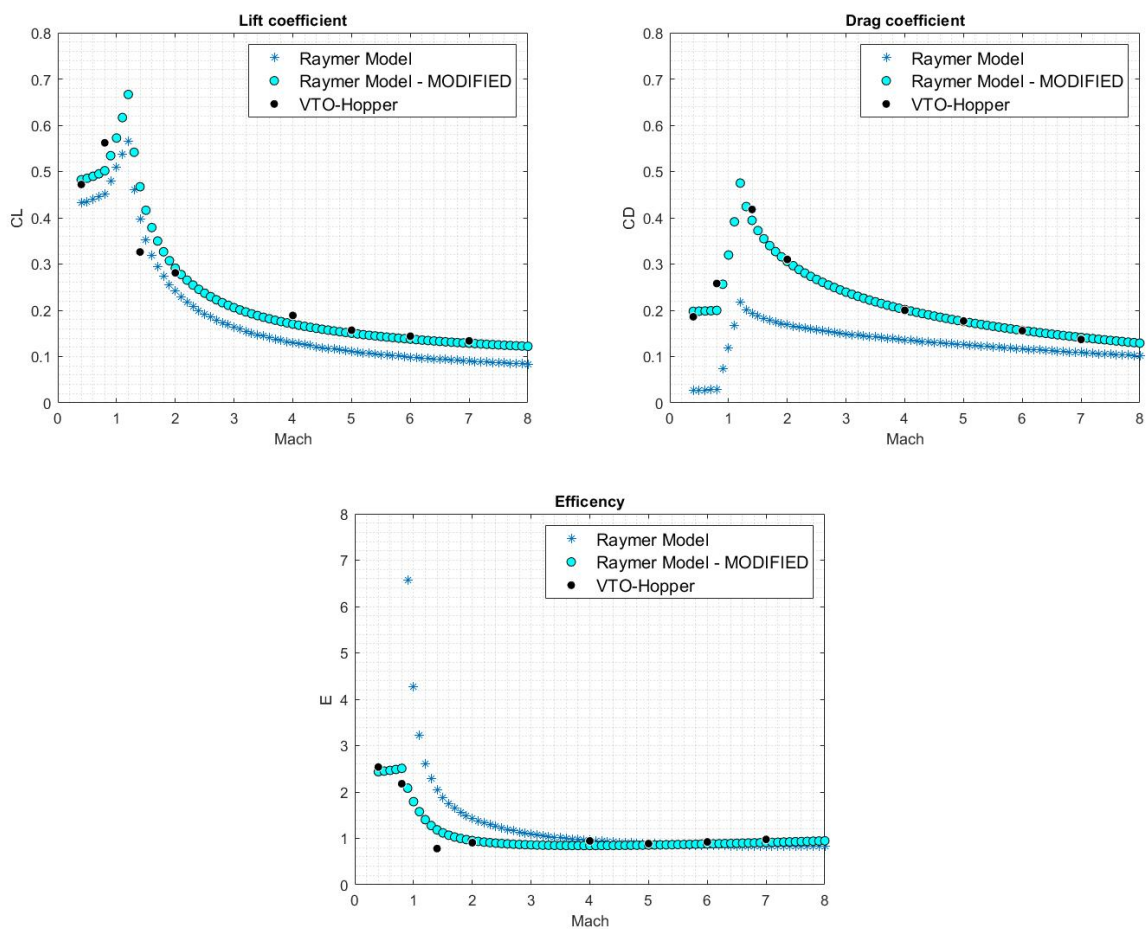


Figure 3.34. Aerodynamic coefficients of the basic Raymer Model compared with the aerodynamic coefficients of the modified Raymer Model for Cylinder Wing configuration

In fact, the estimated coefficients (light blue curves) are not very close to the real ones, especially for the drag. As said before, the reason is that the vehicle under

study is less efficient than the reference geometry: the lower sweep angle, the non very slender fuselage and the large vertical tail are reflected in a higher drag. The observations made for the previous model are still valid for the Torenbeek one. The latter allows the estimation of the aerodynamic coefficients for a generic high speed aircraft configuration with a delta wing, a generic high speed aircraft configuration with an arrow wing and a blended wing body configuration. In this case, given the quite large trailing edge sweep angle, the results of the arrow wing are presented in the figure 3.35 with the light blue curves.

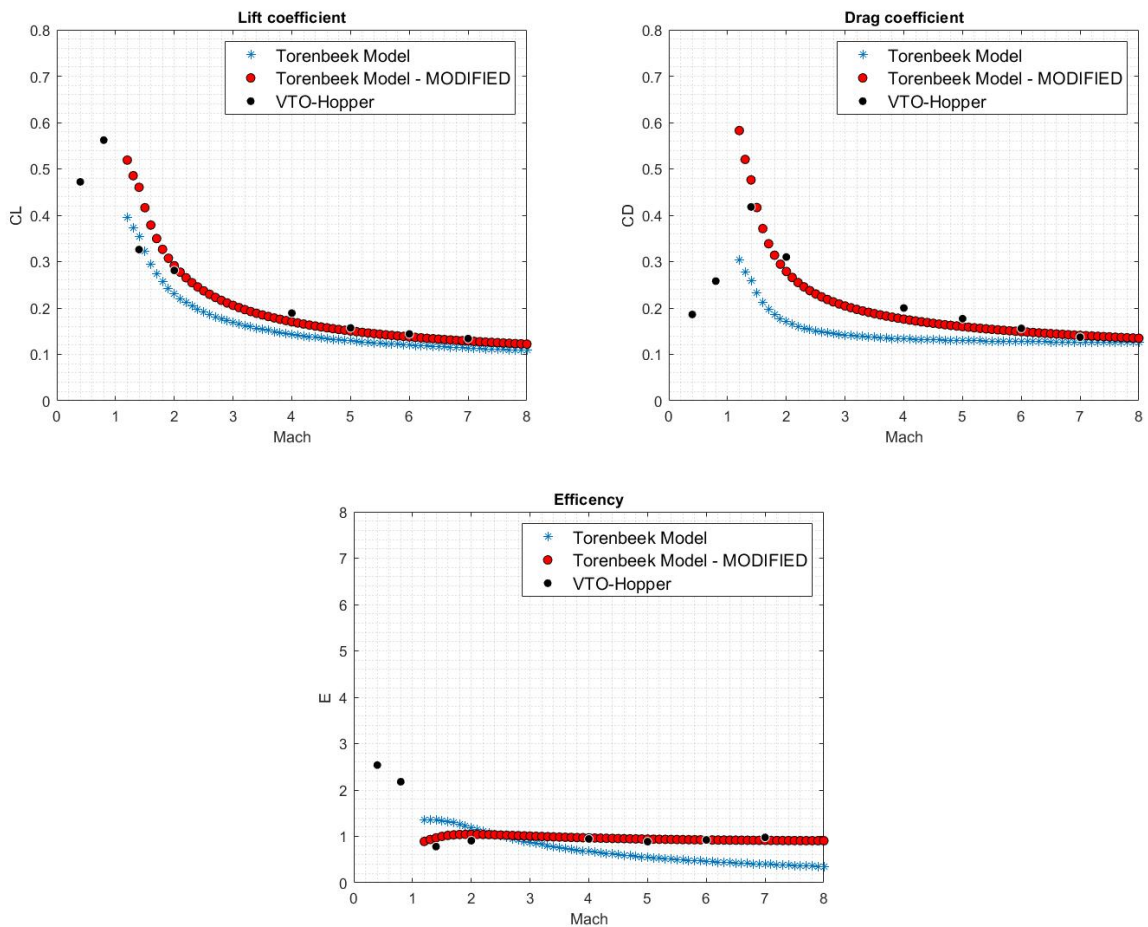


Figure 3.35. Aerodynamic coefficients of the basic Torenbeek Model compared with the aerodynamic coefficients of the modified Torenbeek Model for Cylinder Wing configuration

In order to improve the estimation of aerodynamic behaviour in a preliminary design phase, the corrective coefficients reported in the table below (3.15) were added, found with the help of the "Curve fitting" Matlab tool.

The final results are shown in the figure 3.33, 3.34, 3.35 with the green, cyan and

red cures respectively. In conclusion, it is possible to affirm that the Curran and Raymer Model are reliable for all the flight regime, whereas the Torenbeek one is reliable only for the supersonic flight regime.

CURRAN MODEL	
Flight Regime	Corrective Coefficients
<i>Subsonic</i>	<ul style="list-style-type: none"> • CL: (eq.2.6)·(32 − 21 · M); • CD: (eq.2.4)·1.6;
<i>Supersonic</i>	<ul style="list-style-type: none"> • CL: (eq.2.6)·M · 1.75; • CD: (eq.2.4)·(3 + M/1.1);
RAYMER MODEL	
<i>Subsonic</i>	<ul style="list-style-type: none"> • CL: (eq.2.37)+0.25; • CD: (eq.2.43)+0.165;
<i>Supersonic</i>	<ul style="list-style-type: none"> • CL: (eq.2.37)·(1 + M/4.5); • CD: (eq.2.43)·(3.9/log(2 · M + 3));
TORENBEEK MODEL	
<i>Supersonic</i>	<ul style="list-style-type: none"> • CL: (eq.2.66)·(1 + M/4.5); • CD: (eq.2.71)·(3.3/log(2 · M + 3));

Table 3.15: Corrective coefficients for Cylinder Wing configuration

3.6 Blended Body Configuration

This is the last configurational family being analysed. A blended body is a vehicle having no a clear division between the wings and the main body of the aircraft: this concept is more efficient than a conventional aircraft. Firstly, it reduces the total wetted area and the accompanying form drag and skin friction drag associated with a conventional wing-body junction. Secondly, this shape allows the entire aircraft to generate lift, thus reducing the size and the drag of the wings. Moreover, the leading edges of this slender concept are swept far behind the Mach cone and consequently a lower wave drag due to volume is obtained. Despite the advantage of an higher aerodynamic efficiency in both supersonic and hypersonic regime, the main drawback is that this highly integrated configuration has an unfavorable utilization of the internal volume which is useful for the payload accomodation.

Generally, the aerodynamic control surfaces comprise elevons for both pitch and roll control if their deflection is symmetrical or asymmetrical respectively, due to the absence of a tail.

In the following subsections, the two blended body vehicles SAENGER and ELAC are analysed, in order to test the models' reliability for this configurations.

3.6.1 ELAC

Over the years, space transport systems have continued to evolve and there has been a need for a relatively low-cost, reusable spacecraft capable of horizontal take-off and landing: it seemed possible and more efficient than the conventionally used solid and liquid fuel rockets. Under this scenario, In Germany three Collaborative Research Centers (SFB) where established in 1989, to carry out research into the basic principles required for a possible evolution of the TSTO (two stage to orbit) vehicle [25] [26].



Figure 3.36. ELAC vehicle configuration [25]

In this frame, a two-stage space transportation concept was designed with the lower stage called ELAC (Elliptical Aerodynamic Configuration), represented in the figure 3.36 and the upper stage called EOS (ELAC Orbital Stage). In the following sections, only the lower one is analysed.

As can be seen, the ELAC configuration consists of a lifting body with a delta planform and rounded leading-edges, which allow to reduce the thermal loads. The length of the vehicle amounts to 72 m with a wing span of about 39 meters and a leading-edge sweep angle equal to 75°. In the table 3.16 all the geometrical data are reported. The aerodynamic control surfaces comprise movable rudders on the two vertical tail for directional control and two elevons for both pitch and roll control. The air propulsion system is integrated in the underside of the ELAC. The aerodynamic data base of this vehicle configuration was essentially established by tests in wind tunnels and it is taken from the reference [14].

GEOMETRICAL DATA		Value
Total volume	V_{tot}	5238 [m ³]
Reference surface	S_{plan}	1695.8 [m ²]
Wetted surface	S_{wet}	4210 [m ²]
Exposed surface	$S_{Exposed}$	907 [m ²]
Wing span	$span$	38.6 [m]
Fuselage length	$l_{fuselage}$	72 [m]
Fuselage diameter	$d_{fuselage}$	7 [m]
Nose length	l_{nose}	21 [m]
Tail length	l_{tail}	14 [m]
Maximum cross-sectional area	S_{max}	110 [m ²]
Mean aerodynamic chord of the wing	MAC_{wing}	60 [m]
Leading edge sweep angle of the wing	λ_w	75 [°]
Trailing edge sweep angle of the wing	$\lambda_t e$	0 [°]
Wing thickness ratio	$(t/c)_{wing}$	0.11 none
Flap span	$Flap_{span}$	8.47 [m]
Vertical tail thickness ratio	$(t/c)_{Vtail}$	0.05 none
Vertical tail surface	S_{Vtail}	89.8 [m ²]
Vertical tail span	b_{Vtail}	8.47 [m]
Leading edge sweep angle of the Vertical tail	λ_{Vtail}	56.63 [°]
Mean aerodynamic chord of the Vertical tail	MAC_{Vtail}	10.6 [m]
Vertical tail number	$Vtail_{number}$	2 none

Table 3.16. ELAC geometrical data

3.6.2 SAENGER

Back in the 1990s, space-flight was based on vertically launched transportation systems that were not or only partially reusable and the costs of delivering payloads into Earth orbits were too high. Besides the aspect of greater economy and safety, interest was focusing on more environmental-friendly vehicles. Consequently, worldwide efforts aimed to develop concepts for completely reusable space transportation systems capable of taking off and landing like airplanes.

In 1988 the German Federal Ministry for Research and Technology (BMFT) initiated the Hypersonics Technology Programme, with the aim of finding new solutions for accessing space using advanced space vehicles [27]. The programme's reference concept is the SANGER, depicted in the figure 3.37.



Figure 3.37. Saenger vehicle configuration [14]

it consists of a fully reusable winged two stage to orbit (TSTO) space transportation system. The first stage is a hypersonic vehicle with turboramjet engines using liquid hydrogen. The separation between stages occurs at an altitude of approximately 40 km and a Mach number 6.5 velocity. After that, the first stage return to its starting point while the second stage climbs to the selected orbit, using its own rocket propulsion.

In addition to this mission scenario, in the initial study phase it was planned to analyse whether the lower stage could operate as a hypersonic passenger aircraft. This vehicle took the name European Hypersonic Transport Vehicle (EHTV).

In this thesis, only the first stage is analysed and the main dimensions of which are a total length of 82.4 m, a wing span of 45.2 m and a reference surface of approximately 2722 m². All the geometrical data are reported in the table 3.17.

The airbreathing propulsion system consists of five turboramjet engines, installed in the underside of the aircraft [28].

In conclusion, the aerodynamic database of the SAENGER lower stage is taken from the references [14].

GEOMETRICAL DATA		Value
Total volume	V_{tot}	8692 [m ³]
Reference surface	S_{plan}	2722 [m ²]
Wetted surface	S_{wet}	5208 [m ²]
Exposed surface	$S_{Exposed}$	1265 [m ²]
Wing span	$span$	45.2 [m]
Fuselage length	$l_{fuselage}$	82.4 [m]
Fuselage diameter	$d_{fuselage}$	10 [m]
Nose length	l_{nose}	22.8 [m]
Tail length	l_{tail}	16.4 [m]
Maximum cross-sectional area	S_{max}	150 [m ²]
Mean aerodynamic chord of the wing	MAC_{wing}	14 [m]
Leading edge sweep angle of the wing	λ_w	69 [°]
Trailing edge sweep angle of the wing	λ_{te}	0 [°]
Wing thickness ratio	$(t/c)_{wing}$	0.18 none
Inlet length	l_{Inlet}	18.3 [m]
Inlet diameter	d_{Inlet}	5*3.7 [m]
Flap span	$Flap_{span}$	14.7 [m]
Vertical tail thickness ratio	$(t/c)_{Vtail}$	0.045 none
Vertical tail surface	S_{Vtail}	83.4 [m ²]
Vertical tail span	b_{Vtail}	9.2 [m]
Leading edge sweep angle of the Vertical tail	λ_{Vtail}	59 [°]
Mean aerodynamic chord of the Vertical tail	MAC_{Vtail}	10 [m]
Vertical tail number	$Vtail_{number}$	2 none

Table 3.17. SAENGER geometrical data

3.6.3 Results

The first model to be analysed is the Curran one. As explained in the pages above, the two ELAC and SAENGER vehicles are of the same configurational family and consequently have a very similar geometry and aerodynamic coefficients.

The closeness between these two concepts is also visible from the τ and K_w parameters. In the case of the ELAC, they are equal to $\tau = 0.0750$ and $K_w = 2.4831$, whereas in the case of SAENGER they are equal to $\tau = 0.0612$ and $K_w = 2.2127$. These values are in agreement with the classification made, as can be seen in the graphs 3.1, in the chapter 3.

In the figure 3.38, the results of the basic Curran model for an angle of attack equal to 5° are shown, with the light blue curves. Starting from the top, the ELAC lift coefficients, the drag coefficients and the efficiency respectively are reported on the left, while the SAENGER results are reported on the right.

The All-Body Hypersonic Aircraft Model is the second to be analysed. It only refers to a representative hypersonic configuration: a delta planform with an elliptical cone forebody and an elliptical cross-section afterbody. For this reason, it is the most suitable for this configurational family.

The results obtained for the ELAC and SAENGER vehicles (geometric data reported in the table 3.16, 3.17) for an angle of attack equal to 5° are shown by the light blue curve in the figure (3.39).

As can be seen, the prediction of the coefficients are very close to the real case (light blue curves compared with black points), especially for drag. As regard the lift coefficient, it is linearised from the transonic Mach number up to high supersonic one, depending on the value of the aspect ratio. In the case of ELAC and SAENGER, they are slender vehicles and the AR is very low. This result in a range of linearity quite large and consequently in an unreliable efficiency trend for low supersonic speed.

Unlike the previous model, the Raymer one was generated for a conventional aircraft configuration with a clear distinction between fuselage and wings. This concept is therefore different from the ELAC and SAENGER one.

As can be seen in the graphs below (fig. 3.40) the estimation of the aerodynamic coefficients reflects this aspects. In particular, the Drag coefficient is slightly over-estimated because the vehicles under study are more efficient than the reference geometry: the smooth transition between wing and fuselage avoid the negative interference contribution. In addition, a blended body is characterized by a lower wetted surface and consequently the skin friction drag is lower.

In conclusion, the Torenbeek model is analysed. The results of the blended body estimation are reported in the figure 3.41, with the light blue curves. Also in this case the ELAC and SAENGER geometry are close to the reference model one, so the estimation is quite close to the real coefficients (black points).

In order to improve the results, the corrective coefficients reported in the table below (3.18) were added to the basic models. the final curves trend is good, as can be seen in the figure 3.38, 3.39, 3.40, 3.41 with the green, yellow, cyan and red curves respectively. In particular it is possible to affirm that the Curran and Raymer model are applicable for the all flight regimes, the All-Body Hypersonic Aircraft model is reliable only for the subsonic regime and the high supersonic one and the Torenbeek model is valid for the supersonic flight regime.

CURRAN MODEL	
Flight Regime	Corrective Coefficients
<i>Subsonic</i>	<ul style="list-style-type: none"> • CL: (eq.2.6)·(5.5 – 3 · M); • CD: (eq.2.4)·0.12;
<i>Supersonic</i>	<ul style="list-style-type: none"> • CL: (eq.2.6)·M · 0.55; • CD: (eq.2.4)·(0.20 + M/10);
ALL BODY HYPERSONIC AIRCRAFT MODEL	
<i>Subsonic</i>	<ul style="list-style-type: none"> • CL, (eq.2.11): $c_1 \cdot 0.63$; • CD: (eq.2.12)·(1 + M/3);
<i>Supersonic</i>	<ul style="list-style-type: none"> • CL, (eq.2.11): $c_1 \cdot 0.46, c_2 \cdot 2$; • CD: (eq.2.12)·(0.88 + M/9.5);
RAYMER MODEL	
<i>Subsonic</i>	<ul style="list-style-type: none"> • CL: (eq.2.37)+0.022; • CD: (eq.2.43)+0.005;
<i>Supersonic</i>	<ul style="list-style-type: none"> • CL: (eq.2.37)·(0.3 + M/18); • CD: (eq.2.43)·(1.4/log(2 · M + 0.5));
TORENBEEK MODEL	
<i>Supersonic</i>	<ul style="list-style-type: none"> • CL: (eq.2.66)·(0.35 + (M/20)); • CD: (eq.2.71)·(2.1/(log2 · M + 2));

Table 3.18: Corrective coefficients for Blended Body configuration

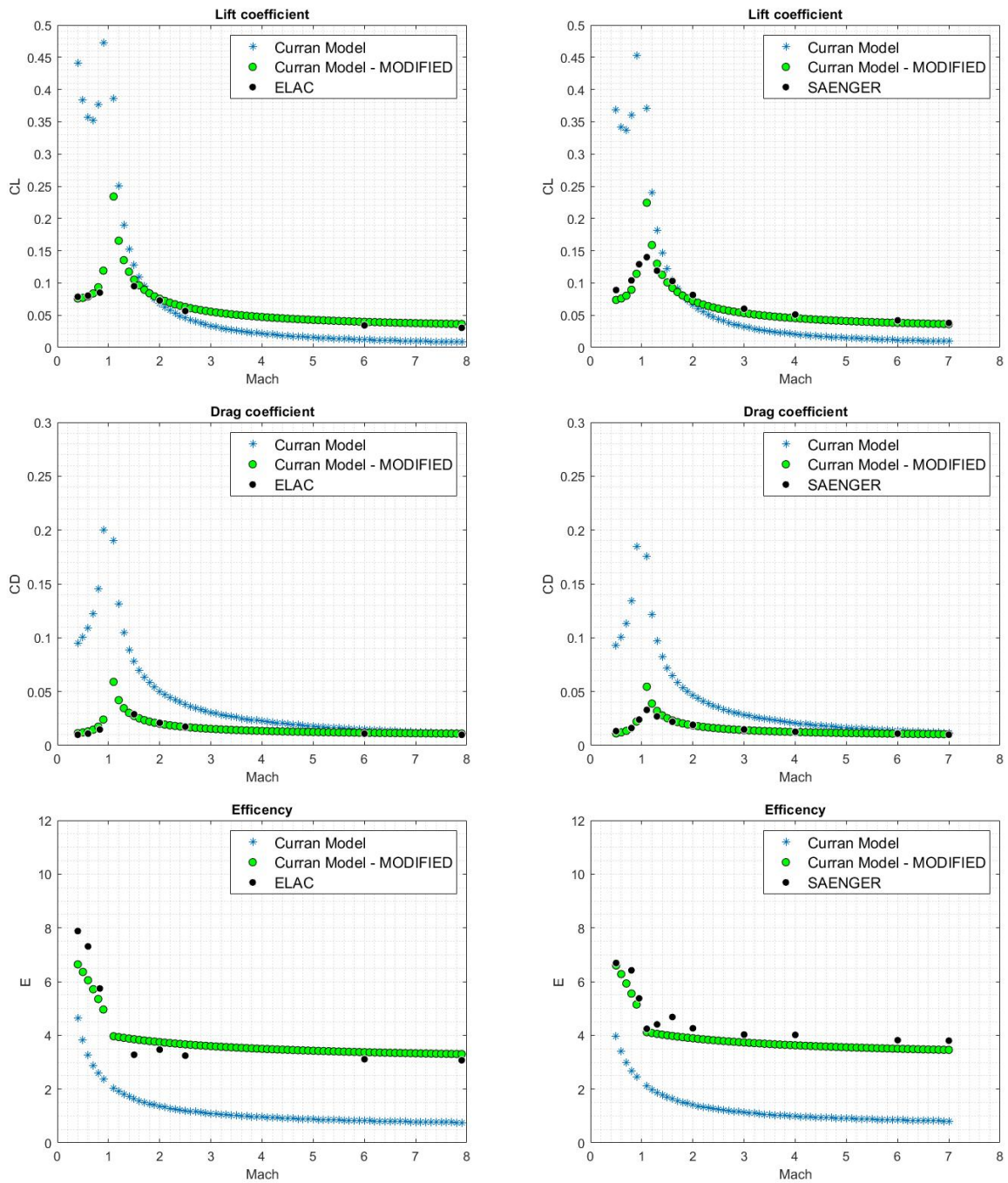


Figure 3.38. Aerodynamic coefficients of the basic Curran Model compared with the aerodynamic coefficients of the modified Curran Model for Blended Body configuration

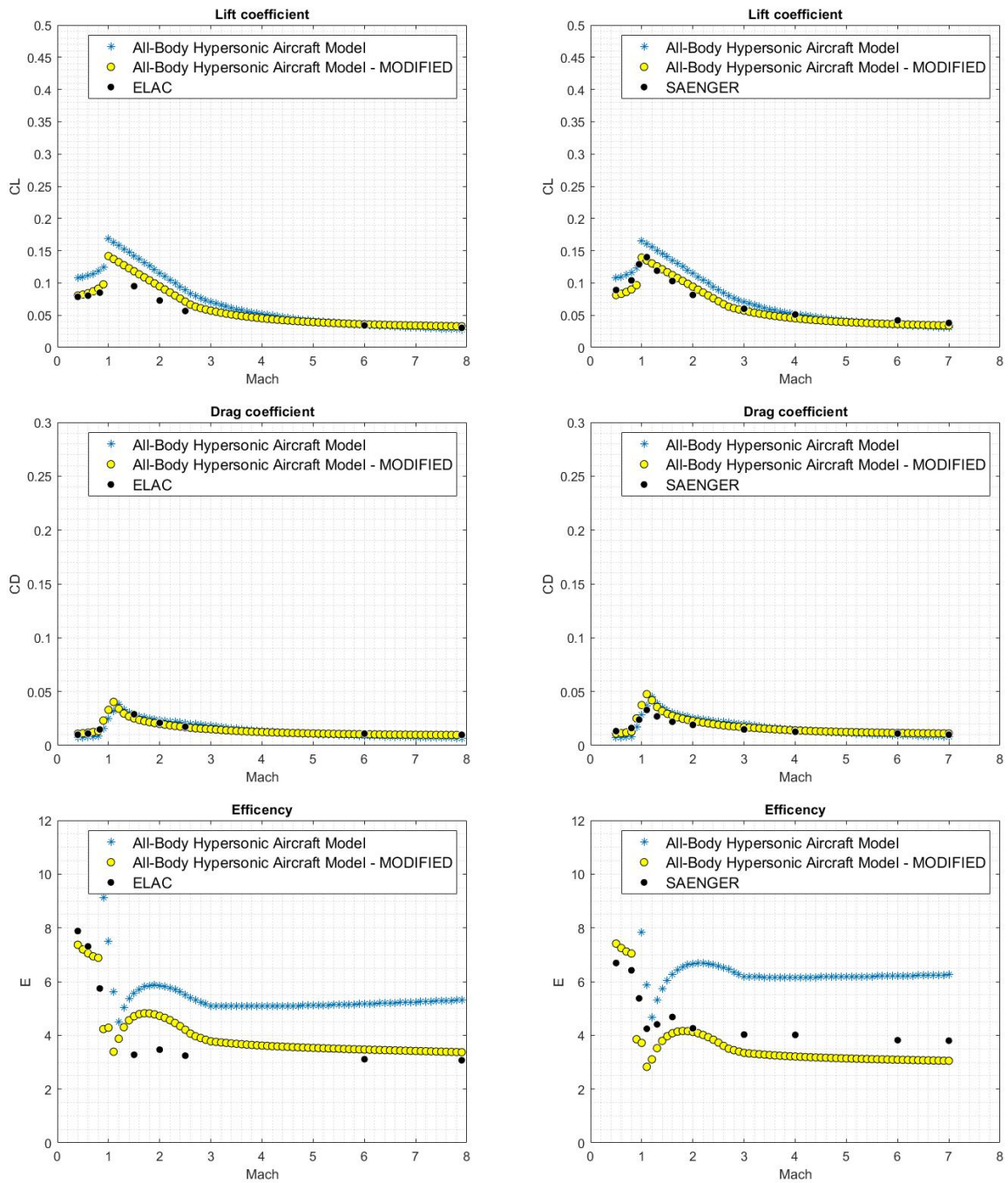


Figure 3.39. Aerodynamic coefficients of the basic All-Body Hypersonic Aircraft Model compared with the aerodynamic coefficients of the modified All-Body Hypersonic Aircraft Model for Blended Body configuration

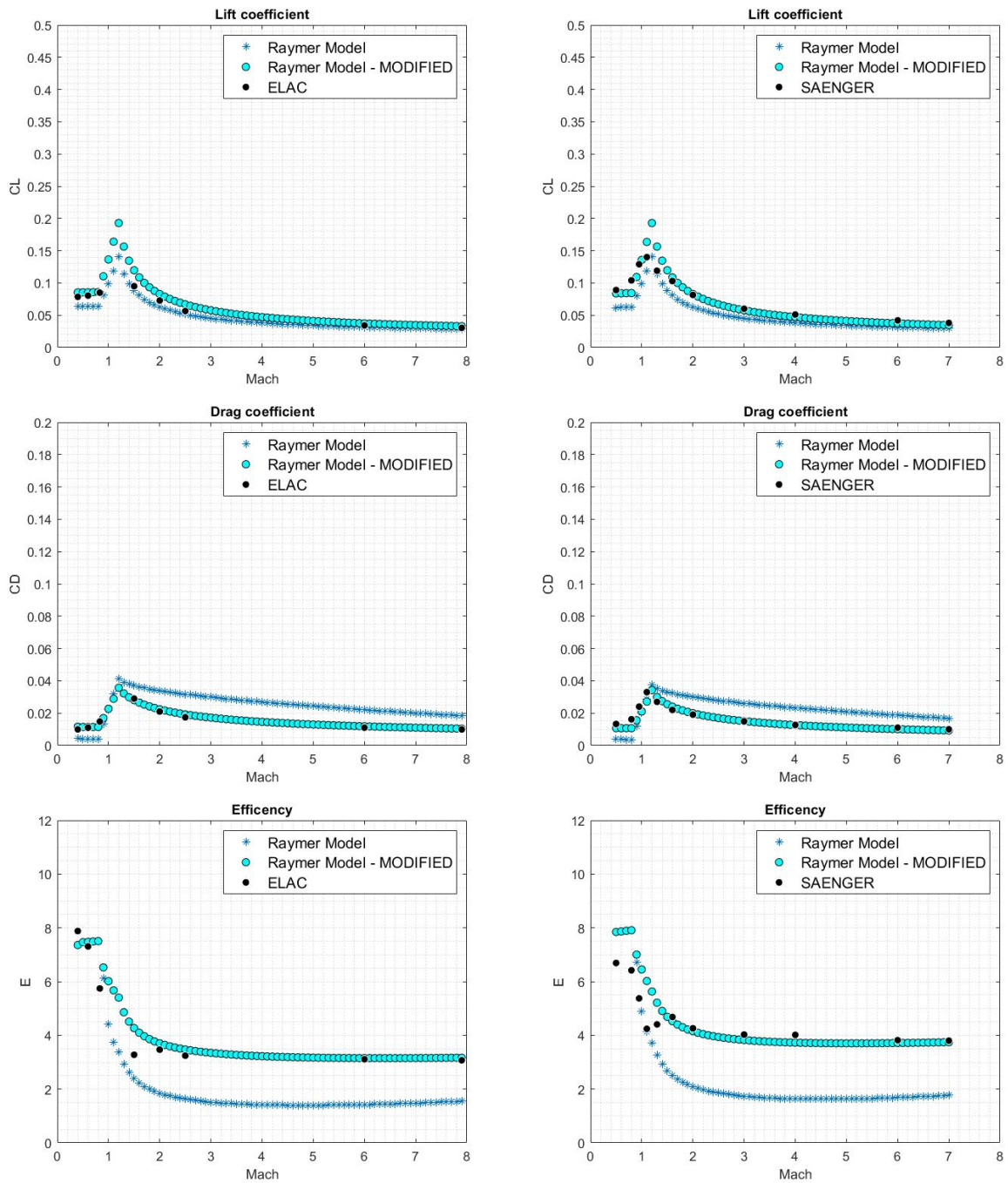


Figure 3.40. Aerodynamic coefficients of the basic Raymer Model compared with the aerodynamic coefficients of the modified Raymer Model for Blended Body configuration

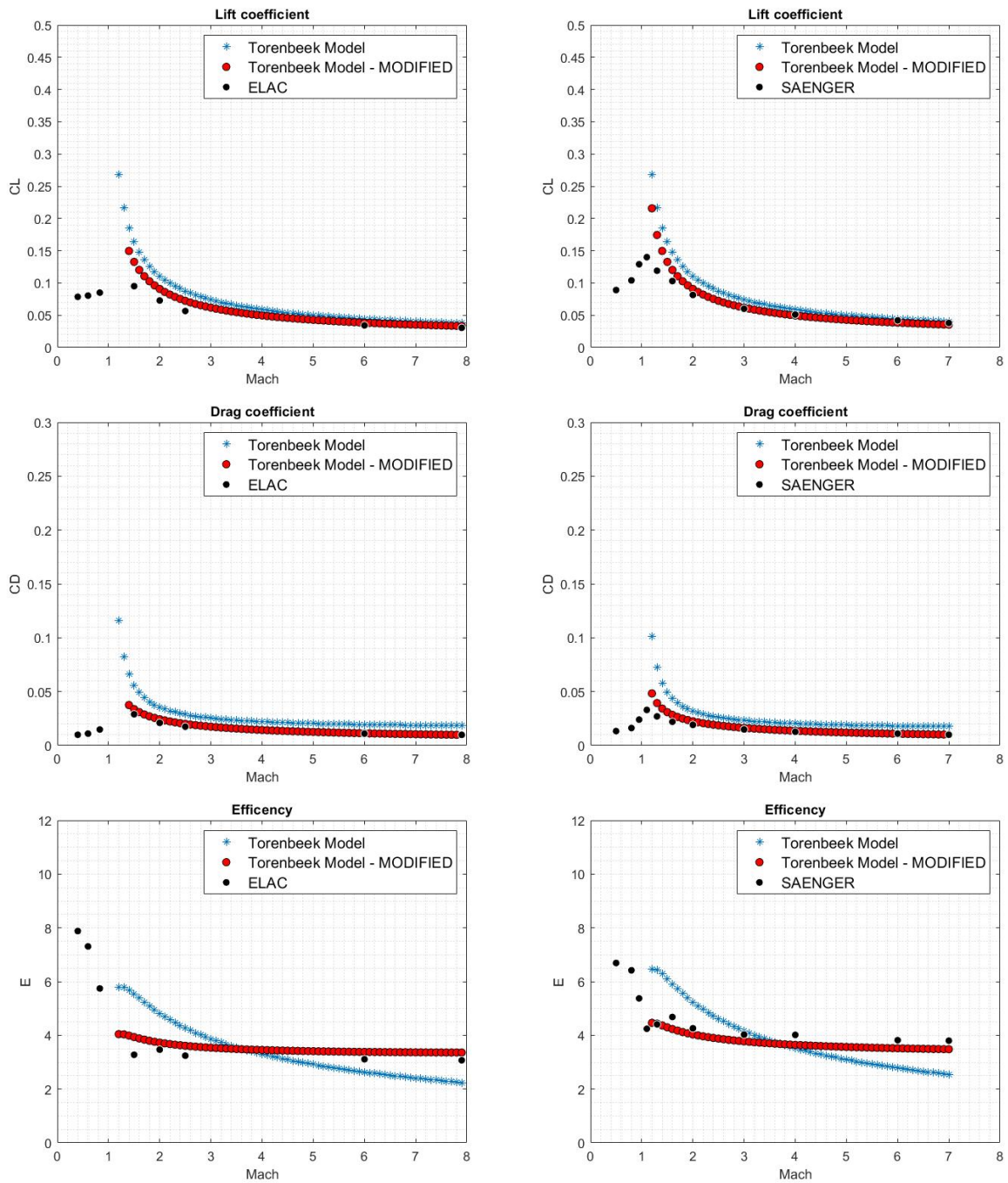


Figure 3.41. Aerodynamic coefficients of the basic Torenbeek Model compared with the aerodynamic coefficients of the modified Torenbeek Model for Blended Body configuration

Chapter 4

Aerodynamic Graphical User Interface Tools

In the previous chapters, all the results obtained following the modifications to the basic aerodynamic models were presented. As seen, thanks to the added corrective coefficients it is possible to obtain a sufficiently reliable estimate of the aerodynamic behaviour, in a preliminary design phase. However, in order to allow any user to take advantage of these results, it was necessary to implement a graphical interface. A GUI (Graphical User Interface) allows interactive use of the implemented functions by the user, who does not necessarily have to know or understand the implementation details of the programming, nor does he have to create scripts or functions to interact with the software. Considering the flexibility, immediacy and usefulness of a GUI, its programming requires design choices that make the interface as immediate and intuitive as possible.

Furthermore, it is possible to consider this tool as a starting point for the improvement of the aerodynamic calculation routine implemented in ASTRID-H, which is already installed at the moment, but it is quite simplified. The ASTRID-H software (Aircraft on-board Systems sizing and TRade-off analysis in Initial Design - High speed), has been developed at Politecnico di Torino in order to provide a valuable support for the design of high-speed vehicles and related subsystems, thus encompassing both the conceptual and preliminary design phases, respectively. In particular, it allows students, researchers and engineers to be guided from the statistical evaluation of the guess data up to the geometrical characterization of the vehicle, guaranteeing a proper integration of the main subsystems [29]. Given that feasible high-speed vehicle design can only be achieved through a high integration between subsystems and airframe, the external layout of the vehicle is usually the best compromise between aerodynamic, propulsive performance and volumetric efficiency. In order to achieve this goal, it is crucial to estimate the basic aerodynamic performance and geometrical parameters for the reference design point selection.

The final part of this work, therefore, is to implement with "Matlab App Designer" a graphical interface that is simple to use and able to provide the required outputs in a clear and complete way.

In the following pages, the main capabilities of this tool and its structure are explained. In the same way, all the required inputs and outputs are listed, depending on the analysis performed. Finally, a small guide is provided with the aim of helping the user step by step and assisting him in the all choices.

4.1 GUI Architecture and Capabilities

The final aerodynamic estimation routine is complete and capable of supporting a wide range of users and high-speed vehicle configurations.

The figures (4.1, 4.2, 4.3) show the flow chart of the tool, which summarises graphically all the operations and choices required to perform the aerodynamic analysis. As can be seen, the user's first choice is the configuration of the aircraft to be analysed. In particular, the family of interest can be chosen between:

- Cylinder Wing configuration;
- Blended Body configuration;
- Wing Body configuration;
- Waverider configuration;

After that, the second user's choice is the accuracy of the analysis to be performed, which can be less or more accurate. These two options are closely linked to the number of available inputs and geometric data, and therefore to the progress of the project. If the analysis is performed in an early stage, there is a poor number of available data and the obvious option is "Simplified analysis with few input required". On the other hand, if the phase of the project is advanced and all or almost all the geometric data of the aircraft are available, it is possible to choose the "More accurate analysis with many input required" option.

At this point, depending on the combination of these two initial choices, the next step is to enter the required inputs. As can be seen from the figure (4.1), the simplified analysis involves the use of the Model I (Curran Model) which is the simplest of those analysed and only requires three geometrical input: the total volume of the aircraft V_{tot} , the reference surface S_{plan} and the wetted surface S_{wet} . In addition, the initial (M_{in}) and final Mach number (M_{fin}) of the analysis and its step of variation (between 0.1 - 0.5 - 1) are required. As introduced in the chapter 2.1, this model is not a function of the angle of attack and therefore the results are only Mach number functions.

On the other hand, the more accurate analysis implies the use of the remaining

three models: the Model II (All-Body Hypersonic Aircraft Model), the Model III (Raymer Model) and the Model IV (Torenbeek Model). These routines are used simultaneously in order to verify that the aerodynamic coefficients are approximately the same for all three cases and to obtain a more reliable results. The curves of the three models are plotted on the same graph in order to have a direct comparison and immediately understand which of the three is less accurate and reliable.

Before entering all the input required, in the case of Wing-Body and Waverider family, a few more choices need to be made. In the first case, it is necessary to define whether the vehicle under consideration has an Aspect Ratio (AR) greater or lower than 2. In the second case, the first choice to do is to define whether the waverider is a dorsal or ventral concept. After that, it is possible to do an only Mach number variation analysis, specifying the desired angle of attack, or a Mach number and Alpha variation analysis, where the the initial (α_{in}) and final angle of attack (α_{fin}) are 1° and 5° respectively. The last choice is to indicate if the analysis refers to an operational condition where the engines are switched on or off.

All the inputs required for this more accurate analysis are listed in the figure (4.2, 4.3): those written in black are mandatory inputs while those in grey must be inserted only if the vehicle under consideration has that particular component within its configuration. As can be seen from the last part of the flow chart (fig. 4.3), in the case of a dorsal waverider, the output are functions of both the Mach number and the angle of attack.

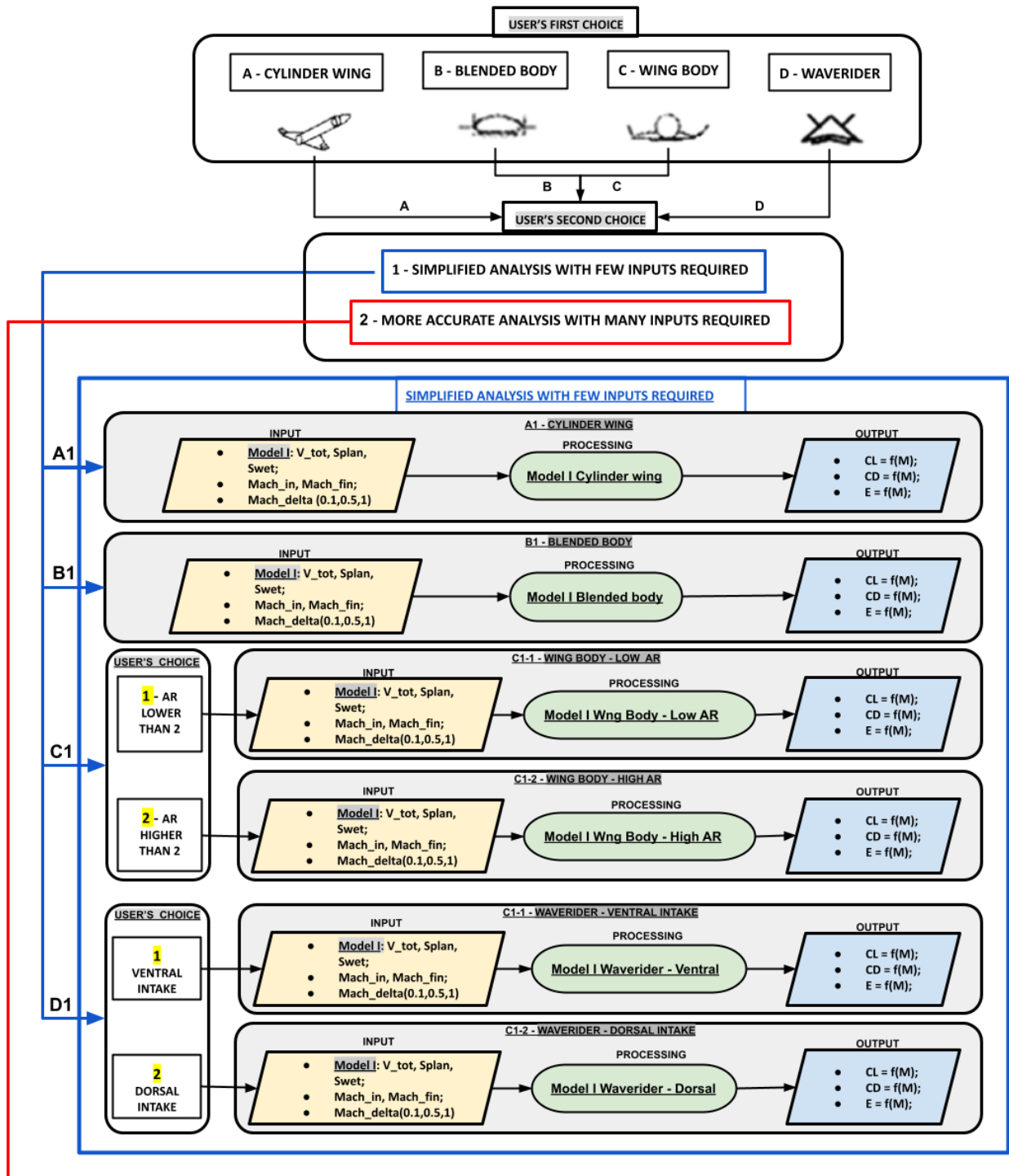


Figure 4.1. Structure of the Aerodynamic GUI, simplified analysis.

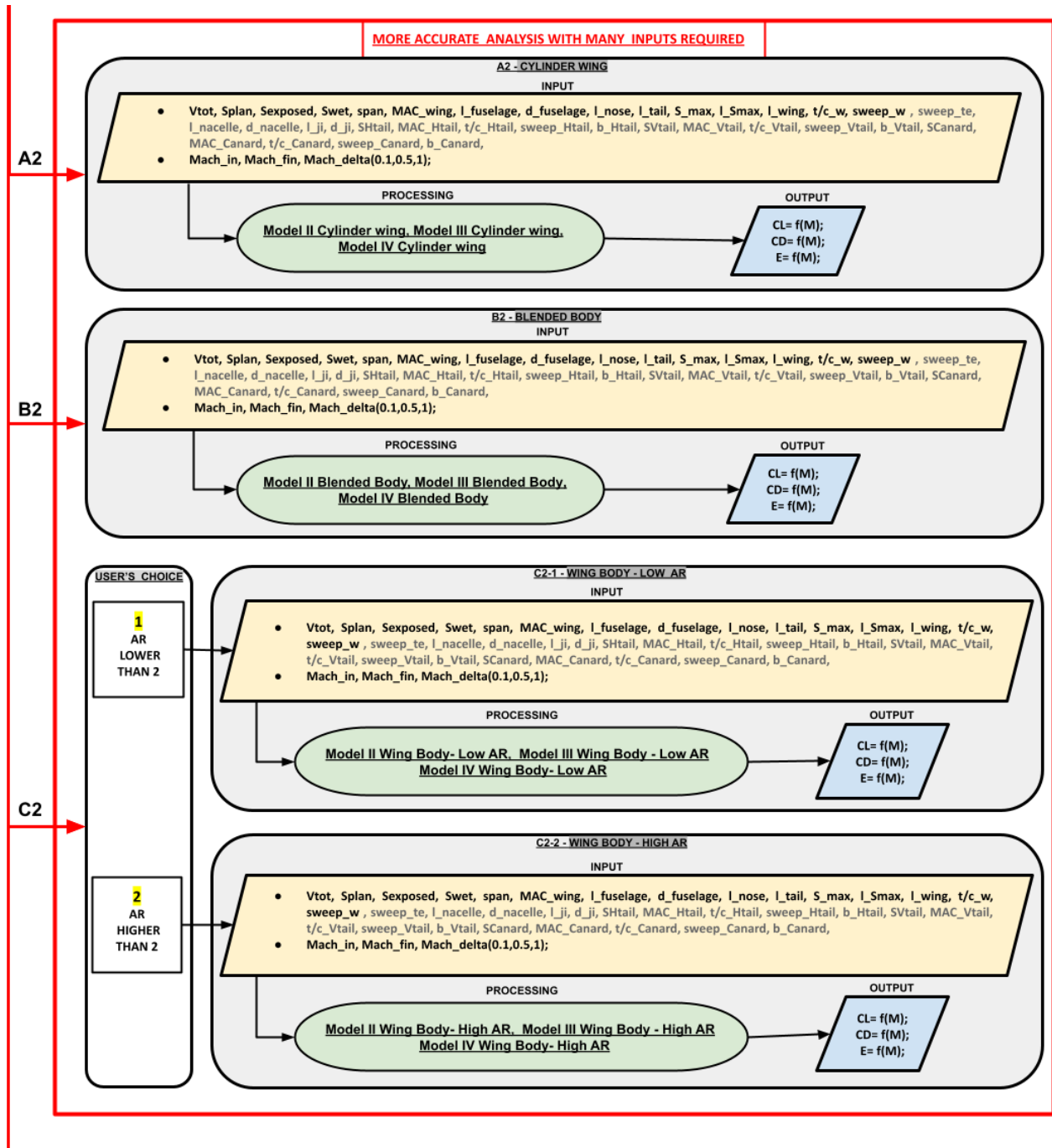


Figure 4.2. Structure of the Aerodynamic GUI, more accurate analysis.

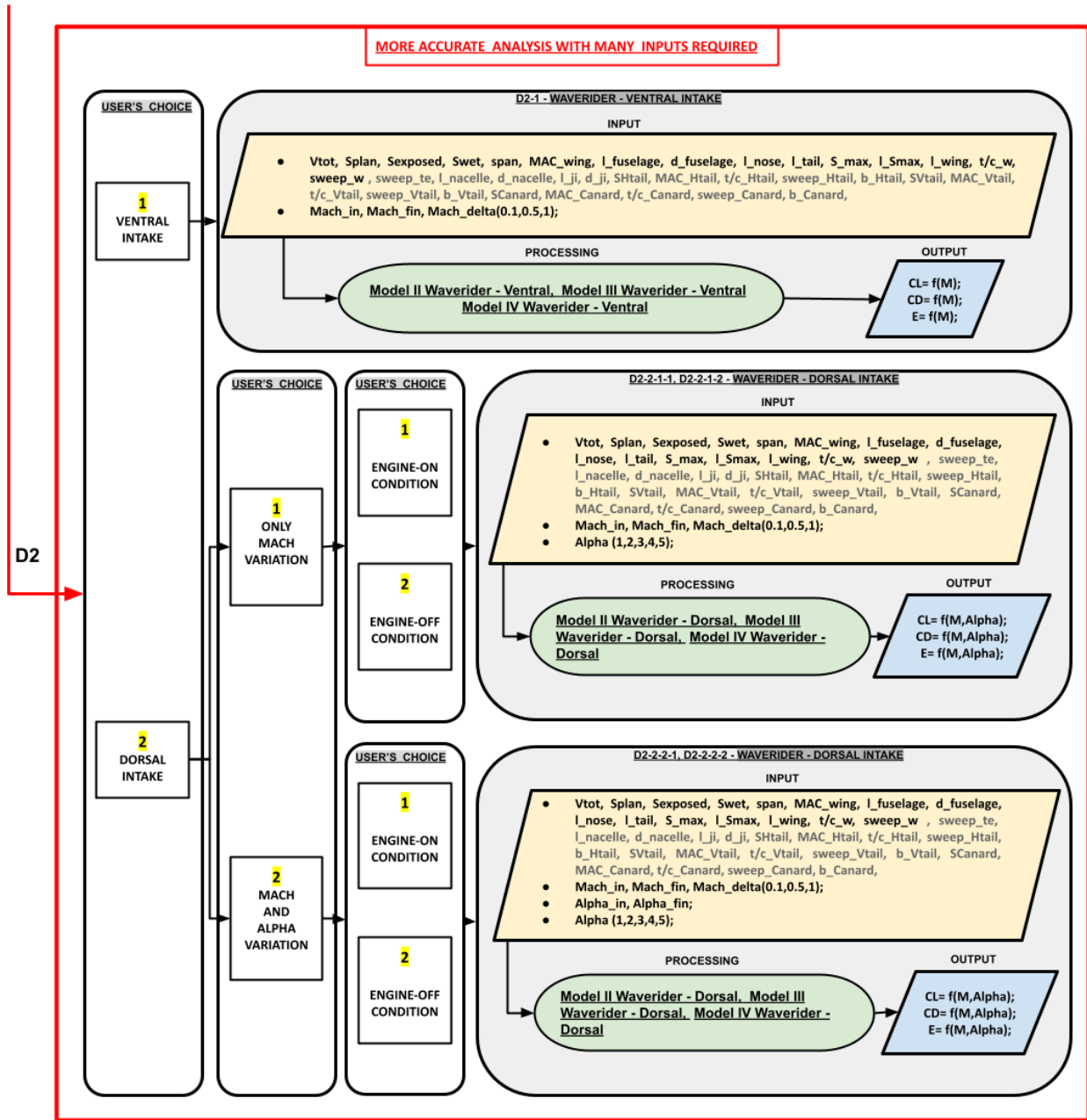


Figure 4.3. Structure of the Aerodynamic GUI, more accurate analysis.

4.2 User Guide

This section aims to provide the user with a quick guide on how to run the aerodynamic tool and to proceed step by step, in order to ensure proper use and to avoid unwanted errors. In particular, two examples are reported in the following pages, one for the simplified analysis and another one for the more accurate analysis. Once the tool is started, the first screen that appears is the following:

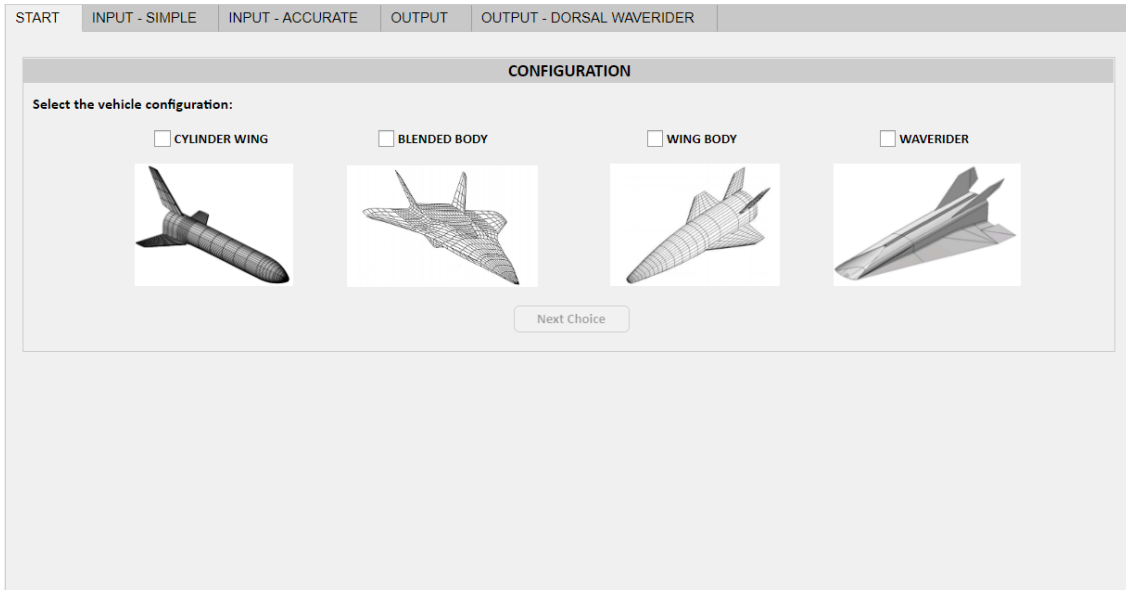


Figure 4.4. First choice of the Aerodynamic tool

As can be seen from the figure above (4.4), the aerodynamic graphical user interface is very simple and intuitive. The first user's choice is the configurational family of the vehicle to be analysed. It is necessary to simply check the box of interest and the button "Next Choice" automatically became enable: clicking on it, the next screen appears (4.5) and it is possible to make the second choice. As mentioned before, it consist of the accuracy of the analysis, which can be simplified if the geometric data are poor, or accurate if all the required input are enable. At this point, depending on the combination of these two initial choices, the selected analysis' screen will appear.

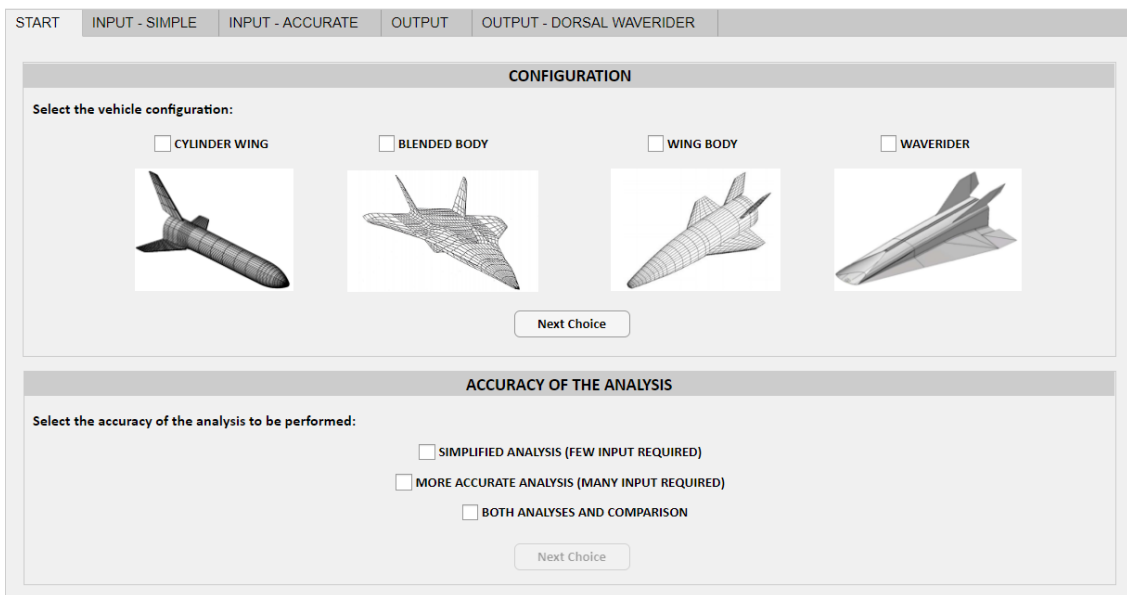


Figure 4.5. Second choice of the Aerodynamic tool

4.2.1 Simplified analysis

As example, the simplified analysis procedure for the cylinder wing configuration is presented.

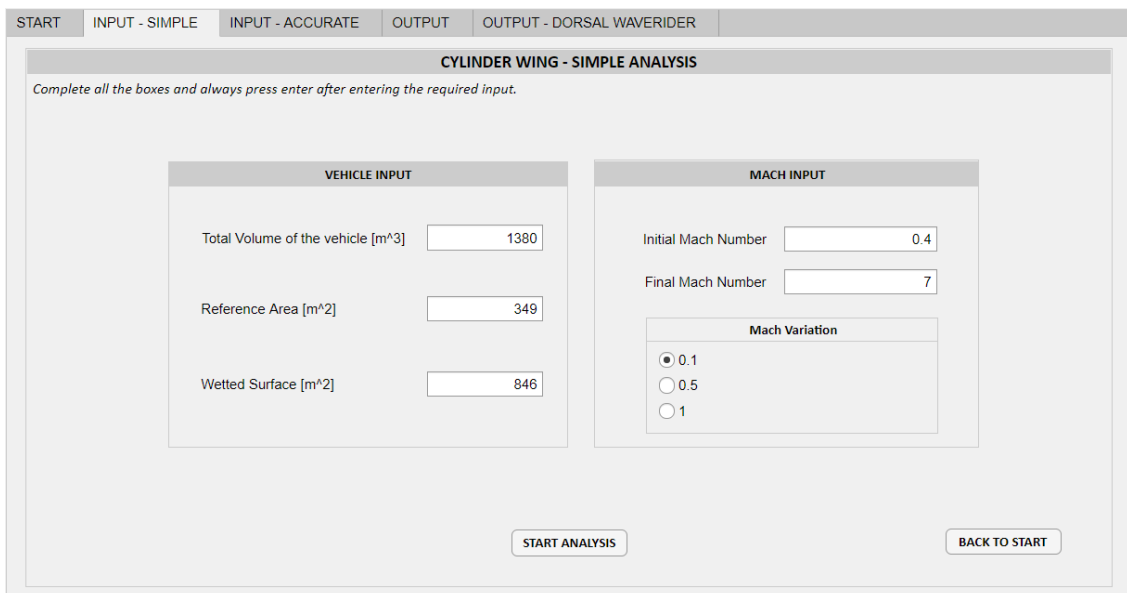


Figure 4.6. Cylinder wing - simplified analysis - INPUT

Selecting the boxes of interest and clicking on the button "Next Choice", the INPUT screen will open (figure 4.6). As can be seen, the geometrical data required are the Curran Model ones. Then, it is necessary to digit in all the values by always pressing "enter" and once the last has been entered, the button "START ANALYSIS" will became enable. Clicking on it, the programme automatically switches to the final OUTPUT screen (fig.4.7).

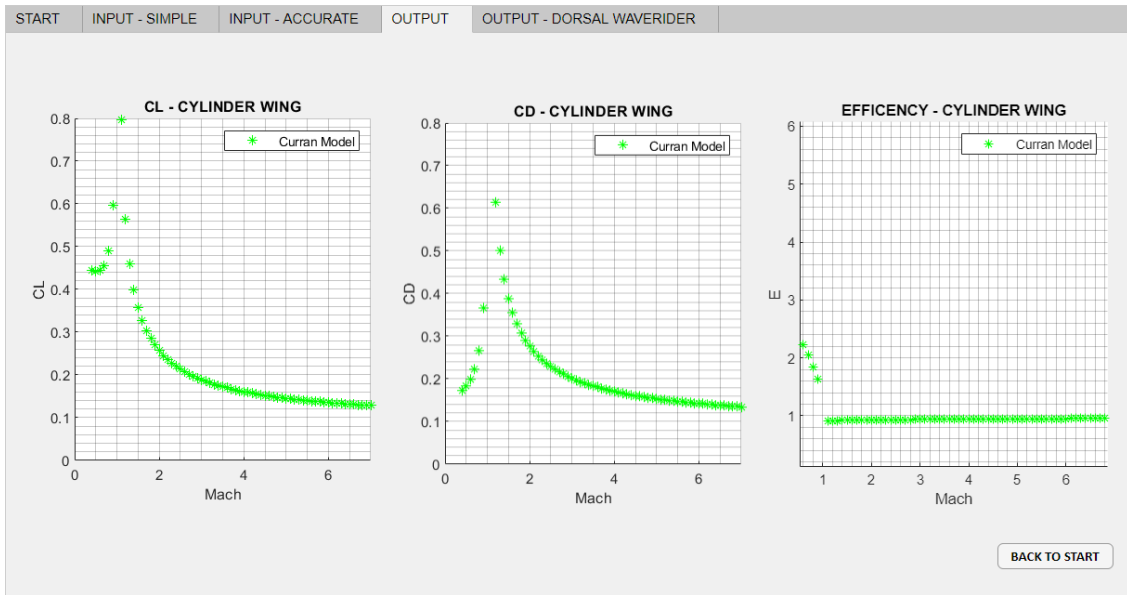


Figure 4.7. Cylinder wing - simplified analysis - OUTPUT

Starting from the left graph, the lift coefficient, drag coefficient and the aerodynamic efficiency, obtained as the ratio between the first two, are presented respectively. As can be seen, the flight range is the one specified in the inputs, which in this case is between 0.4 and 7, with a selected variation step equal to 0.1. As specified in the chapter 3.5, The Curran Model approximates well the aerodynamic behaviour for the subsonic and supersonic regime, while it overestimates it in the transonic regime. For a more accurate reading of the results, it is possible to manipulate the graph by zooming in on the range of interest, or by moving the curves as desired.

The tool is therefore very intuitive and easy to use, and the results are clear and visible. At any time, if there is an error or any data to change, simply select the button "BACK TO START" and the software will return to the initial screen.

4.2.2 Accurate analysis

In order to provide an example of the more accurate analysis, the procedure for the dorsal waverider configuration is reported.

Selecting the boxes of interest (fig. 4.5), the button "Next Choice" became enable: clicking on it, the INPUT screen will appear (fig.4.8), where all the necessary data are required. As said before, the choice of the more accurate analysis implies the request of a much larger number of geometrical data: in the previous case there were only six, while now there are three screens to fill.

Figure 4.8. Dorsal waverider - accurate analysis - first INPUT screen

As can be seen in the figure 4.8, in the first screen "Initial Input" it is necessary to set the analysis: in this case, the Dorsal Intake check-box is chosen, together with the only Mach variation for an angle of attack equal to $\alpha = 3^\circ$ and the engine - ON condition. The question mark's box specifies that the α value must be between 1° and 5° .

Clicking the button "Next", the tool will pass to the second INPUT screen, called "Vehicle". The general data of the aircraft are here requested, such as the length and the diameter of the fuselage, the total volume, ecc. The values reported in the figure 4.9 are those relating to the STRATOFly MR3 vehicle, which can therefore also be read in the table 3.1, chapter 3.1.1. Finally, the speed range within which the analysis will be carried out is defined.

WAVERIDER - ACCURATE ANALYSIS
 Complete all the boxes and always press enter after entering the required input.

Initial Input	Vehicle	Wing	Tail and Canard
Total Volume of the vehicle [m ³]	1e+04		
Wetted Surface of the vehicle [m ²]	5422		
Fuselage length [m]	94.54		
Fuselage diameter [m]	11.07		
Nose length [m]	20		
Tail length [m]	20		
Maximum cross-sectional area [m ²]	210		
Distance from nose to maximum cross-sectional point [m]	70		

MACH INPUT

Initial Mach Number:

Final Mach Number:

Mach Variation

0.1
 0.5
 1

Figure 4.9. Dorsal waverider - accurate analysis - second INPUT screen

The third INPUT screen ("Wing"), depicted in the figure 4.10, asks for wing data such as the span, the reference surface, the leading-edge sweep angle and others.

WAVERIDER - ACCURATE ANALYSIS
 Complete all the boxes and always press enter after entering the required input.

Initial Input	Vehicle	Wing	Tail and Canard
Wing span [m]	41		
Wing length [m]	93.93		
Wing thickness ratio	0.22		
Mean chord of the wing [m]	14		
Leading edge sweep angle [°]	81		
Trailing edge sweep angle [°]	0		
Reference area [m ²]	2365		
Exposed surface [m ²]	1265		
		Nacelle length[m]	<input type="text" value="0"/>
		Nacelle diameter [m]	<input type="text" value="0"/>
		Air intake length [m]	<input type="text" value="26"/>
		Air intake diameter [m]	<input type="text" value="8"/>

If any of the following required data is not available or the aircraft configuration does not foresee the relevant component, enter 0

Figure 4.10. Dorsal waverider - accurate analysis - third INPUT screen

In conclusion, the fourth and last INPUT screen is the "Tail and Canard" one (fig. 4.11). Obviously, depending on the aircraft being analysed, some parts may not

be installed, such as the horizontal tail or the canards for the STRATOFly MR3 case study.

Figure 4.11. Dorsal waverider - accurate analysis - fourth INPUT screen

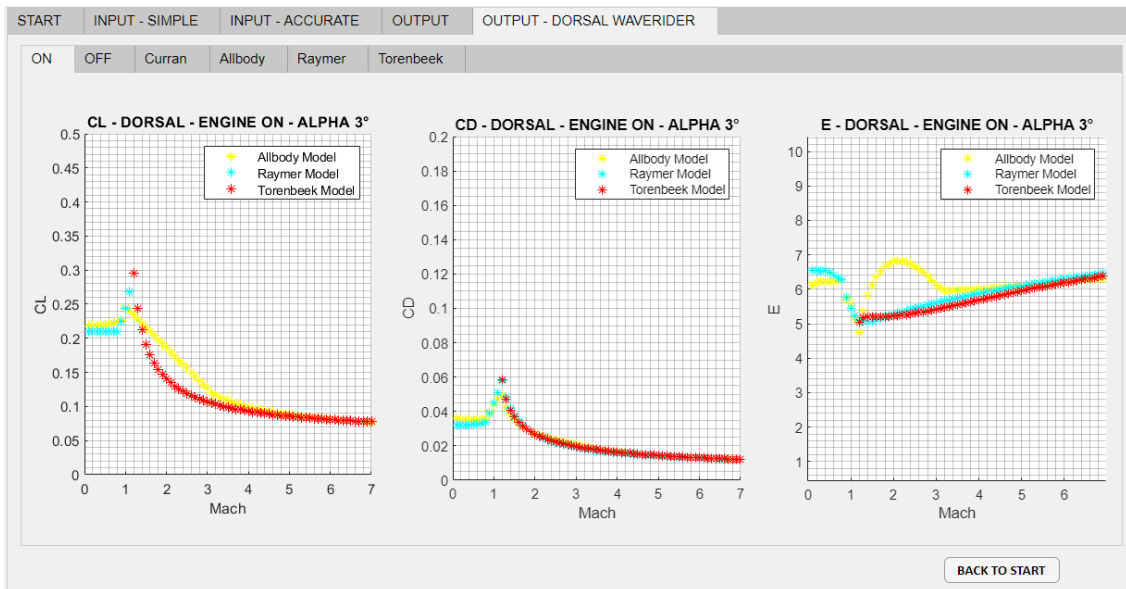


Figure 4.12. Dorsal waverider - accurate analysis - OUTPUT screen

In order to specify which are the surfaces of the vehicle, it is simply necessary

to select the appropriate check-box and enter all the values required, so that the button "START ANALYSIS" becomes enable: clicking it, the OUTPUT screen will appear.

As mentioned before, the accurate analysis involves the use of the Allbody, Raymer and Torenbeek models. The curves of these three models are plotted on the same graphs in order to have a direct comparison of the aerodynamic coefficients. The results depicted in the figure 4.12 are the STRATOFLY ones and starting from the left, the CL coefficients, CD coefficients and Efficiency are shown respectively.

As explained previously, it is possible to see that the Raymer model is applicable for all the flight regimes, from subsonic to supersonic (cyan curves), while the Torenbeek model is only applicable for supersonic regimes (red curves). Finally, it can be seen that the Allbody model (yellow curves), due to lift linearization, is only reliable for subsonic and high supersonic - hypersonic regimes.

4.2.3 Both analysis and comparison

Looking at the initial screen of the Aerodynamic GUI (figure 4.5), it is clear that in addition to the simple and accurate analysis, if all the necessary data are available, it is possible to choose another option: "both analysis and comparison". In this way, the results will be provided not only for the three models of the accurate analysis, but also for the Curran model of the simplified analysis. The OUTPUT screen is the one reported in the figure 4.13.

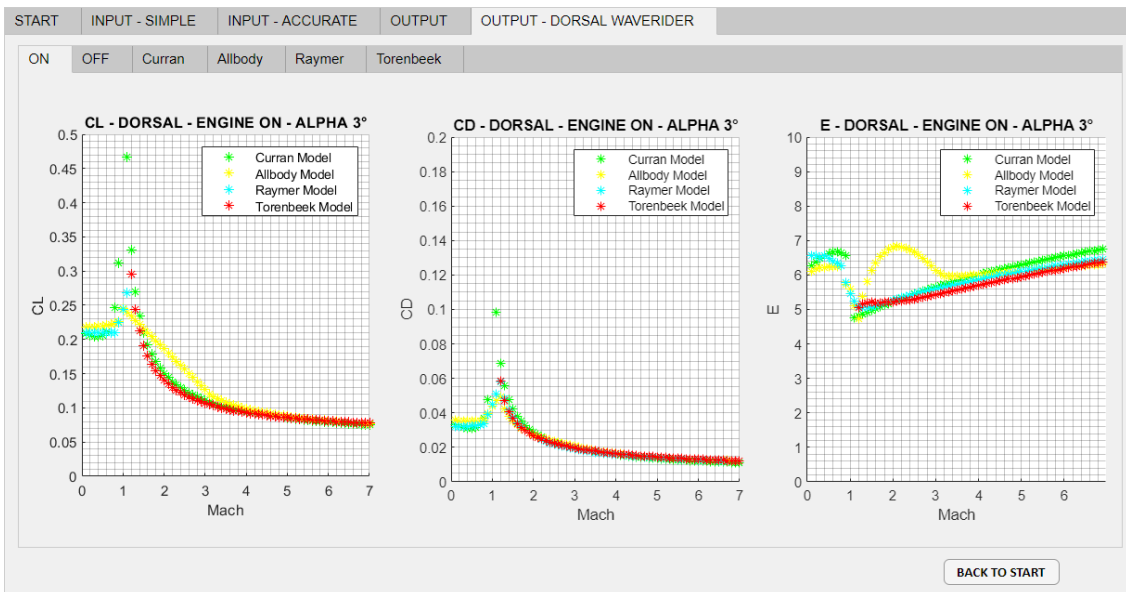


Figure 4.13. Dorsal waverider - both analysis and comparison - Engine ON

in addition to the previous case (4.12), it can be seen that there are the Curran

model results (green curves).

The three INPUT screens for this case are exactly the same of the ones presented for the dorsal waverider STRATOFly MR3 case study.

4.2.4 Other Results

In the previous sections, three possible uses of the GUI were presented, depending on the user's choices. For all the configurational families, the procedure and the geometrical data required as input are approximately the same, for both simple and accurate analysis.

However, as explained in the chapter 4.1, in the case of the dorsal waverider, many more choices can be made. In addition to the analysis with only the Mach variation and the engines switched on, it is also possible to estimate the aerodynamic coefficients with the engines switched off and the variation of both the Mach and the angle of attack. In this last section, some additional results are given as examples.

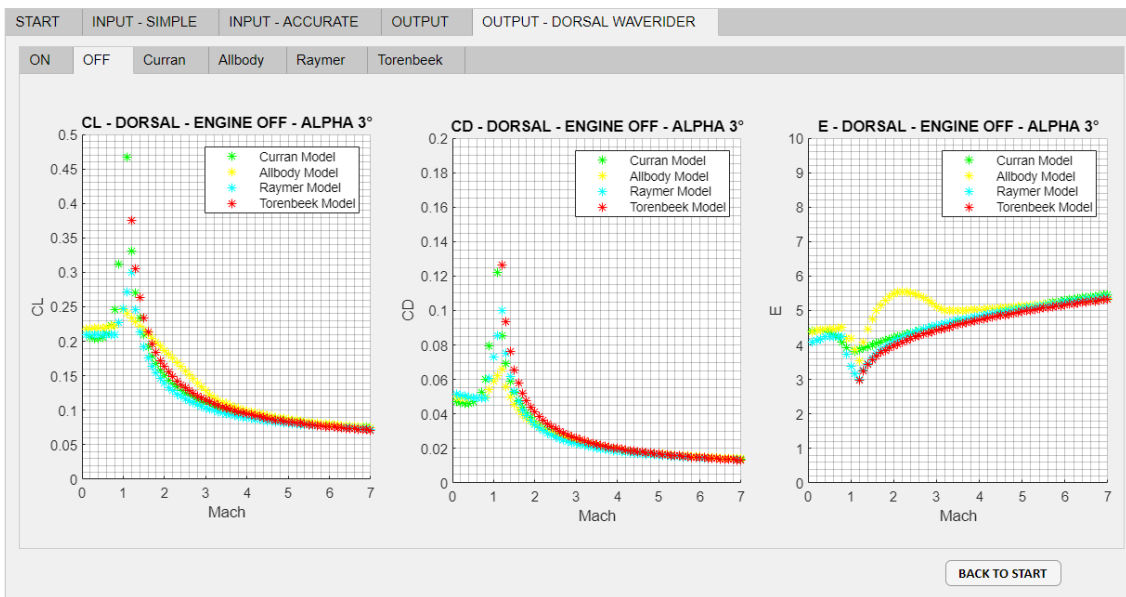


Figure 4.14. Dorsal waverider - both analysis and comparison - Engine OFF

The first OUTPUT screen depicted in the figure 4.14 shows the results for the case in which the engines are switched off, for both the simple and accurate analysis. When compared with the engine on case study (figure 4.13), it is clear that now the CD coefficients are higher and consequently the Efficiency is lower, for the reason that is explained in the chapter 3.1.1.

The last two examples concern the analysis as a function of both Mach number and

angle of attack: the latter varies from $\alpha_{in} = 1^\circ$ up to $\alpha_{fin} = 5^\circ$. In fact, five curves are shown in the figures 4.15, 4.16, obtained by the Raymer model.

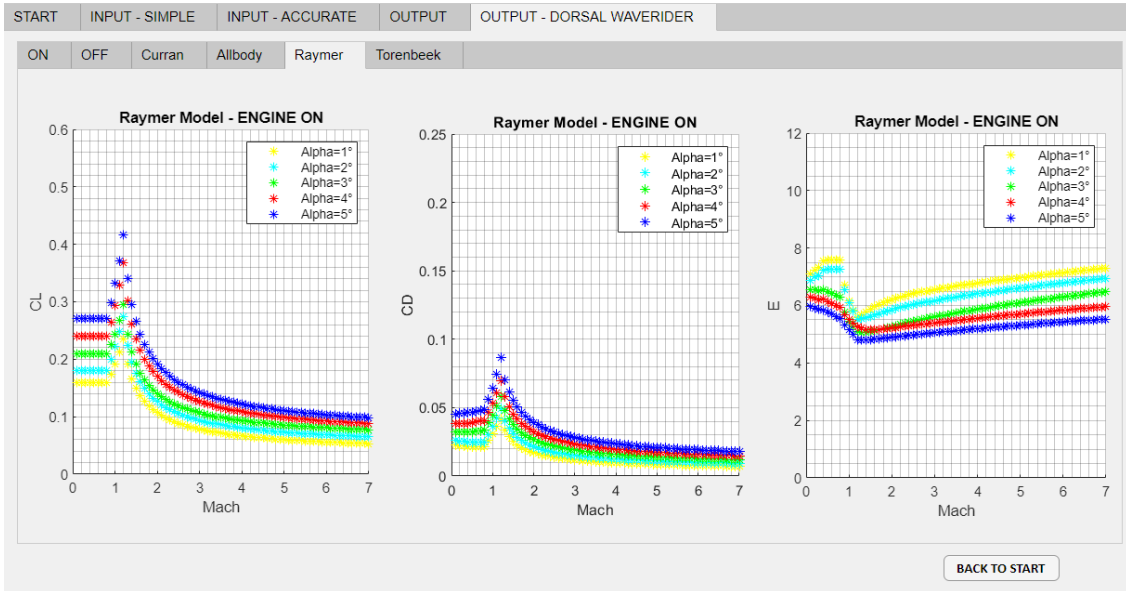


Figure 4.15. Dorsal waverider - Mach and α variation - Engine ON - Raymer Model results

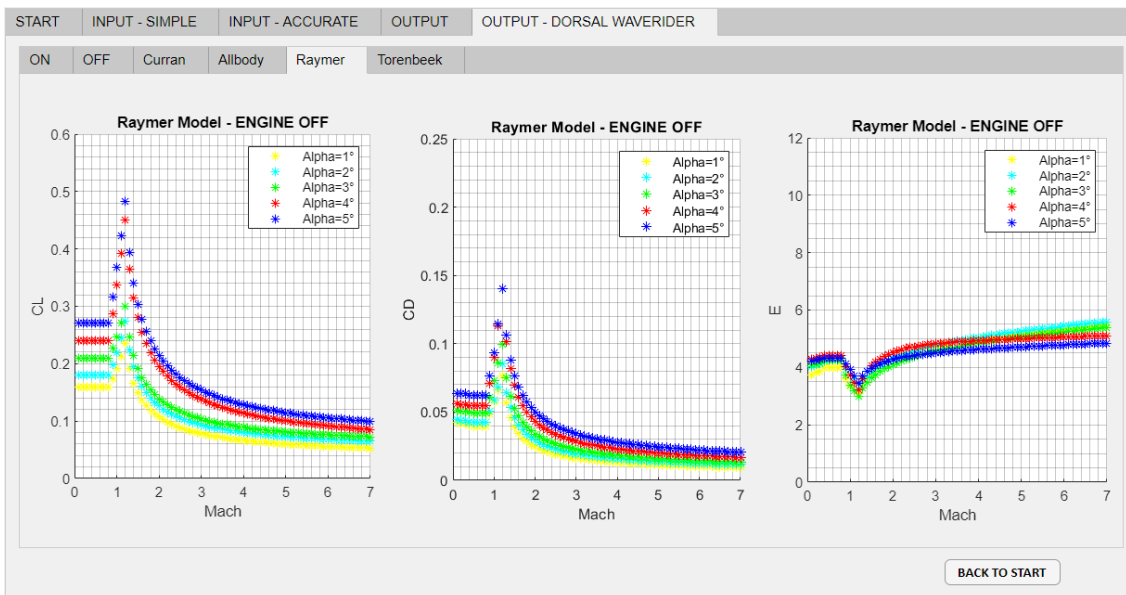


Figure 4.16. Dorsal waverider - Mach and α variation - Engine OFF - Raymer Model results

As can be seen, as the angle of attack increases, the lift increases. However, In the same way, there is an increase in drag coefficient, which is greater than the previous one, and consequently the efficiency decreases. In conclusion, comparing the two figures, it is possible to see the negative effect of the engines switched off.

Chapter 5

Conclusions

The initial objective of this thesis was to obtain a simple and reliable aerodynamic procedure, capable of estimating the performance of a high-speed aircraft in the initial design phases. All the effort made to achieve this goal has been described in the previous pages, from the analysis of the basic models found in the literature, up to the modifications of the same and finally the presentation of the outcomes. In addition, an intuitive graphical interface has been implemented, so that any user can benefit from the work done and obtain desired results in a few simple steps.

As explained in the previous chapters, the main part of the work was carried out on the STRATOFly MR3 case study. The available aerodynamic database of this vehicle is very complete and within it the coefficients depend on the Mach number, the angle of attack and also the operative condition of the engines, which can be either switched on or off. It was therefore possible to obtain accurate results, for angle of attack between $\alpha = 1^\circ$ and $\alpha = 5^\circ$, and a speed range between $M = 0.4$ and $M = 8$.

In addition to the dorsal intake waverider configuration, five other families were analysed: ventral intake waverider, cylinder wing, blended body and wing body, for both high aspect ratio and low aspect ratio. Unfortunately, for all these families it was only possible to fit the models according to flight speed, due to the lack of accurate databases: all the curves taken as reference are relative to an angle of attack of 5° .

There is a good similarity of the results with the real curves, for all four models studied. The least accurate model is usually the Curran one, which tends to overestimate the transonic phase more than the others; however, this is due to its simplicity and to the negligible number of data required as input. On the other hand, the remaining three models require a considerable amount of data, but they certainly provide more reliable results, depending on the configuration under analysis. Thanks to the implemented tool, however, it is possible to have a direct comparison of the four models, for a speed range from subsonic to hypersonic regime.

In conclusion, it is possible to consider this work as an excellent starting point for

the complete achievement of the initial objectives: it has been demonstrated that it is possible to adapt the analysed models for a wide range of configurations. The greatest limitation encountered during this thesis was certainly the difficulty in finding geometric and aerodynamic data of existing high-speed aircraft. In fact, in order to improve the outcomes, a future development could be to increase the number of vehicles in the database, useful for models' validation, especially for those configurational families in which only one aircraft has been tested (Cylinder wing for example). By doing so, it would certainly be possible to improve the coefficients for a more efficient, but above all more reliable results. In the same way, it would be possible an increase in the number of configurational families to be included in the Aerodynamic Graphical User Interface, so that the user can classify more precisely the aircraft to be analysed in the first choices, especially for unconventional hypersonic geometries.

Bibliography

- [1] S. N. B. M. E. T. Curran, *Scramjet propulsion, Cambridge, Massachusetts, 2000.*
- [2] Vinh, N. X., *Flight Mechanics of High-Performance Aircraft, Cambridge Aerospace Series 4, Cambridge Univ. Press, 1993.*
- [3] L. J. Williams, *Estimated Aerodynamics of All-Body Hypersonic Aircraft Configurations*, National Aeronautics and Space Administration, Moffett Field, California, March 1971.
- [4] Raymer, Daniel. *Aircraft design: a conceptual approach. American Institute of Aeronautics and Astronautics, Inc.*, 2012.
- [5] Egbert Torenbeek, *Essentials of Supersonic Commercial Aircraft Conceptual Design (Aerospace Series)*, 2020, Wiley-Blackwell.
- [6] Feng Ding, Jun Liu, Chi-bing Shen, Zhen Liu, Shao-hua Chen, Xiang Fu, *An overview of research on waverider design methodology Acta Astronautica*, August 2017.
- [7] A. J. Eggers, Jr., and Clarence A. Syvertson, *Aircraft configurations developing high Lift-Drag Ratios at high supersonic speeds*, NACA, March 1956.
- [8] R. Scigliano, V. De Simone, M. Marini, P. Roncioni, R. Fusaro, N. Viola, *Preliminary Finite Element Thermal Analysis of STRATOFly Hypersonic Vehicle*, 2020.
- [9] R. Fusaro, N. Viola, *Design and integration of a cryogenic propellant subsystem for the hypersonic STRATOFly MR3 Vehicle*, Politecnico di Torino, 2019.
- [10] T. Langener, J. Steelant, *Trajectory Analysis for the Updated LAPCAT-MR2.4 Waverider based Vehicle*, October 2013.

- [11] Laurie A. Marshall, Griffin P. Corpening, Robert Sherrill, *A Chief Engineer's View of the NASA X-43A Scramjet Flight Test*, NASA, March 27, 2004.
- [12] Walter C. Engelund, Scott D. Holland, Charles E. Cockrell Jr, *Aerodynamic Database Development for the Hyper-X Airframe-Integrated Scramjet Propulsion Experiments*, December 2001.
- [13] Scott D. Holland, William C. Woods, Walter C. Engelund, *Hyper-X Research Vehicle (HXRV) Experimental Aerodynamics Test Program Overview*, August, 2000.
- [14] Claus Weiland, *Aerodynamic Data of Space Vehicles*, 2014.
- [15] Giuseppe C. Rufolo, P. Roncioni, M. Marini, *USV FTB-1 reusable vehicle aerodatabase development*, January 2007.
- [16] G. Pezzella, *Aerodynamic and aerothermodynamic trade-off analysis of a small hypersonic flying test bed*, Capua, April 2011.
- [17] G. C. Rufolo, P. Roncioni, M. Marini, R. Vott *Experimental and Numerical Aerodynamic Data Integration and Aerodatabase Development for the PRORA USV-FTB-1 Reusable Vehicle*, November 2006.
- [18] V. D'Oriano, R. Savino, M. Visone, *Aerothermodynamic Study of a Small Hypersonic Plane*, Aircraft Engineering and Aerospace Technology, 2018.
- [19] Savino R., Russo G., Carandente V., D'Oriano V *Hyplane: Challenges for Space Tourism and Business Transportation*, Journal of Aeronautics & Aerospace Engineering, 2013.
- [20] G. Zuppari, R. Savino, G. Russo, L. Spano' Cuomo, E. Petrosino *Aerodynamic analysis of the aerospaceplane HyPlane in supersonic rarefied flow*, Napoli, March 2016.
- [21] G. Pezzella, M. Marini, P. Roncioni, J. Kauffmann, C. Tomatis, *Aerodynamic and Aerothermodynamic evaluation of the VTO Hopper concept in the frame of ESA Future Launchers Preparatory Program*, Dayton, Ohio, 2008.
- [22] G. Pezzella, *Preliminary Aerodynamic and Aerothermodynamic Assessment of the VTO Hopper Booster*, ISRN Mechanical Engineering. Volume, 2011.

- [23] G. Pezzella, M. Marini, P. Roncioni, C. Tomatis, J. Kauffmann *Preliminary Design of Vertical Takeoff Hopper Concept of Future Launchers Preparatory Program*, Journal of Spacecraft and Rockets 2009.
- [24] Hyoung Woo Oh, *Applied Computational Fluid Dynamics*, March, 2012.
- [25] Vaibhav B Jadhav 1, Arundhati Warke, *Investigation of ELAC 1 Aerodynamics Using CFD in Supersonic Flow*, 2014.
- [26] Jacob D., Sachs G., Wagner S., *Basic Research and Technologies for Two-Stage-To-Orbit Vehicles*, Weinheim (2005).
- [27] S. Weingartner, *The Reference Concept of the German Hypersonics Technology Program* , December 1993.
- [28] Dietrich E. KOELLE, *SAENGER II, A Hypersonic Flight and Space Transportation System*, ICAS-88-1.5.1.
- [29] D. Ferretto, R. Fusaro, N. Viola, *A conceptual design tool to support high-speed vehicle design*, Politecnico di Torino, Italy.
- [30] CORDIS European Commission, *Stratospheric Flying Opportunities for High-Speed Propulsion Concepts*, <https://cordis.europa.eu/project/id/769246>.
- [31] N. Viola, R. Fusaro, O. Gori, M. Marini, P. Roncioni, et al., *STRATOFly MR3 – how to reduce the environmental impact of high-speed transportation*, Torino, 2019.